CHARACTERIZATION OF THE REDOX SWITCHES IN HUMAN HEME OXYGENASE-2 AND A HUMAN HEME-RESPONSIVE POTASSIUM CHANNEL

By

Li Yi

A dissertation submitted in partial fulfillment
of the requirements for the degree of
Doctor of Philosophy
(Biological Chemistry)
in The University of Michigan
2010

Doctoral Committee:

Professor Stephen W. Ragsdale, Chair
Professor Ruma Banerjee
Professor David P. Ballou
Associate Professor Jeffrey R. Martens
Associate Professor Ursula Jakob

ACKNOWLEDGMENTS

I was fortunate to get tremendous support from a lot of people throughout my Ph.D degree pursuit over the last six years – my mentor, my committee members, my labmates, the department, the university, my collaborators, and my family. This dissertation would not have been possible without their unselfish assistance, encouragement and support.

First and foremost, I would like to sincerely thank Dr. Stephen W. Ragsdale, who has been my mentor for the last six years at both the University of Nebraska-Lincoln and the University of Michigan-Ann Arbor. I am very lucky to have had the opportunity of studying under his supervision, and learning from him, not only in science but also in my daily life. Steve's constant enthusiasm, unceasing dedication, and numerous brilliant ideas have made this dissertation fruitful and accomplished smoothly. Over the past six years, Steve has always supported me, encouraged me, and guided me through my entire graduate studies with his endless patience and passion. I can not imagine any achievement without his tremendous help and encouragement. Besides, Steve is such a nice and approachable person that he makes me feel that six years' graduate study under his mentoring have taken only one day.

For their help and guidance, I also thank all my committee members: Dr. Ruma Banerjee, Dr. David Ballou, Dr. Ursula Jakob, and Dr. Jeffrey R. Martens. Thanks for serving as my committee members for the last three years and giving suggestions and instructions for my research. I would like to specially thank Ruma for also serving as a member of my Master's committee at the University of Nebraska-Lincoln before we moved to Michigan. Her great insights into science and tremendous support have guided me through the last six years, and I see her as an unofficial Ph.D supervisor for my graduate studies.

My thesis would have been impossible without help and support from all of the current and past members in Steve's lab. People in Steve's lab are just like a family,

where you always can find cooperation, assistance, encouragement, and fun. I would like to express my greatest appreciation to Dr. Javier Seravalli, Dr. Mathias Antoine, Dr. Hisashi Hemmi, Dr. Vekalet Tek, Dr. Kuljeet Singh, Dr. Mishtu Dey, Dr. Ryan Kunz, Dr. Gunes Bender, Dr. Joe Darty, Dr. Xianghui Li, Dr. Yuzhen Zhou, Dr. Ireena Bagai, Stelian Pop, Elizabeth Pierce, Nirupama Gupta, Andrea Morris, Ali Bogart, and Jeff Morgan. I would thank people in Ruma's lab as well, in which most people are six years' old friends. And here, I will also acknowledge my appreciation for other people's assistance for my projects over the last three years. I would like to thank Christopher Bianchetti and Dr. George Phillips (University of Wisconsin-Madison) for collaborating on the HO-2 crystallization project, Jessica Gardner and Dr. Thomas Brunold (University of Wisconsin-Madison) for collaborating on the HO-2 spectroscopic studies, and Dr. Paul Jenkins (Dr. Jeff Marten's lab, University of Michigan) and Dr. Lars Leichert (Dr. Ursula Jakob's lab, University of Michigan) for collaborating on the HO-2 *in vivo* thiol trapping experiments. I also thank everyone in the Department of Biological Chemistry. Thanks for your great help over the last three years!

I have been blessed with luck and encouragement from my parents and other family members, although they are on the other side of the planet. They always put my needs before theirs. I have no words to describe how important they are to me. I thank them for raising me and supporting every decision I made!

At last, I dedicate this thesis to my wife, Wenwen Shen, who is always ready to make any sacrifice to cherish and support my ambitions. She always stands behind me, building a shelter of love and encouragement. My life and career can not be successful without her support. This thesis is also dedicated to my newborn daughter, Ella (Anbing) Yi. Life has never been the same ever since her arrival-it has been much better. She is another great accomplishment during my Ph.D degree pursuit.

TABLE OF CONTENTS

LIST OF FIGURES

LIST OF TABLES

LIST OF ABBREVIATIONS

Biliverdin reductase: BVR
Charge transfer: CT
Circular dichroism : CD
Cys-Pro motif: CP motif
Dimethyl sulfoxide: DMSO
Diamide: DA
Dithiothreitol: DTT
Estimated standard uncertainty: ESU
Electronic absorption: Abs
Electron paramagnetic resonance: EPR
Glutathione S-transferase: GST
Glutathione disulfide : GSSG
Heme binding domain : HBD
Heme binding peptide : HBP
Heme oxygenase; HO
Heme regulatory motif: HRM
Large-conductance Ca^{2+} and voltage-activated K^{+} channel : BK channel
Isopropyl-beta-D-thiogalactopyranoside: IPTG
Isotope coded affinity tag: ICAT
Low temperature: LT
Luria-Bertani medium: LB medium
Magnetic circular dichroism: MCD
mPEG-Maleimide, MW 5000: MAL-PEG
N-acetyl-cysteine: NAC
Nicotinamide adenine dinucleotide phosphate: NADPH
Phosphate buffered saline: PBS
Potassium chloride: KCl
Potassium phosphate monobasic: KH_2PO_4
Protein Data Bank: PDB
resonance Raman: rR

Room temperature: RT
Root mean square deviation: r.m.s.d.
Sodium chloride: NaCl
Sodium phosphate dibasic: Na_2HPO_4
tert-butyl hydroperoxide: t-BuOO
Trichloroacetic acid: TCA
Tris(2-carboxyethyl)phosphine: TCEP
Zinc protoporphyrin: ZnPP
5,5′-Dithiobis(2-nitrobenzoic acid): DTNB

ABSTRACT

CHARACTERIZATION OF THE REDOX SWITCHES IN HUMAN HEME OXYGENASE-2 AND A HUMAN HEME-RESPONSIVE POTASSIUM CHANNEL

By

Li Yi

Chair: Stephen W. Ragsdale

Heme oxygenase (HO) catalyzes heme catabolism, generating CO, biliverdin, and Fe^{2+}. HO-2, the constitutively expressed isoform of HO, contains three Cys-Pro signatures (heme-regulatory-motifs, HRMs). In HO-2, we demonstrated that the C-terminal HRMs constitute a thiol/disulfide redox switch, regulating affinity of HO-2 for heme. HO-2 has lower affinity for Fe^{3+}-heme (K_d=350 nM) when the C-terminal HRMs are in the dithiol state, but 10-fold higher affinity for Fe^{3+}-heme (K_d=33 nM) when the C-terminal HRMs switch to the disulfide state. The three-dimensional structure of the core domain in HO-2 was determined in our research and found to be nearly identical to that of other HOs. Furthermore, our *in vivo* thiol trapping results demonstrated that the thiol/disulfide switch in human HO-2 is physiologically relevant, with its redox potential near the ambient intracellular redox potential (-200 mV). In human HEK293 cells, the

C-terminal HRMs were found to be 60-70% reduced under normal growth conditions, while oxidative stress conditions convert most (86-89%) of the C-terminal HRMs to the disulfide state. Treatment with reductants converts the C-terminal HRMs largely (81-87%) to the dithiol state.

Our research on the human large-conductance Ca^{2+} and voltage-activated K^{+} (BK) channel demonstrates a novel thiol/disulfide-mediated regulatory mechanism by which it can respond to cellular hypoxic/normoxic conditions. Our results demonstrate that heme, CO, and HO-2 bind to the 134-residue heme-binding domain (HBD) of human BK channel, which contains a characteristic CXXCH motif. The histidine residue in this motif serves as the axial heme ligand, with the CXXC forming a thiol/disulfide redox switch that regulates the HBD's affinity for Fe^{3+}-heme and CO. The dithiol state was demonstrated to bind Fe^{3+}-heme (K_d=210 nM) 14-fold more tightly than the disulfide state. Furthermore, the HBD-Fe^{2+}-heme complex demonstrated tight binding of CO (K_d=50 nM), with the CXXC motif regulating its affinity for CO. Fluorescence quenching experiments suggested that HBD is the key domain for BK channel's interaction with HO-2. These combined findings indicate that thiol/disulfide redox switches in the C-terminal HRMs of HO-2 and the CXXCH motif of the BK channel establish a novel mechanism that allows hemoproteins to respond to variations in redox environments of cell.

Chapter 1

General Introduction

1.1 Heme degradation catalyzed by heme oxygenase

Heme is a prosthetic group that consists of an iron atom that is contained in the center of a porphyrin ring. There are several major types of heme in cells, including heme A, heme B, heme C, and heme O. The heme in heme oxygenase (HO) is a b-type heme with the iron coordinated to the four nitrogen atoms of the porphyrin and has a chemical formula of $C_{34}H_{32}FeN_4O_4$. In the presence of NADPH - cytochrome P450 reductase (CPR), heme oxygenase (HO, EC 1:14:99:3) catalyzes the degradation of heme into iron, CO and biliverdin, which is quickly reduced to bilirubin by biliverdin reductase (**Figure 1.1**). (1,2). The degradation of one molecule of heme to biliverdin requires seven electrons to be transferred and three molecules of oxygen to be consumed (**Equation 1**). Subsequently, biliverdin reductase (BVR) catalyzes the two-electron reduction of biliverdin to bilirubin using NADPH as an electron donor (**Equation 2**). A distinct color change occurs in this process: from purple (heme) to green (biliverdin), then finally to yellow (bilirubin).

HO is present in organisms ranging from bacteria to eukaryotes, and is the only known enzyme that can degrade heme. In mammals, the electrons are provided by NADPH–cytochrome P450 reductase (3); however, alternative electron donors are employed by bacteria and plants (4,5). For example, Hmu O was identified as the heme degradation enzyme in *Corynebacterium diphtheriae*, with a hemoglobin-like protein (HMP) as the electron donor (6). In *Cyanidium caldarium*, cyanobacteria, and plants, reduced ferredoxin is used as the source of reducing equivalents that are needed for the reaction (7,8). In plants, biliverdin is further reduced to phytochromobilins instead of bilirubin because of the absence of biliverdin reductase (9).

In HO, heme acts as not only a cofactor but also as a substrate that catalyzes its own destruction (**Figure 1.2**). The HO-bound heme is first oxidized to α-*meso*-hydroxyheme through a peroxy intermediate. The deprotonated state of α-*meso*-hydroxyheme has free radical character, which can react with oxygen to produce α-verdoheme and eliminate the α carbon atom from the porphyrin ring as CO. The α-verdoheme is subsequently converted to biliverdin and free iron in a reaction that requires NADPH–cytochrome P450 reductase and O_2. Recent studies indicated that product release involves sequential reduction of the ferric to the ferrous biliverdin complex, release of the ferrous iron, and finally dissociation of the biliverdin from the protein (10).

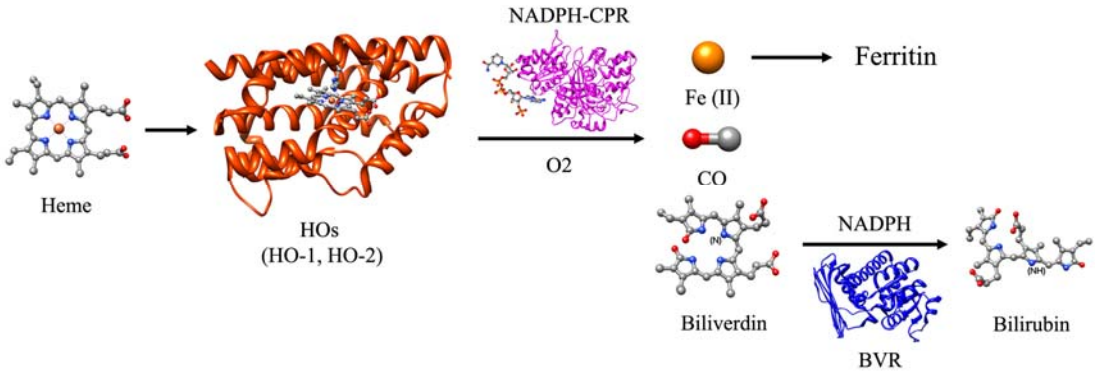

Heme + 7 e^- + 3 O_2 → Biliverdin + CO + Fe(II) + 3 H_2O (Eq.1)

Biliverdin + 2 e^- → Bilirubin (Eq.2)

FIGURE 1.1. **Heme degradation catalyzed by heme oxygenase.** Heme oxygenase (HO-1, HO-2) catalyzes the NADPH-cytochrome P450 reductase (CPR)-dependent degradation of heme into iron, CO and biliverdin, which is quickly reduced to bilirubin. Seven electrons are transferred and three molecules of O_2 are consumed when one molecule of heme is oxidized to generate one molecule of biliverdin, one molecule of CO, one molecule of Fe(II), and three molecules of H_2O. Two electrons are required for the reduction of one molecule of biliverdin.

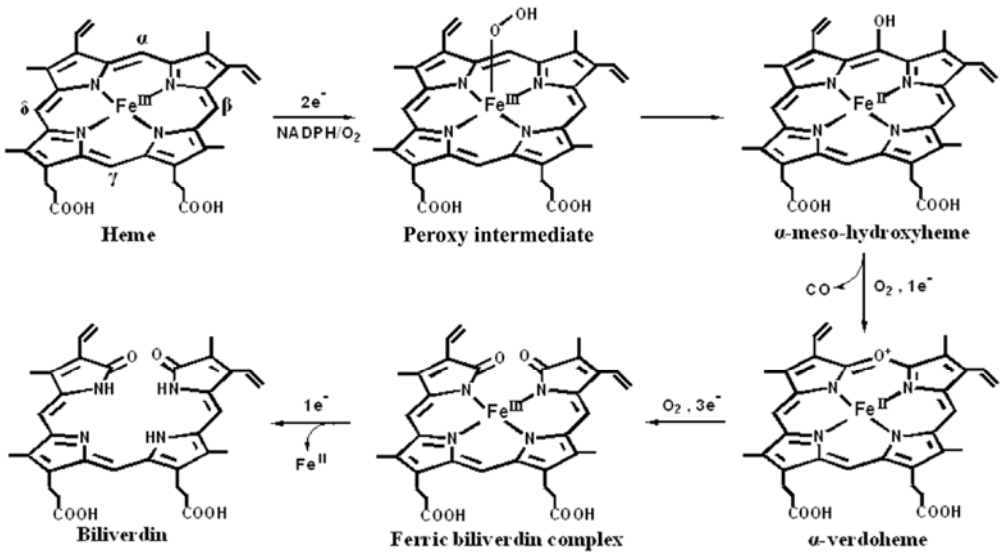

FIGURE 1.2. **Heme degradation pathway.** Heme is degraded to biliverdin through several key intermediates, including a peroxy intermediate, α-*meso*-hydroxyheme, α-verdoheme, and a ferric biliverdin complex.

1.2 Physiological functions of heme oxygenase

1.2.1 Heme and iron homeostasis

Iron is an essential element for all living organisms. It acts as a cofactor for many heme-containing proteins such as CPR and HO, forms iron-sulfur clusters in many non-heme-containing proteins such as ferredoxins and CODH, and provides oxygen transport and storage for hemoglobin and myoglobin, respectively. However, excess iron can be toxic (11), since it can produce large amounts of highly reactive hydroxyl radical (·OH) by the Fenton reaction in cells (12). An efficient way to maintain iron balance in cells is through regulation of its uptake. Dietary iron mainly exists as iron salts and heme iron. Uptake of inorganic iron is mainly mediated by the iron transporters located in the brush border membrane, including DMT1 (divalent metal transporter-1) (13) and Dcytb (duodenal cytochrome b) (14). In comparison to inorganic iron uptake, heme uptake is very different and its transport mechanism has not been fully elucidated. A very recent report indicated that the HRG (histidine-rich glycoprotein) family proteins are potential heme transporters in *Caenorhabditis elegans* (15). However, the heme transport pathway in mammals remains mysterious. After heme is transported into cells, the iron is released by heme degradation in a reaction that is catalyzed by HO. In addition to playing a role as

an iron reservoir, heme has other critical physiological functions in cells. Heme is a common prosthetic group that is structurally associated with many electron transfer and redox enzymes and regulates genes involved in oxygen utilization in lower eukaryotes and prokaryotes (16-18). Although heme plays crucial roles in various physiological processes, free heme can be toxic at concentrations greater than 1 μM (19), causing oxidative stress induced by reactive oxygen species (ROS), hemolytic effects, and abnormal inflammation (20). Because of the contradictory biological functions for heme and iron, their metabolism in mammals needs to be tightly and delicately regulated.

HO is the only known enzyme that can degrade heme in cells, playing a critical role in heme and iron homeostasis. Although the precise molecular mechanisms by which HO confers tissue protection are not clearly defined, it is believed that HO-dependent protection is mediated by the reaction products of heme degradation, including biliverdin, CO, and iron (**Figure 1.3**). Each product could contribute alone or in concert to the restoration of cellular homeostasis under inducing conditions. One potential mechanism of the HO-mediated cytoprotective effect is that HO may provide a possible antioxidative function by accelerating the removal of heme to limit oxidative stress sustained through heme-dependent mechanisms. It has recently been reported that free iron, at physiological levels, has crucial effects on cytoprotection (21,22). Furthermore, iron can also promote the ferritin-mediated cytoprotective process against mitochondrial dysfunction and oxidative stress (23). In contrast, evidence showed that iron released from the HO reaction may potentially act as a catalyst of deleterious pro-oxidant reactions, such as the metal-catalyzed Haber-Weiss cycle, or iron-dependent lipid peroxidation (24). In addition, HO-derived iron may also stimulate ferritin synthesis, sequestering reactive iron (25).

1.2.2 CO signaling in cells

Historically, CO has been regarded as a lethal gas and is toxic at high levels (>500 ppm). The first identified molecular target of CO was the heme iron center of hemoproteins, such as hemoglobin. High CO concentrations cause hypoxemia by competitive binding to the oxygen-binding sites of hemoglobin to form carboxyhemoglobin (CO-Hb), with an affinity that is > 200-fold higher than that of oxygen (26). In humans, prolonged or elevated CO exposure can cause a number of acute clinical effects, including nausea, dizziness, and loss of consciousness (26). Symptoms of

CO poisoning begin to appear at 20% CO-Hb, while death occurs between 50 and 80% CO-Hb (26). However, when CO is applied at low concentrations (typically within the 15 to 20% CO-Hb) range, it can influence a number of signaling pathways in cells to confer various cytoprotective effects, including anti-inflammation, anti-apoptosis, and anti-proliferation (**Figure 1.3**) (27,28).

The CO signaling pathway is still not clearly elucidated. At a physiological level, CO can trigger the production of cyclic-guanosine-monophosphate (cGMP) to stimulate neuronal signaling processes and regulate vascular functions, including vessel tone, smooth muscle proliferation and platelet aggregation (29,30). Furthermore, recent studies indicate that the activation of MAPK pathways, particularly the p38 MAPK signaling pathway, can be modulated by CO treatment (31). MAPK pathways have been demonstrated to be critical for cellular response to inflammatory, apoptotic and proliferative stress (31-34). The activation of p38 MAPK by CO has been reported to be dependent or independent of soluble guanylate cyclase (sGC), depending on the cell type. In addition, modulation of cellular ROS production, inhibition of cellular O_2 production, membrane NADPH-oxidase, and Toll-like receptor (TLR) trafficking and activation have also been implicated in CO dependent signaling (35-37). Thus, CO can confer tissue protection in various models of acute lung injury, vascular injury, pulmonary hypertension, liver injury, organ I/R injury, organ transplantation, and numerous other conditions (30,38). Observations of CO-mediated tissue protection have also been described in transplantation of heart, lung, kidney, liver, and intestinal allografts or xenografts, whereby application of CO to the recipient or to the graft reduced inflammation and apoptosis associated with I/R injury, thus reducing the probability of graft, rejection (39,40). In fact, CO-based inhalation therapies have been applied in the clinic. A recently reported clinical trial demonstrates that reduction of sputum eosinophils and improvement of methacholine responsiveness through inhalation of CO was observed in patients with stable chronic obstructive pulmonary disease (COPD) (41).

In cells, HO-catalyzed heme degradation is the major source of CO, especially in neurons and in the carotid body (42). HO-derived CO is usually produced locally within tissues, serving as an endogenous physiological mediator. In the early 1990s, HO-derived CO was discovered as a neurotransmitter in olfactory neurotransmission (43). Since then,

increasing evidence has been presented that HO-derived CO, instead of being a waste product of heme oxidation, actually plays critical roles in various physiological phenomena, including circadian modulation of heme biosynthesis, regulation of T cell function, modulation of caveolin-1 status in growth control (44), activation of guanylate cyclase (45), and mediation of O_2 sensing and the hypoxic response (46). It is now believed that CO acts as a signaling molecule like another diatomic molecule, nitric oxide (NO), possessing anti-apoptotic, anti-inflammatory, and anti-proliferative properties (33,44,47,48).

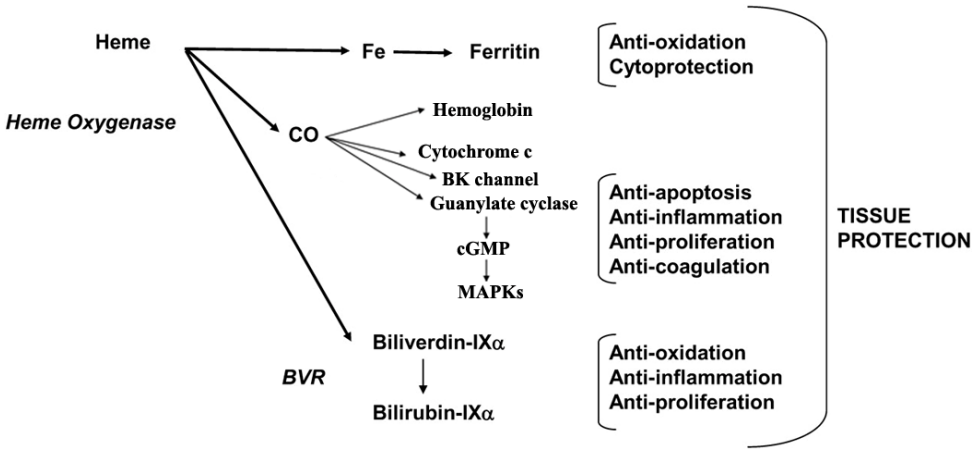

FIGURE 1.3. **Tissue protection conferred by HO end-products (modified from (38))**. All three end-products of heme degradation, including Fe, CO, and bilverdin/bilirubin, can contribute to the cytoprotective process. Iron released by HO activity stimulates a cytoprotective pathway involving the synthesis of ferritin. CO has been implicated in anti-inflammatory, anti-apoptotic, and anti-proliferative pathways. Biliverdin and bilirubin, potent lipid antioxidants, can exert anti-inflammatory and anti-proliferative effects.

1.2.3 Biliverdin and bilirubin homeostasis

Bilirubin, the final product of heme metabolism, is rapidly derived from biliverdin by biliverdin reductase (BVR) in mammals. Bilirubin can revert to biliverdin via oxidation, although the mechanism is unclear. The function of the BVR pathway in cells is not clearly understood because bilirubin is toxic and insoluble, while biliverdin is more water soluble. Bilirubin must be glucuronidated before its excretion in bile, which is

primarily catalyzed by UDP-glucuronyl transferase (UDPGT) in liver (49). Compared to bilirubin, biliverdin is more easily excreted. Bilirubin was first reported to mainly exist in the plasma and can cause brain damage (50). However, it has been recently reported that biliverdin and bilirubin can act as chain-breaking antioxidants *in vitro*, which may provide cytoprotection (**Figure 1.3**) (51).

The cytotoxicity associated with deletion of HO appears to reflect a loss of bilirubin. Mice with targeted deletion of either HO-1 or HO-2 have reduced bilirubin levels and are more susceptible to neurotoxic damage, seizures, stroke damage, and traumatic brain injury (52,53). The antioxidant actions of bilirubin are dramatically amplified by BVR in a biliverdin–bilirubin cycle. Depletion of BVR by RNA interference markedly diminishes the cytoprotective effects of exogenous bilirubin and leads to increased cellular levels of oxygen free radicals and cell death (54,55). A recent study suggested that water-soluble glutathione (GSH) primarily protects water soluble proteins, whereas lipophilic bilirubin protects against lipid peroxidation of cell membranes (55). Mice with deletion of HO-2, which generates biliverdin, display more oxidation of lipid than that of protein, while the reverse holds for GSH depletion. Pharmacologic application of biliverdin and bilirubin can protect cultured cells against injury by oxidative or nitrosative stress (56). One possible mechanism is that bilirubin can surpass α-tocopherol as the most potent protector against lipid peroxidation and acts as an antioxidant that is involved in resistance to oxidative stress (51,57,58).

1.3 Differences between HO-1 and HO-2

There are two forms of HO (HO-1 and HO-2), which share similar physical and kinetic properties, but are differentially regulated and exhibit dissimilar physiological roles and tissue distributions (59,60). Another isoform, HO-3, was recently reported in rat (61); however, no activity was detected for this isoform and it is considered to be a pseudogene. Phylogenetic analysis of heme oxygenase indicates that HO-1 and HO-2 have a very high degree of evolutionary conservation among mammals (62). Bacterial heme oxygenases have a closer evolutionary relationship with those in plants. However, the bacterial, plant and mammalian HOs have high structural similarity in their catalytic domains. A bacterial HO-2 crystal structure has been reported recently, which shows a

high similarity at the core domain region with human HO-1 and HO-2 structures (63). Plants contain several HOs, including one named HO-2, but these lack the C-terminal membrane spanning region seen in mammalian HOs (64) and are more closely related to the bacterial and insect HO-1 than to the mammalian HOs (62). In higher plants, ferredoxin is utilized instead of NADPH-cytochrome P450 reductase as the reducing partner in the HO reaction (7). Many plants do not produce bilirubin since they lack biliverdin reductase (9).

HO-1, considered to be the inducible HO, is also known as heat-shock protein 32 and is found in most tissues, with particularly high levels in spleen and liver (65,66). Expression of HO-1 is regulated by heat shock and various oxidative stress conditions such as ischemia, hypoxia, hyperoxia, and alterations in glutathione levels (60,67). On the other hand, HO-2 appears to be constitutively expressed, but exhibits a narrow tissue distribution, with high levels in the brain and in testes (61,68,69). HO-2 has been implicated in oxygen sensing by the carotid body (46,70), mediating oxidative stress in neurons (71), and regulating cerebral blood flow and vascular tone in certain tissues (72).

Human HO-1 and HO-2 exhibit similar catalytic activities and share a high level of homology (55% identity, 76% similarity), including related stretches of 20 hydrophobic residues at their C-termini that anchor them to the microsomal membrane (**Figure 1.4**) (60). However, in addition to the 30 residues at the N-terminus, HO-1 and HO-2 diverge significantly around residue 127 and between residues 240-295 (HO-2 numbering throughout unless otherwise stated). While HO-1 typically lacks Cys residues, there are three "CP" sequences in regions that have been proposed to contain heme regulatory (or responsive) motifs (HRMs) centered at Cys127, Cys265, and Cys282. It is interesting to note that the C-terminal HRMs in HO-2 appear to be a fairly recent evolutionary development, estimated to have occurred about 250 million years ago, since HRM1 and HRM2 co-occur only in amniotes (**Figure 1.5**) (62). HRM1 is found in all HO-2s, which emerged with the jawed vertebrates; however, HRM2 is lacking in ray fish and amphibians, suggesting that the HRM1 and HRM2 may be involved in oxygen sensing in all amniotes.

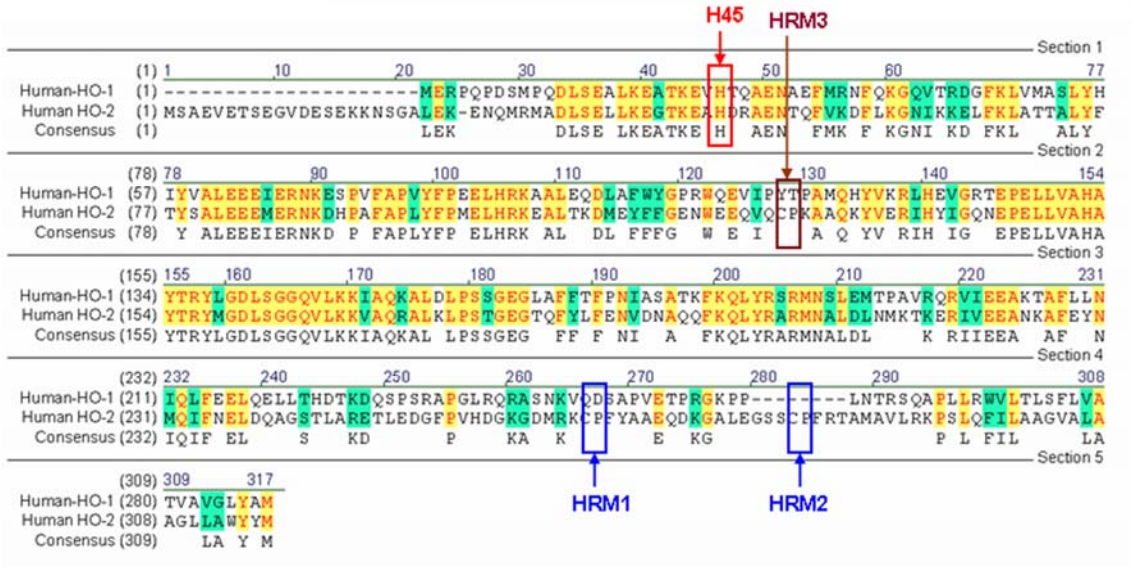

FIGURE 1.4: **Sequence alignment of human HO-1 and HO-2.** Human HO-1 contains 288 resides and human HO-2 contains 316 residues. His45, the residue that coordinates the heme, is highlighted in red. The three heme regulatory motifs (HRM) that are found in HO-2 but not in HO-1 are marked in the sequence alignment. The HRMs in HO-2 are located at amino acids 265-266, 282-283, and 127-128, termed as HRM1, HRM2, and HRM3, respectively.

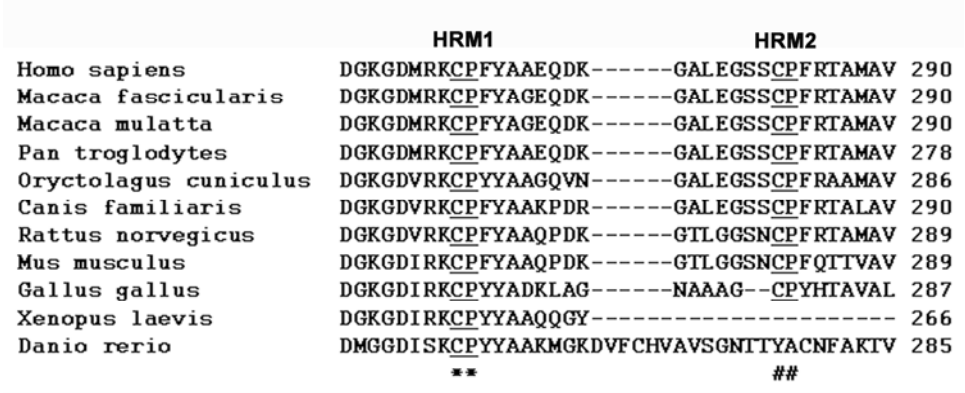

FIGURE 1.5: **Sequence alignment of HO-2 in different organisms.** HRM1 and HRM2 in HO-2s co-occur only in amniotes. HRM1 is found in all HO-2s, however, HRM2 is lacking in ray fish and amphibians. HRM contains a characteristic Cys-Pro dipeptide, followed by 2-3 hydrophobic residues.

1.4 Functions of heme regulatory motifs in heme containing proteins

Heme regulatory motifs (HRM), short amino acid sequences containing the characteristic Cys-Pro dipeptide, exist in diverse heme proteins. Numerous heme-

mediated functions of proteins require HRMs. It has been indicated that HRMs play critical roles in regulating protein activity, stability, and functions.

Three HRMs exist in the iron responsive regulator (Irr). Among other results, substitution of Cys29 by Ala in one of the HRMs in Irr significantly decreases heme dependent degradation, leading to proposal that the HRM controls Irr activity and stability (73-75). The yeast transcriptional activator Hap1 contains seven HRMs (HRMs 1–7) with HRM7 proposed to bind heme and mediate the heme activation of Hsp1 under heme-sufficient conditions and HRMs 1–6 perhaps cooperatively involved in heme binding and scavenging under heme-depleted conditions (76,77).

The first and rate-limiting enzyme in the mammalian heme biosynthetic pathway, 5-aminolevulinate synthase, has two tissue-specific isozymes: the housekeeping enzyme ALAS1 and the erythroid tissue-specific enzyme ALAS2 (78). Three HRMs are located in the C-terminal end in both ALAS1 and ALAS2, but perform different functions. The HRMs in ALAS1 are required for regulation of its mitochondrial import, while heme showed no effect on the mitochondrial import of ALAS2 under the same conditions (79). Recently, it was reported that heme inhibited the DNA-binding activity of Bach1–MafK heterodimers by directly interacting with Bach1 through HRMs (80,81). In Reverb-β, a HRM is involved in a ligand switch in which the Cys residue in the HRM can ligate to the heme iron, enhancing its affinity for heme (unpublished data, Gupta, Ragsdale 2010). As described in this thesis, in the case of HO-2, cysteines in the C-terminal HRMs can form an intramolecular disulfide bond, affecting the affinity of HO-2 for heme under different redox conditions.

1.5 Heme binding to HO-2 is regulated by a thiol/disulfide redox switch in the HRMs

The function of HO-1 is regulated mainly through stimulation or repression of its gene expression, which can be triggered by various factors. However, the regulatory mechanism of HO-2 remains largely unknown. HO-1 and HO-2 differ in their tissue distributions and their expression patterns. At the protein level, HO-1 and HO-2 exhibit 76% similarity, including related C-terminal membrane anchoring regions (60). The major difference between HO-1 and HO-2 is the presence of Cys residues within three

HRM motifs in HO-2 (**Figure 1.4**), which were recognized to be involved in regulation (82).

The functions of the HRMs in HO-2 have been investigated in my previous research (82). Interestingly, instead of serving as a heme ligand or influencing protein stability like in other HRM-containing proteins, we found that an intramolecular disulfide bond was formed between the two cysteines (Cys265 and Cys282) contained in the two C-terminal HRMs (HRM1 and HRM2), constituting a redox switch (**Figure 1.6**). This redox switch affects the heme affinity of HO-2. The K_d value for the protein-heme complex was found to be 348 nM when the cysteines of the HRMs are in the reduced (free thiol) state. However, this value drops significantly to 33 nM, similar to the intracellular free heme level, when the HRMs switch to the oxidized (disulfide) state, indicating a much stronger affinity of oxidized HO-2 for its substrate. This thiol/disulfide redox switch is likely to be physiologically important because it shifts the K_d for ferric heme into the concentration range of the cellular heme pool (~0.03 μM) (80). Thus, elevation of the K_d into the 0.35 μM range would be expected to impact heme homeostasis by decreasing intracellular HO-2 activity. It was proposed that that redox switch could have important physiological roles, including the ability of organisms to regulate intracellular heme and oxygen concentrations.

Sequence alignment of selected HO-2s indicated that HRM1 and HRM2 in HO-2s co-occur only in amniotes (**Figure 1.5**). Perhaps the redox switch involving HRM1 and HRM2 provided a selective advantage for amniotes that improved their ability to respond to high atmospheric oxygen levels as they moved from water onto dry land.

1.6 Involvement of heme and thiol/disulfide redox chemistry in oxygen-sensing by the human BK channel

Ion channels are pore-forming proteins that regulate the flow of ions across the membrane in all cells. For most ion channels, the pore-forming subunits are called α subunits while the regulatory subunits are denoted β, γ, and so on. Some channels permit the passage of ions based solely on their positive (cation) or negative (anion) charge. However, in some ion channels, passage through the pore is governed by a "gate," which may be opened or closed by chemical or electrical signals, temperature, or mechanical

force, depending on the channel. Two major types of ion channel exist in cells: voltage-gated ion channels and ligand-gated ion channels, whose opening or closing depend on the voltage gradient across the plasma membrane or the binding of ligands to the channel, respectively. Large-conductance Ca^{2+} and voltage-activated K^+ channels, also known as Slo or BK channels, are both voltage- and ligand-gated potassium channels, since they can be activated (opened) by changes in membrane electrical potential as well as by increases in concentrations of intracellular Ca^{2+} and CO (83,84).

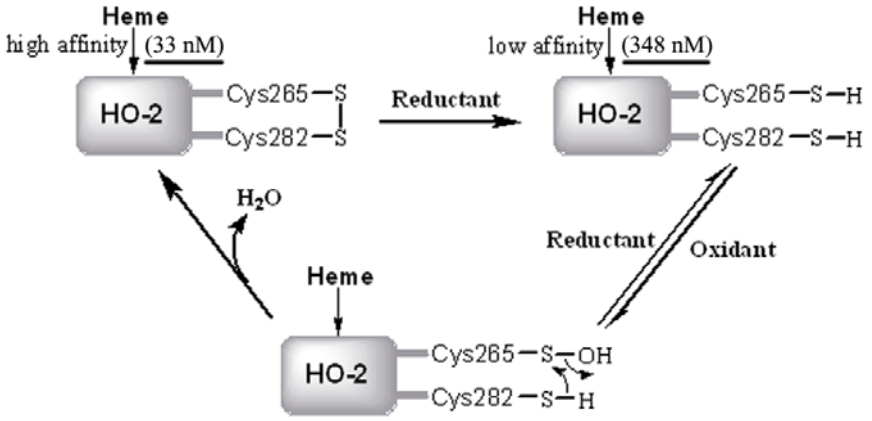

FIGURE 1.6: **Proposed mechanism for the formation of the intra-molecular disulfide bond between HRM1 and HRM2 in HO-2 (modified from (62)).** Cys265 and Cys282 in HRM1 and HRM2, respectively, can form an intramolecular disulfide bond. Under oxidizing conditions, Cys265 is oxidized to a sulfenic acid, which undergoes nucleophilic attack by Cys282 to eliminate water and form a disulfide bond. HO-2 has higher affinity for heme (K_d = 33 nM) when Cys265 and Cys282 form a disulfide bond than when both Cys residues exist in the free thiol state (K_d = 348 nM).

BK channels are expressed in a wide variety of cells including most neurons, muscle, epithelia, and endocrine cells. Like other voltage-gated K^+ channels, a BK channel complex exists as a tetramer, composed of four pore-forming α subunits that contain both transmembrane and cytoplasmic regions (**Figure 1.7**) (85). Each α subunit contains 7 transmembrane spanning domains (S0-S6) at the N-terminus, with the voltage sensor located in S4 and the pore-forming loop located between S5 and S6 (86). A major

difference between BK channels and other Ca^{2+}- activated K^+ channels, such as SKCa and IKCa channels, is that an extra seven-helix transmembrane segment (S0) exists in BK channels that leads to the extracellular N-terminus, with its function unknown (87). The N-terminus of the BK channel α subunit is also involved in its interaction with BK channel β-subunits, which are regulatory subunits. Both the COOH- and NH_2-termini of β-subunits are located in the cytoplasm, forming two putative transmembrane (TM) domains, TM1 and TM2 (88,89). The extracellular loop of the β-subunit can induce an appropriate conformation within the α-subunit, facilitating the binding of α subunits with β-subunits. β-subunits have been reported to activate the BK channel by increasing the affinity of the channel for Ca^{2+} (90). However, the β-subunit is unequally distributed in different tissues, so its function still remains unclear (91).

Four hydrophobic segments (S7–S10) exist at the large intracellular carboxyl (C) terminus of the BK channel, forming two homologous domains termed "regulators of conductance of potassium" (RCK1 and RCK2) by S7-S8 and S9-S10, respectively (92,93). Both RCK1 and RCK2 can form a gating ring that is essential for Ca^{2+} activation of the channel, with RCK1 also serving as a H^+ sensor (93,94). Between RCK1 and RCK2, a linker segment connects these two domains, which has been identified to be involved in the heme and CO mediated regulatory mechanisms of the BK channel (83,95). RCK domains also exist in other potassium channels, such as MthK (*Methanobacterium thermautotrophicum*), KtrAB (*Vibrio alginolyticus*), and EcoliTrkA2 (*Escherichia coli*) K^+ transporters (96-98).

The human BK channel plays pivotal and specific roles in many physiological phenomena, including oxygen sensing, vasodilation, synaptic transmission, and hormone secretion (99,100). In BK channel knockout mice, progressively developing outer hair cell (OHC) dysfunction and degeneration were observed, indicating a crucial role for the BK channel in maintaining outer hair cells that receive different feedback from the brain (101). Furthermore, the BK channel was also suggested to be involved in the spontaneous firing of the cerebellar Purkinje neurons (102).

Similar to other types of K^+ channels, BK channels are also modulated by various post-translational modifications such as oxidation and reduction (103), phosphorylation (104), and glycosylation (88,104,105). In addition, the BK channel has recently been

identified as a heme protein (83,95,106,107). Heme binding under hypoxic conditions strongly inhibits the channel, while under normoxic conditions, CO, which is generated by HO during heme degradation, activates the BK channel. HO-2, an enzyme responsible for heme degradation to generate CO, can form a complex with the BK channel, acting as a CO donor (106). Previous studies and our studies have indicated that some key residues, such as His and Cys residues, play critical roles in the heme and CO mediated regulatory mechanisms. A CXXCH motif, which is located in the linker segment between RCK1 and RCK2, is involved in the heme/CO regulation, with His as the heme ligand and Cys residues in CXXCH motif forming a redox switch affecting the affinities of BK channel for heme and CO. Furthermore, mutagenesis studies of an Asp and two His residues (H365, H394 and D367) within the RCK1 domain demonstrated that these residues are required for the stimulatory action of CO on the BK channel (108). Cysteine oxidation (109,110), including C430 and C911, leads to the decreased K^+ transfer of the BK channel, with Cys911 also playing a role in the sensitivity of the BK channel for CO (111). Recently, hydrogen sulfide (H_2S) was reported to inhibit the channel through a mechanism that is non-competitive with CO, but that is still poorly characterized (112).

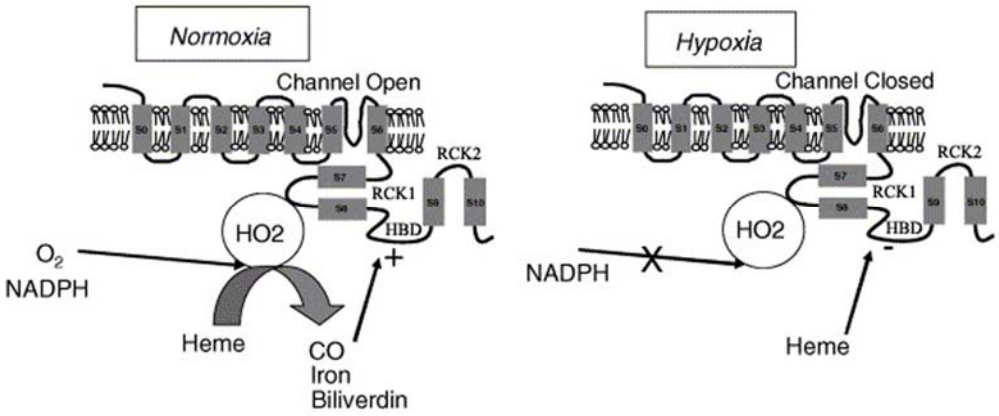

FIGURE 1.7: **Schematic representation of the structure of the α-subunit of the BK channel, and proposed HO-2 mediated mechanism of inhibition/activation of the BK channel under hypoxic/normoxic conditions (modified from (113))** A BK channel complex is composed of transmembrane (S0-S6) and cytoplasmic regions (S7-S10, and a HBD (heme binding domain). Two RCK domains were identified in the cytoplasmic region. Under hypoxic conditions, O_2 availability is limited and heme binds to the BK channel to evoke channel closure instead of being metabolized. However, during normoxia, cellular heme is catabolized by HO-2 and CO is generated. Then CO binds the BK channel, promoting channel opening at normal systemic O_2 levels.

1.7 References

1. Maines, M. D. (2004) *Antioxid Redox Signal* 6, 797-801
2. Maines, M. D. (2005) *Physiology (Bethesda)* 20, 382-389
3. Schacter, B. A., Nelson, E. B., Marver, H. S., and Masters, B. S. (1972) *J Biol Chem* 247, 3601-3607
4. Beale, S. I. (1993) *Chemical Reviews* 93, 785-802
5. Wilks, A., and Schmitt, M. P. (1998) *J Biol Chem* 273, 837-841
6. Sano, S., Sano, T., Morishima, I., Shiro, Y., and Maeda, Y. (1986) *Proc Natl Acad Sci U S A* 83, 531-535
7. Muramoto, T., Tsurui, N., Terry, M. J., Yokota, A., and Kohchi, T. (2002) *Plant Physiol* 130, 1958-1966
8. Cornejo, J., and Beale, S. I. (1988) *J Biol Chem* 263, 11915-11921
9. Kohchi, T., Mukougawa, K., Frankenberg, N., Masuda, M., Yokota, A., and Lagarias, J. C. (2001) *Plant Cell* 13, 425-436
10. Montellano, P. R. (2000) *Curr Opin Chem Biol* 4, 221-227
11. Baker, H. M., Anderson, B. F., and Baker, E. N. (2003) *Proc Natl Acad Sci U S A* 100, 3579-3583
12. Papanikolaou, G., and Pantopoulos, K. (2005) *Toxicol Appl Pharmacol* 202, 199-211
13. Garrick, M. D., Dolan, K. G., Horbinski, C., Ghio, A. J., Higgins, D., Porubcin, M., Moore, E. G., Hainsworth, L. N., Umbreit, J. N., Conrad, M. E., Feng, L., Lis, A., Roth, J. A., Singleton, S., and Garrick, L. M. (2003) *Biometals* 16, 41-54
14. Sargent, P. J., Farnaud, S., and Evans, R. W. (2005) *Curr Med Chem* 12, 2683-2693
15. Rajagopal, A., Rao, A. U., Amigo, J., Tian, M., Upadhyay, S. K., Hall, C., Uhm, S., Mathew, M. K., Fleming, M. D., Paw, B. H., Krause, M., and Hamza, I. (2008) *Nature* 453, 1127-1131
16. Qi, Z., Hamza, I., and O'Brian, M. R. . (1999) *Proc. Natl. Acad. Sci. USA* 96, 13056-13061
17. Ogawa, K., Sun, J., Taketani, S., Nakajima, O., Nishitani, C., Sassa, S., Hayashi, N., Yamamoto, M., Shibahara, S., Fujita, H., and Igarashi, K. (2001) *Embo J.* 20, 2835-2843
18. Dioum, E. M., Rutter, J., Tuckerman, J. R., Gonzalez, G., Gilles-Gonzalez, M. A., and McKnight, S. L. . (2002) *Science* 298, 2385-2387
19. Sassa, S. (2006) *J. Clin. Biochem. Nutr.* 38, 138-155
20. Kumar, S., and Bandyopadhyay, U. (2005) *Toxicol Lett* 157, 175-188

21. Grosser, N., Oberle, S., Berndt, G., Erdmann, K., Hemmerle, A. and Schroder, H. . (2004) *Biochem. Biophys. Res. Commun* 314, 351-355
22. Ragsdale, S. W. (2006) *Chem. Rev.* 106, 3317 - 3337
23. MacKenzie, E. L., Ray, P. D., and Tsuji, Y. (2008) *Free Radic Biol Med* 44, 1762-1771
24. Ryter, S. W., and Tyrrell, R. M. (2000) *Free Radical Biology and Medicine* 28, 289-309
25. Beale, S. I., and Yeh, J. I. (1999) *Nat Struct Biol* 6, 903-905
26. Von Burg, R. (1999) *J Appl Toxicol* 19, 379-386
27. Dolinay, T., Szilasi, M., Liu, M., and Choi, A. M. (2004) *Am J Respir Crit Care Med* 170, 613-620
28. Hoetzel, A., Dolinay, T., Vallbracht, S., Zhang, Y., Kim, H. P., Ifedigbo, E., Alber, S., Kaynar, A. M., Schmidt, R., Ryter, S. W., and Choi, A. M. (2008) *Am J Respir Crit Care Med* 177, 1223-1232
29. Morita, T., Perrella, M. A., Lee, M. E., and Kourembanas, S. (1995) *Proc Natl Acad Sci U S A* 92, 1475-1479
30. Ryter, S., Alam, J., and Choi, AM.,. (2006) *Physiol Rev.* 86, 583-650
31. Otterbein, L. E., Bach, F. H., Alam, J., Soares, M., Tao Lu, H., Wysk, M., Davis, R. J., Flavell, R. A., and Choi, A. M. (2000) *Nat Med* 6, 422-428
32. Otterbein, L. E., Zuckerbraun, B. S., Haga, M., Liu, F., Song, R., Usheva, A., Stachulak, C., Bodyak, N., Smith, R. N., Csizmadia, E., Tyagi, S., Akamatsu, Y., Flavell, R. J., Billiar, T. R., Tzeng, E., Bach, F. H., Choi, A. M., and Soares, M. P. (2003) *Nat Med* 9, 183-190
33. Otterbein, L. E., Otterbein, S. L., Ifedigbo, E., Liu, F., Morse, D. E., Fearns, C., Ulevitch, R. J., Knickelbein, R., Flavell, R. A., and Choi, A. M. (2003) *American Journal of Pathology* 163, 2555-2563
34. Brouard, S., Otterbein, L. E., Anrather, J., Tobiasch, E., Bach, F. H., Choi, A. M. K., and Soares, M. P. (2000) *Journal of Experimental Medicine* 192, 1015-1025
35. Wang, X. M., Kim, H. P., Nakahira, K., Ryter, S. W., and Choi, A. M. K. (2009) *Journal of Immunology* 182, 3809-3818
36. Nakahira, K., Kim, H. P., Geng, X. H., Nakao, A., Wang, X., Murase, N., Drain, P. F., Wang, X., Sasidhar, M., Nabel, E. G., Takahashi, T., Lukacs, N. W., Ryter, S. W., Morita, K., and Choi, A. M. K. (2006) *Journal of Experimental Medicine* 203, 2377-2389
37. Kim, H. P., Wang, X., Nakao, A., Kim, S. I., Murase, N., Choi, M. E., Ryter, S. W., and Choi, A. M. K. (2005) *Proceedings of the National Academy of Sciences of the United States of America* 102, 11319-11324

38. Ryter, S. W., and Choi, A. M. (2009) *Am J Respir Cell Mol Biol* 41, 251-260
39. Song, R. P., Kubo, M., Morse, D., Zhou, Z. H., Zhang, X. C., Dauber, J. H., Fabisiak, J., Alber, S. M., Watkins, S. C., Zuckerbraun, B. S., Otterbein, L. E., Ning, W., Oury, T. D., Lee, P. J., McCurry, K. R., and Choi, A. M. K. (2003) *American Journal of Pathology* 163, 231-242
40. Kohmoto, J., Nakao, A., Kaizu, T., Tsung, A., Ikeda, A., Tomiyama, K., Billiar, T. R., Choi, A. M., Murase, N., and McCurry, K. R. (2006) *Surgery* 140, 179-185
41. Bathoorn, E., Slebos, D. J., Postma, D. S., Koeter, G. H., van Oosterhout, A. J., van der Toorn, M., Boezen, H. M., and Kerstjens, H. A. (2007) *Eur Respir J* 30, 1131-1137
42. Boehning, D., and Snyder, S. H. (2002) *Science* 298, 2339-2340
43. Verma, A., Hirsch, D. J., Glatt, C. E., Ronnett, G. V., and Snyder, S. H. (1993) *Science* 259, 381-384
44. Kim, H. P., Ryter, S. W., and Choi, A. M. (2006) *Annu Rev Pharmacol Toxicol* 46, 411-449
45. Baranano, D. E., and Snyder, S. H. (2001) *Proc Natl Acad Sci U S A* 98, 10996-11002
46. Williams, S. E., Wootton, P., Mason, H. S., Bould, J., Iles, D. E., Riccardi, D., Peers, C., and Kemp, P. J. (2004) *Science* 306, 2093-2097
47. Moore, B. A., Overhaus, M., Whitcomb, J., Ifedigbo, E., Choi, A. M., Otterbein, L. E. and Bauer, A. J (2005) *Crit. Care Med.* 33, 1317-1326
48. Ryter S.W., M. D., and Augustine M. K. . (2004) *Sci STKE.* 230, RE6
49. Childs, B., Sidbury, J. B., and Migeon, C. J. (1959) *Pediatrics* 23, 903-913
50. Calabrese, V., Butterfield, D. A., Scapagnini, G., Stella, A. M., and Maines, M. D. (2006) *Antioxid Redox Signal* 8, 444-477
51. Stocker, R., Yamamoto, Y., McDonagh, A. F., Glazer, A. N., and Ames, B. N. (1987) *Science* 235, 1043-1046
52. Chang, E. F., Wong, R. J., Vreman, H. J., Igarashi, T., Galo, E., Sharp, F. R., Stevenson, D. K., and Noble-Haeusslein, L. J. (2003) *J Neurosci* 23, 3689-3696
53. Yachie, A., Niida, Y., Wada, T., Igarashi, N., Kaneda, H., Toma, T., Ohta, K., Kasahara, Y. and Koizumi, S. (1999) *J. Clin. Invest.* 103, 129-135
54. Sedlak, T. W., and Snyder, S. H. (2004) *Pediatrics* 113, 1776-1782
55. Sedlak, T. W., Saleh, M., Higginson, D. S., Paul, B. D., Juluri, K. R., and Snyder, S. H. (2009) *Proc Natl Acad Sci U S A* 106, 5171-5176
56. Foresti, R., Green, C. J., and Motterlini, R. (2004) *Biochem Soc Symp*, 177-192
57. Baranano, D. E., Rao, M., Ferris, C. D. and Snyder, S. H. (2002) *Proc. Natl. Acad. Sci. USA* 99, 16093-16098

58. Fondevila, C., Shen, X. D., Tsuchiyashi, S., Yamashita, K., Csizmadia, E., Lassman, C., Busuttil, R. W., Kupiec-Weglinski, J. W. and Bach, F. H. . (2004) *Hepatology* 40
59. Maines, M. D. (2005) *Antioxid Redox Signal* 7, 1761-1766
60. Maines, M. D. (1997) *Annu Rev Pharmacol Toxicol* 37, 517-554
61. McCoubrey WK Jr, H. T., and Maines MD. (1997) *Eur J Biochem.* 247, 725-732
62. Yi, L. (2007) *Master thesis, University of Nebraska-Lincoln*
63. Sugishima, M., Hagiwara, Y., Zhang, X., Yoshida, T., Migita, C. T., and Fukuyama, K. (2005) *Biochemistry* 44, 4257-4266
64. Davis SJ, B. S., Durski AM, Walker JM, and Vierstra RD. (2001) *Plant Physiol.* 126, 656-669
65. Pimstone, N. R., Engel, P., Tenhunen, R., Seitz, P. T., Marver, H. S., and Schmid, R. (1971) *J Clin Invest* 50, 2042-2050
66. Adlercreutz, H., and Tenhunen, R. (1970) *Am J Med* 49, 630-648
67. Maines, M. D. (1992) *Heme Oxygenase: In Clinical Applications and Functions, Boca Raton,* ,
68. Maines, M. D., Eke, B. C., and Zhao, X. (1996) *Brain Res* 722, 83-94
69. Trakshel, G. M., Kutty, R. K., and Maines, M. D. (1986) *J Biol Chem* 261, 11131-11137
70. Hoshi, T., and Lahiri, S. (2004) *Science* 306, 2050-2051
71. Regan, R. F., Chen, J., and Benvenisti-Zarom, L. (2004) *BMC Neurosci* 5, 34
72. Galbraith, R. (1999) *Proc Soc Exp Biol Med* 222, 299-305
73. Yang, J., Ishimori, K., and O'Brian, M. R. (2005) *J. Biol. Chem.* 280, 7671-7676
74. Qi, Z., Hamza, I., and O'Brian, M. R. (1999) *Proc. Natl. Acad. Sci. USA* 96, 13056-13061
75. Yang, J., Panek, H. R., and O'Brian, M. R. (2006) *Mol. Microbiol.* 60, 209-218
76. Hon, T., Hach, A., Lee, H. C., Cheng, T., and Zhang, L. (2000) *Biochem. Biophys. Res. Commun.* 273, 584-591
77. Lee, H. C., Hon, T., Lan, C., and Zhang, L. (2003) *Molecular and cellular biology* 23, 5857-5866
78. Sadlon, T. J., Dell'Oso, T., Surinya, K. H., and May, B. K. (1999) *Int J Biochem Cell Biol* 31, 1153-1167
79. Munakata, H., Sun, J. Y., Yoshida, K., Nakatani, T., Honda, E., Hayakawa, S., Furuyama, K., and Hayashi, N. (2004) *J Biochem (Tokyo)* 136, 233-238
80. Ogawa, K., Sun, J., Taketani, S., Nakajima, O., Nishitani, C., Sassa, S., Hayashi, N., Yamamoto, M., Shibahara, S., Fujita, H., and Igarashi, K. (2001) *Embo J.* 20, 2835-2843

81. Chefalo, P. J., Oh, J., Rafie-Kolpin, M., Kan, B., and Chen, J. J. (1998) *Eur. J. Biochem.* 258, 820-830
82. Yi, L., and Ragsdale, S. W. (2007) *J Biol Chem* 282, 21056-21067
83. Tang, X. D., Xu, R., Reynolds, M. F., Garcia, M. L., Heinemann, S. H., and Hoshi, T. (2003) *Nature* 425, 531-535
84. Marrion, N. V., and Tavalin, S. J. (1998) *Nature* 395, 900-905
85. Lu, R., Alioua, A., Kumar, Y., Eghbali, M., Stefani, E., and Toro, L. (2006) *J Physiol* 570, 65-72
86. Ghatta, S., Nimmagadda, D., Xu, X., and O'Rourke, S. T. (2006) *Pharmacol Ther* 110, 103-116
87. Adelman, J. P., Shen, K. Z., Kavanaugh, M. P., Warren, R. A., Wu, Y. N., Lagrutta, A., Bond, C. T., and North, R. A. (1992) *Neuron* 9, 209-216
88. Knaus, H. G., McManus, O. B., Lee, S. H., Schmalhofer, W. A., Garcia-Calvo, M., Helms, L. M., Sanchez, M., Giangiacomo, K., Reuben, J. P., Smith, A. B., 3rd, and et al. (1994) *Biochemistry* 33, 5819-5828
89. McManus, O. B., Helms, L. M., Pallanck, L., Ganetzky, B., Swanson, R., and Leonard, R. J. (1995) *Neuron* 14, 645-650
90. Cox, D. H., and Aldrich, R. W. (2000) *J Gen Physiol* 116, 411-432
91. Jiang, Z., Wallner, M., Meera, P., and Toro, L. (1999) *Genomics* 55, 57-67
92. Xia, X. M., Zeng, X., and Lingle, C. J. (2002) *Nature* 418, 880-884
93. Yusifov, T., Savalli, N., Gandhi, C. S., Ottolia, M., and Olcese, R. (2008) *Proc Natl Acad Sci U S A* 105, 376-381
94. Hou, S., Xu, R., Heinemann, S. H., and Hoshi, T. (2008) *Nat Struct Mol Biol* 15, 403-410
95. Jaggar, J. H., Li, A., Parfenova, H., Liu, J., Umstot, E. S., Dopico, A. M., and Leffler, C. W. (2005) *Circ Res* 97, 805-812
96. Dong, J., Shi, N., Berke, I., Chen, L., and Jiang, Y. (2005) *J Biol Chem* 280, 41716-41724
97. Nakamura, T., Yuda, R., Unemoto, T., and Bakker, E. P. (1998) *J Bacteriol* 180, 3491-3494
98. Jiang, Y., Pico, A., Cadene, M., Chait, B. T., and MacKinnon, R. (2001) *Neuron* 29, 593-601
99. Salkoff, L., Butler, A., Ferreira, G., Santi, C., and Wei, A. (2006) *Nat Rev Neurosci* 7, 921-931
100. Hou, S., Heinemann, S. H., and Hoshi, T. (2009) *Physiology (Bethesda)* 24, 26-35
101. Ruttiger, L., Sausbier, M., Zimmermann, U., Winter, H., Braig, C., Engel, J., Knirsch, M., Arntz, C., Langer, P., Hirt, B., Muller, M., Kopschall, I., Pfister, M.,

Munkner, S., Rohbock, K., Pfaff, I., Rusch, A., Ruth, P., and Knipper, M. (2004) *Proc Natl Acad Sci U S A* 101, 12922-12927

102. Sausbier, M., Hu, H., Arntz, C., Feil, S., Kamm, S., Adelsberger, H., Sausbier, U., Sailer, C. A., Feil, R., Hofmann, F., Korth, M., Shipston, M. J., Knaus, H. G., Wolfer, D. P., Pedroarena, C. M., Storm, J. F., and Ruth, P. (2004) *Proc Natl Acad Sci U S A* 101, 9474-9478
103. Zeng, X. H., Xia, X. M., and Lingle, C. J. (2003) *Nat Struct Biol* 10, 448-454
104. Jin, P., Weiger, T. M., and Levitan, I. B. (2002) *J Biol Chem* 277, 43724-43729
105. Jin, P., Weiger, T. M., Wu, Y., and Levitan, I. B. (2002) *J Biol Chem* 277, 10014-10020
106. Williams, S. E. W., P. Mason, H. S. Bould, J. Iles, D. E. Riccardi, D. Peers, C. and Kemp, P. J. (2004) *Science* 306, 2093-2097
107. Horrigan, F. T., Heinemann, S. H., and Hoshi, T. (2005) *J Gen Physiol* 126, 7-21
108. Hou, S., Xu, R., Heinemann, S. H., and Hoshi, T. (2008) *Proc Natl Acad Sci U S A* 105, 4039-4043
109. Brazier, S. P., Telezhkin, V., Mears, R., Muller, C. T., Riccardi, D., and Kemp, P. J. (2009) *Adv Exp Med Biol* 648, 49-56
110. Zhang, G., Xu, R., Heinemann, S. H., and Hoshi, T. (2006) *Biochem Biophys Res Commun* 342, 1389-1395
111. Tang, X. D., Daggett, H., Hanner, M., Garcia, M. L., McManus, O. B., Brot, N., Weissbach, H., Heinemann, S. H., and Hoshi, T. (2001) *J Gen Physiol* 117, 253-274
112. Telezhkin, V., Brazier, S. P., Cayzac, S., Muller, C. T., Riccardi, D., and Kemp, P. J. (2009) *Adv Exp Med Biol* 648, 65-72
113. Kemp, P. J. (2005) *Biochem Biophys Res Commun* 338, 648-652

Chapter 2

Heme Regulatory Motifs in Heme Oxygenase-2 Form a Thiol/Disulfide Redox Switch That Responds to the Cellular Redox State

This project was a collaboration with Dr. Ursula Jakob and Dr. Jeffrey R. Martens's research groups at the University of Michigan. The results in this chapter were published in *J. Biol. Chem.*(2009, 284(31):20556-61.): **Yi, L., Jenkins, P. M., Leichert, L. I., Jakob, U., Martens, J. R, Ragsdale, S. W.** " Heme regulatory motifs in heme oxygenase-2 form a thiol/disulfide redox switch that responds to the cellular redox state".

In this chapter, Li Yi and Paul M. Jenkins generated the HEK293 stable cell line, Li Yi and Lars I. Leichert established the mass spectroscopic analysis method, and Li Yi performed the experiments, analyzed the data, and wrote the first draft of the paper.

2.1 Abstract

Heme oxygenase (HO) catalyzes the rate-limiting step in heme catabolism to generate CO, biliverdin, and free iron. Two isoforms of HO have been identified in mammals, inducible HO-1 and constitutively expressed HO-2. HO-1 and HO-2 share similar physical and kinetic properties, but have different physiological roles and tissue distributions. Unlike HO-1, which lacks cysteine residues, HO-2 contains three Cys-Pro signatures, known as heme regulatory motifs (HRMs), which are known to control processes related to iron and oxidative metabolism in organisms from bacteria to humans. In HO-2, the C-terminal HRMs constitute a thiol/disulfide redox switch that regulates affinity of the enzyme for heme (Yi & Ragsdale, *J. Biol. Chem.*, 2007, 282, 20156-21067). Here we demonstrate that the thiol/disulfide switch in human HO-2 is physiologically relevant. Its redox potential was measured to be -200 mV, which is near the ambient intracellular redox potential. We expressed HO-2 in bacterial and human cells and measured the redox state of the C-terminal HRMs in growing cells by thiol trapping experiments using the isotope coded affinity tag technique. Under normal growth conditions, the HRMs are 60-70% reduced, while oxidative stress conditions convert most (86-89%) of the HRMs to the disulfide state. Treatment with reductants converts the HRMS largely (81-87%) to the reduced dithiol state. Thus, the thiol-disulfide switch in HO-2 responds to cellular oxidative stress and reductive conditions, representing a paradigm for how HRMs can integrate heme homeostasis with CO signaling and redox regulation of cellular metabolism.

2.2 Introduction

Heme oxygenase (HO, EC 1:14:99:3) catalyzes the O_2- and NADPH-dependent conversion of heme to biliverdin, CO, and iron in a reaction that is coupled to cytochrome P450 reductase. Then, biliverdin reductase catalyzes the NADPH-dependent reduction of biliverdin to the antioxidant bilirubin. Several recent reviews on HO (1-5) and BVR (6) are available. HO is present in organisms from bacteria to eukaryotes and, as the only known enzyme that can degrade heme, plays a critical role in heme and iron homeostasis.

There are two major heme oxygenase (HO) isoforms in mammals, inducible HO-1, which is ancient and widely distributed among organisms from bacteria to man, and constitutively expressed HO-2, which emerged 250 million years ago with the amniotes (7). HO-1 is found in most tissues, and is highly expressed in spleen and liver (8). Conversely, HO-2 has a narrow tissue distribution, exhibiting high expression levels in the brain, testes and carotid body (8,9). Both HO-1 and HO-2 catalyze the NADPH- and cytochrome P450 reductase-dependent degradation of heme to CO, iron, and biliverdin, which is quickly reduced to bilirubin in the presence of biliverdin reductase (10). Controlling cellular heme concentrations is crucial because heme is required as a prosthetic group by regulatory and redox proteins, yet concentrations higher than 1 μM free heme are toxic (11). Thus, as the only mammalian proteins known to degrade heme, HOs play a key role in cellular heme homeostasis; furthermore, *in vitro* and *in vivo* studies of cellular and tissue injuries, such as oxidative stress and hemin-induced cytotoxicity, indicate that HO is cytoprotective (9).

HO-1 and HO-2 share high sequence and three-dimensional structural homology in their core domains (12,13); however, their sequences diverge near their C-termini, in which HO-2 contains two conserved HRMs, involving Cys265 in HRM1 and Cys282 in HRM2 (12,14) (**Figure 2.1**). It was recently shown that the HRMs in HO-2 do not bind heme *per se*, but instead form a reversible thiol/disulfide redox switch that indirectly regulates the affinity of HO-2 for heme (14). However, for this redox switch to have any physiological consequence, the midpoint redox potential of the thiol/disulfide couple must be near the ambient intracellular redox potential, estimated to range from -170 mV to -250 mV (15).

The heme regulatory motif (HRM) has been proposed to constitute a heme binding site (16,17) that regulates key metabolic processes from bacteria to humans. The HRM consists of a conserved Cys-Pro core sequence that is usually flanked at the N-terminus by basic amino acids and at the C-terminus by a hydrophobic residue. HRM-heme interactions have been proposed to regulate the activity and/or stability of proteins that play central roles in respiration and oxidative damage (18,19), coordination of protein synthesis and heme availability in reticulocytes (20,21), and controlling iron and heme homeostasis (22-26). An important component of the latter process is heme oxygenase-2 (HO-2).

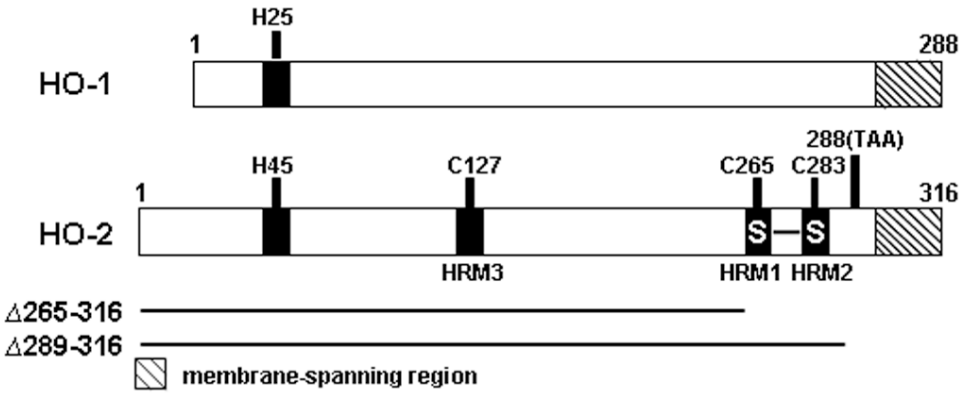

FIGURE 2.1 **Major structural regions in HO-1 and HO-2.** His25 in HO-1 or His45 in HO-2 are the heme-binding ligands

2.3 Materials and methods

2.3.1 Cloning, expression, and purification of human HO-2

The in vitro studies were performed using a truncated form of HO-2 (HO-2Δ289-316, denoted HO-2_t here) that lacks the C-terminal membrane binding region (14), while the full-length protein was used for experiments with growing cells. The C127A and F253W variants were generated from HO-2_t using the QuikChange site-directed mutagenesis protocol (Stratagene, La Jolla, CA). HO-2 purification and enzymatic assay were performed as previously described (14).

2.3.2 Construction of HO-2 stable transfected HEK293 cells

Full-length human HO-2 cDNA was subcloned into a pcDNA 3.1 (-) vector using XhaI and HindIII restriction sites. Human 293 embryonic kidney (HEK293) cells were transfected with the recombinant pcDNA plasmid using TransIT-LT1 (Mirus, Madison, WI), as described by the manufacturer. Cells were cultured at 37 ^{o}C with selective medium containing 600 $\mu g.ml^{-1}$ geneticin every 3-4 days until geneticin-resistant foci were identified. Then colonies were picked and expanded in 60 mm^2 plastic dishes. The HO-2 expression levels in colonies were determined using western blotting with an antibody generated against human HO-2.

2.3.3 Determination of the midpoint reduction potential of the thiol/disulfide redox couple in HO-2

Two truncated forms of HO-2, HO-2_t, which contains all three HRMs, and C127A, which contains HRM1 and HRM2 but lacks HRM3, were used in these experiments, because the full-length purified protein is subject to proteolysis and to precipitation. In a total 20 µl reaction system, 40 µg of HO-2_t in Buffer A (50 mM KCl, 50 mM Tris-HCl pH 7.5) was incubated with 2 µl Buffer A and 8 µl of a solution containing various ratios of reduced (GSH) and oxidized (GSSG) glutathione, with the total GSH and GSSG concentrations fixed at 20 mM. The GSH/GSSG ratio was varied to establish a gradient of ambient redox potentials between -130 and -250 mV, calculated by the Nernst equation according to a midpoint reduction potential of -240 mV (27). The reaction mixtures were incubated at 37 °C with shaking for 2 hr, and the reaction was terminated by adding 20 µl of 40% ice-chilled trichloroacetic acid (TCA) and incubating on ice for 30 min. The suspension was centrifuged at 20,300 x g for 15 min at 4 °C. After removing

the supernatant, the protein pellet was washed three times with -20 °C cold 100% acetone. The acetone-washed pellet was then resuspended in 20 µl of reaction buffer, containing 50 mM Tris-HCl, 4% SDS, and 20 mM purified Mal-PEG 5000 (Laysan Bio, Arab, AL), pH 5.0. After shaking at 25 °C for 30 min, 20 µl of non-reducing SDS loading buffer was added to the reaction buffer and the samples were boiled for 5 min and analyzed by SDS-PAGE. After staining the gel with Coomassie blue, the intensities of the bands from the unmodified and Mal-PEG-modified HO-2 were measured using UN-SCAN-IT gel 6.1 (Silk Scientific, Inc. Orem, Utah), and the midpoint reduction potential of the thiol/disulfide couple from the C-terminal HRMs in HO-2 was calculated using the Nernst Equation 1. In this equation, E is the ambient potential in solution; $E^{\ominus}$ is the midpoint reduction potential of HO-2; R is the universal gas constant: $R = 8.31\ JK^{-1}mol^{-1}$; T is the absolute temperature; F is the Faraday constant: $F = 9.65\times10^{4}\ Cmol^{-1}$; and z is the number of electrons transferred in the reaction.

$$E = E^{0} - \frac{RT}{zF}\ln\frac{[\text{Reduced HO-2}]}{[\text{Oxidized HO-2}]} \quad (1)$$

2.3.4 Determination of the redox states of the HRMs in HO-2 using the isotope coded affinity tag technique

OxICAT experiments were performed as previously described (28), with minor modifications. For trapping the redox states of purified HO-2, 100 µg as-isolated HO-2_t or HO-2_t that had been reduced with 1 mM Tris(2-carboxyethyl)phosphine (TCEP) for 30 min were applied to a two-step alkylation procedure with light/heavy ICAT reagents as described previously. The alkylated protein was then digested with typsin and the cysteine containing peptides, which are linked to biotin, were enriched on a cation exchange cartridge followed by an avidin affinity cartridge (Applied Biosystems, Foster City, CA). After removing the biotin tag conjugated to the cysteine containing peptides, samples were analyzed by Nano-LC/MS/MS at the Michigan Proteome Consortium to quantify the amounts of reduced (dithiol) protein containing the light ICAT and oxidized (disulfide) protein containing the heavy ICAT adduct. For determining the redox state of the C-terminal HRMs, two peptides (Peptide A containing amino acid residues 264-285 and Peptide B containing residues 265-285), which differ in relative abundance (since both 264 and 265 are Lys residues) among various experiments, were analyzed. As

expected, the high-resolution mass spectra consist of envelopes of multiple peaks reflecting the presence of 0.018% ^{2}H, 1.11% ^{13}C, 0.45% ^{15}N and 0.20% ^{18}O in each peptide. The m/z ratios for the oxidized form of these peptides (2877.0 for Peptide A and 2748.8 for Peptide B) are 18 mass units larger than those for the reduced protein (2858.9 and 2730.8, respectively).

For analysis of the redox state of HO-2 expressed in *E. coli*, a pGEX4T-2 plasmid containing the full-length human HO-2 cDNA was transformed into *E. coli* strain BL21 (DE3). Cells were grown in 50 ml MOPS minimal medium containing 100 μg/ml ampicillin at 37 °C. When the OD_{600} reached 0.2, 0.01 mM IPTG was added to induce HO-2 expression. To generate oxidative stress, cells were treated with 400 μM t-butylperoxide (t-BuOOH) or 1 mM diamide (DA), and to generate a reducing environment, cells were treated with 1 mM N-acetyl cysteine (NAC). In addition, the redox states of the HRMs were investigated under normoxic (continuously sparged with air) and anaerobic conditions. Anaerobic conditions were achieved by inoculating the aerobically growing cells into anaerobic MOPS minimal medium at a ratio of 1:500 (cells:medium). Cells were cultured at 37 ^{o}C during each of these treatments.

When the OD_{600} reached 0.4, 0.2 mL of ice cold 100% TCA was mixed with 1.8 mL of cell culture to lyse the cells, precipitate the proteins, and trap the thiol status. After washing with a solution containing 5% TCA and 100% acetone (kept at -20 °C), the protein pellet was then applied to the two-step alkylation procedure with light/heavy ICAT reagents as described above.

The redox states of the C-terminal HRMs in HEK293 cells were determined as just described for the *E. coli* system, with modifications. HO-2-transfected HEK293 cells were cultured in a 60 mm^2 plastic dish with DMEM containing 10% (vol/vol) FBS, 10 U/ml penicillin, 100 mg/ml streptomycin and 300 μg/ml geneticin. After obtaining 50-60% cell confluence, 50% medium was replaced with fresh medium followed by treatment with t-BuOOH (200 μM, 12 h) or NAC (1 mM, 2h). Then, the cells were processed by quickly washing three times with ice cold PBS, pipetting off the dishes with 1.8 ml of PBS, and immediately treating with 0.2 ml of ice-chilled 100% TCA, and briefly sonicating with a Misonix sonicator 4000 (Misonix Inc. Farmingdale, NY). All these steps were carried out on ice. The following ICAT alkylation steps were performed

as described above, except that 1% NP-40 was added into the denaturing alkylation solution to facilitate resuspension of the protein pellet.

2.3.5 Intrinsic fluorescence quenching and circular dichroism analysis

Tryptophan fluorescence is not detectable in as-isolated HO-2; therefore, we engineered a Phe-to-Trp substitution near the C-terminal HRMs. This F253W variant exhibits intrinsic tryptophan fluorescence that increases upon reduction of the disulfide bond, providing a straightforward and direct measure of the redox state of the thiol/disulfide couple. Intensity of the fluorescence emission at 340 nm of the F253W (200-500 nM) variant of HO-2 was measured with a Shimadzu RF-530 1 PC Spectrofluorophotometer (Columbia, MD) at room temperature. CD measurements were performed at 4 °C with a JASCO J-715 instrument (Jasco Inc., Easton, MD). For secondary structure analysis, experiments were performed in a 0.1-mm-path length cell with 20 μM $HO\text{-}2_t$ in 10 mM potassium phosphate buffer, pH 7.5. The F253W variant exhibited approximately 50% of the specific activity of the wild-type protein.

2.4 Experimental results

2.4.1 Structural changes between oxidized and reduced HO-2

To investigate the structural differences between the oxidized and reduced forms of HO-2, the circular dichroism (CD) spectra of as-isolated and TCEP reduced HO-2 were recorded. These spectra are nearly identical (**Figure 2.2**), indicating that if there are any secondary structural changes in HO-2 upon oxidation or reduction of the thiol/disulfide redox switch, these would be minor local changes.

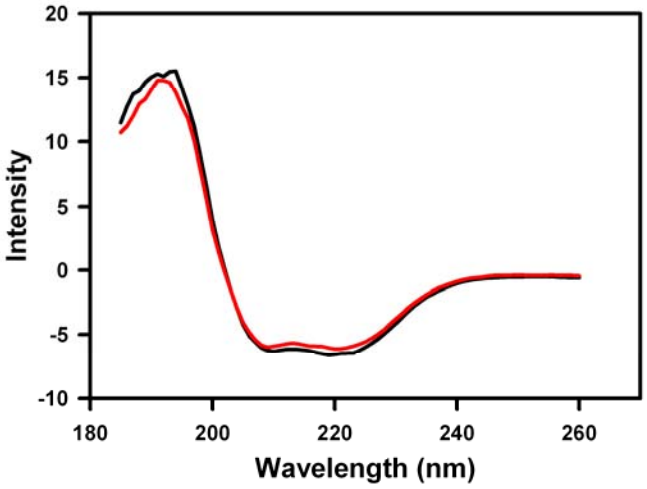

FIGURE 2.2 **CD spectroscopic spectra of oxidized and reduced HO-2_t.** CD spectra of as-isolated (20 μM, black) and 1mM TCEP-reduced (20 μM, red) HO-2_t, TCEP-reduced protein was prepared by incubating 125 μM HO-2Δ289-316 with 1 mM TCEP for 30 min at 4 oC

2.4.2 Determination of the redox potential of thiol/disulfide redox switch in HO-2

To test the hypothesis that the C-terminal HRMs in HO-2 form a physiologically relevant redox switch that is poised to sense the intracellular redox potential, the midpoint reduction potential of the thiol/disulfide redox couple was determined. HO-2_t samples were equilibrated with solutions of oxidized/reduced glutathione (GSSG/GSH) at ratios that established a gradient of ambient redox potentials between -130 and -250 mV. Then, the proteins were precipitated by treating the samples with trichloroacetic acid and alkylated with MAL-PEG, which traps the free thiols as an adduct resulting in a mass increase of 5 kDa per thiol modification. Thus, the oxidized (non-modified disulfide,

lower band) and reduced (modified, upper band) forms of HO-2_t can be conveniently quantified by analyzing the migration pattern on non-reducing SDS-PAGE (**Figure 2.3A**). To unambiguously assign the titrated disulfide bond to Cys265 and Cys282, we used a form of HO-2 containing all three HRMs (HO-2_t) as well as the HO-2_t variant (C127A) containing only the two C-terminal HRMs (**Figure 2.3**). After quantifying the ratio of oxidized/reduced protein at each ambient redox potential and fitting the data to the Nernst equation, the calculated midpoint reduction potentials of the thiol/disulfide redox switches in C127A (-191 mV) and HO-2_t (-199 mV) (**Figure 2.3B**) were nearly identical.

To confirm the value of the midpoint potential determined by the MAL-PEG approach, we performed intrinsic tryptophan fluorescence experiments of an HO-2_t variant (F253W) in which a Phe to Trp substitution was engineered near the C-terminal HRMs. Fluorescence quenching of excited Trp by nearby disulfide bridges is common in proteins and is proposed to occur through an energy transfer mechanism from excited Trp to the disulfide bond (29). The activity of the F253W variant is ~ two-fold lower than that of HO-2_t (**Figure 2.4A**), indicating that major structural changes have not occurred by the replacement of Phe with Trp at this position. Reduction of the disulfide bond in the F253W variant leads to approximately a two-fold increase in fluorescence intensity (**Figure 2.4B**). When solutions of the F253W variant are equilibrated at different redox potentials, set by establishing a gradient of GSSG/GSH ratios as above, the fluorescence intensity is quenched by the disulfide bond. Fitting the data to the Nernst equation provides a midpoint reduction potential of -200 mV (**Figure 2.3B**). Thus, both thiol modification and intrinsic tryptophan fluorescence experiments provide similar values of -190 to -200 mV for the midpoint potential of the thiol/disulfide redox switch in HO-2_t. This value is within the range of redox potentials for proteins known to catalyze key thiol/disulfide oxidoreductase reaction, from -122 mV for the oxidase DsbA (30) to -270 mV for the reductase thioredoxin (31). It lies precisely within the range measured for the intracellular redox potential, from -170 (15) to -325 mV (32), indicating that the thiol/disulfide redox switch in HO-2 is poised to respond to the redox state within the cell.

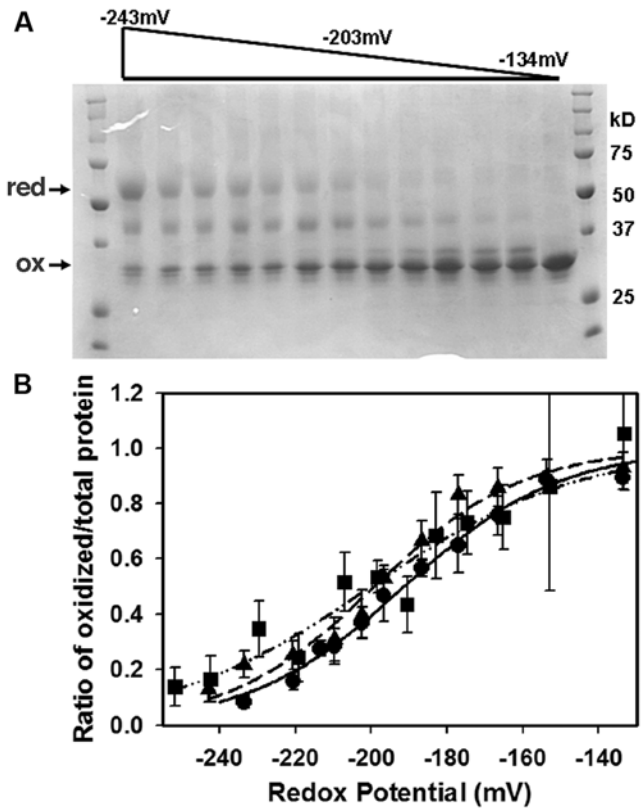

FIGURE 2.3 **Measurement of the midpoint redox potential of the thiol/disulfide couple in HO-2_t.** C127A was used in the alkylation experiment to determine the redox potential of the C-terminal HRMs. The ambient redox potential, set by variation of the GSSG/GSH ratio, ranged from -133 mV to -252 mV. (See details in "Materials and Methods"). **A,** SDS-PAGE analysis of the alkylation of C127A by Mal-PEG 5000. **B,** Nernst analysis of results from non-reducing PAGE shown in (A) and fluorescence quenching studies of F253W. The redox potential of the C-terminal HRMs, analyzed using the Nernst Equation, provided an E^0 = -191 ± 1 mV for C127A (Solid line, closed circle), E^0 = -199 ± 2 for HO-2_t (dash line, closed triangle), and E^0 = -200 ± 3 mV for F253W (dash-dot, closed squares).

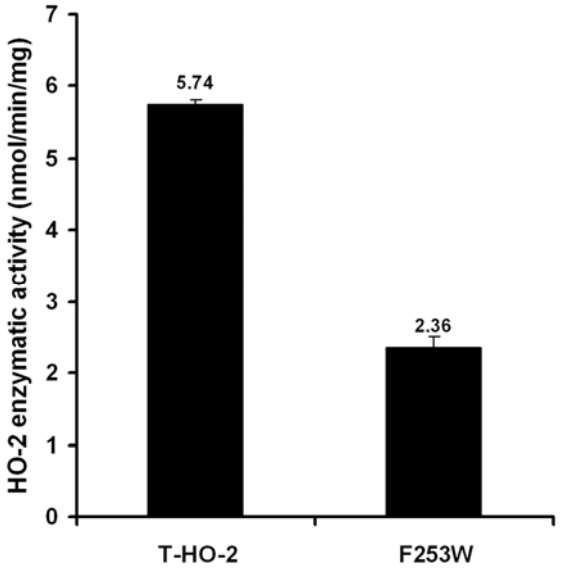

A

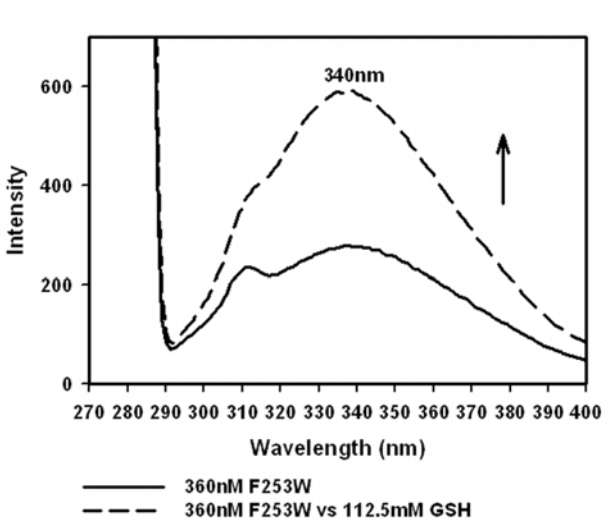

B

FIGURE 2.4 **Properties of HO-2$_t$ and variants. A,** HO-2 activity of the F253W variant was determined by measuring the rate of bilirubin synthesis. **B,** Intrinsic tryptophan fluorescence of 360 nM as-isolated (solid line) and GSH-reduced (dash line) F253W. GSH-reduced protein was prepared by incubating 360 nM F253W with 112.5 mM GSH for 1hr.

2.4.3 Response of the thiol/disulfide redox couple to alteration in the cellular redox potential

To further test the hypothesis that the thiol/disulfide switch in HO-2 responds to changes in intracellular redox conditions, the redox state of the HRMs was measured by OxICAT, a novel mass spectrometric method that combines thiol trapping with the ICAT technique to quantify oxidative thiol modifications (28). ICAT consists of an iodoacetamide group linked to a cleavable biotin affinity tag via an isotopically light (^{12}C) or heavy (^{13}C) nine-carbon linker (33).

Before initiating experiments with growing cells, we performed the OxICAT analysis on pure HO-2. To determine the redox status of freshly purified protein, we treated HO-2_t with the light ICAT reagent, the reduced all existing oxidative thiol modifications and alkylated all newly reduced thiols with heavy ICAT. Thus, a peptide containing a free Cys thiol(ate) will have an m/z value that is 9 units smaller than one containing a Cys that is engaged in a disulfide bond. Mass spectral analysis of the affinity-purified tryptic peptide harboring HRM1 and HRM2 (Peptide A, residues 264-285) generated from as-isolated HO-2 reveals peaks at 2858.9, 2868.0 (+9), and 2877.0 (+18), with the major peak at 2877.0, resulting from labeling with two heavy ICAT molecules (**Figure 2.5**). Thus, the majority of the as-isolated protein contains cysteines in HRM1 and HRM2 that are engaged in an intramolecular disulfide bond. In contrast, when HO-2 is reduced by TCEP before the OxICAT procedure, the light ICAT-labeled peptide is in significantly greater abundance. Thus, the cysteines of HRM1 and HRM2 in purified HO-2 are mainly (90.6%) in the disulfide state, and TCEP converts the HRMs nearly quantitatively (94.2%) to the dithiol state (**Figure 2.5**). This result indicates that HO-2 is highly oxidation sensitive and accumulates in its disulfide bond form when reducing agents are absent during its purification.

The minor peak in Fig. 2.5 at m/z 2868.0 (+9) in the as-isolated protein is likely due to the presence of a small amount of the sulfenate (S-OH) of Cys265 in the sample. The peak has a +9 value of m/z because the S-OH does not react with iodoacetamide; however, TCEP reduces the S-OH to the SH in the second step of the OxICAT protocol. Furthermore, the intermediate band shown in Fig 2A also probably arises from to a small amount of Cys-sulfenate in the sample (see above). Similarly, a sulfenate intermediate

was reported in OxICAT analysis of Hsp33 and GapA (28). Our assignment of Cys265-SOH is consistent with earlier studies, involving the C127A/C282A HO-2_t variant, in which the sulfenate of Cys265 was trapped as an adduct with 7-chloro-4-nitrobenzo-2-oxa-1,3-diazole and was identified as the sulfonate by mass spectrometry; thus we proposed that the sulfenate of Cys265 is an intermediate in the formation of the disulfide (14).

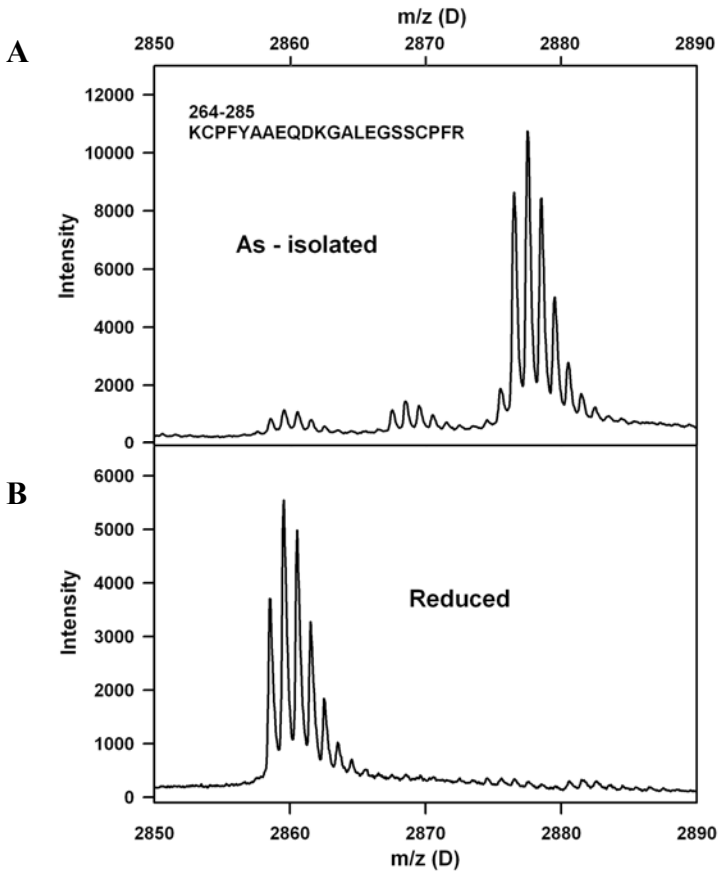

FIGURE 2.5 **OxICAT analysis of the redox state of the C-terminal HRMs in purified HO-2_t.** Purified HO-2_t was treated as described in "Materials and Methods". **A,** as-isolated HO-2_t. **B,** TCEP-reduced HO-2_t, generated by incubating 100 μM HO-2_t with 1 mM TCEP for 30 min.

2.4.3.1 Response of the thiol/disulfide redox couple to alteration in the cellular redox potential in reconstructed *E.coli* cells

To determine whether the thiol/disulfide switch in HO-2 responds to changes in intracellular redox conditions, full-length HO-2 was expressed in human and in *E. coli* cells, and the redox states of the HRMs were determined by the OxICAT method (**Figure 2.6A**) (also see **Figure 2.7** and **Table 2.1**). When *E. coli* was grown under aerobic conditions, the C-terminal HRMs were nearly equally distributed between the reduced (63%) and oxidized (37%) states, which corresponds well with the determined redox potential of HO-2_t, suggesting that truncation of the membrane spanning region has little effect on the thiol/disulfide redox potential and that HO-2 is in equilibrium with the cellular GSSG/GSH ratio. The proportion of reduced HRMs increased to 75.0% or 87.0% when cells were grown either anaerobically or treated with 1 mM NAC, respectively. On the other hand, when cells were subjected to oxidative stress generated by addition of 1 mM DA or 400 μM t-BuOOH, the proportion of reduced HRMs decreased to 11.0% and 12.2%, respectively.

2.4.3.2 Response of the thiol/disulfide redox couple to alteration in the cellular redox potential in human HO-2 expressing HEK293 cells

Similar experiments were performed with stably transfected HEK293 cells containing the full-length HO-2 gene, which was integrated into the genome and constitutively expressed (**Figure 2.8**). When this cell line was cultured under normoxic conditions, the C-terminal HRMs were mostly (70%) in the reduced dithiol state, while under oxidative stress conditions (200 μM t-BuOOH), the HRMs were converted predominantly (86%) to the disulfide state; in contrast, after treatment with 2 mM NAC, the HRMs were found mostly (82%) in the reduced dithiol state (**Figure 2.6B**, **Figure 2.8**) (also see **Table 2.1**). Thus, the C-terminal HRMs in HO-2 form a physiologically relevant redox rheostat that responds to the intracellular redox potential. The amount of HO-2 that accumulates in the stably transfected HEK293 cell line is unaffected by treatment with oxidants or reductants or by adding hemin to the cells (**Figure 2.9**). This is consistent with prior studies, which demonstrated that expression of HO-1, but not HO-2, is induced by oxidative stress (10). Thus, the shifts in intracellular redox potential alter

the redox states of the C-terminal HRMs in HO-2, but do not appear to alter the expression or stability of HO-2.

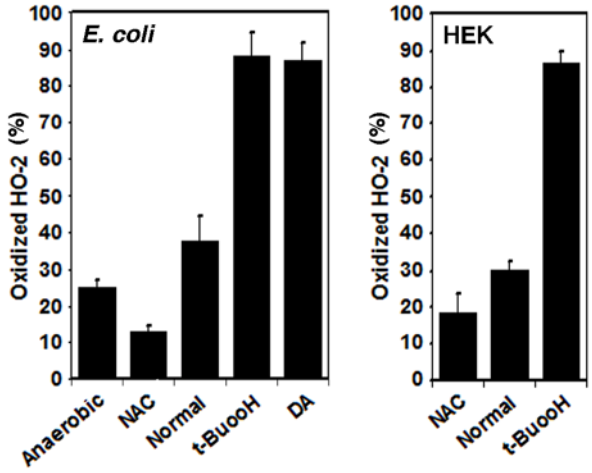

FIGURE 2.6 **The redox state of the C-terminal HRMs of HO-2 expressed in *E. coli* and in HEK293 cells under different cellular redox conditions.** The oxICAT technique was applied to investigate the redox states of the C-terminal HRMs of HO-2 expressed under different conditions, as described in "Materials and Methods". **A,** Wild type HO-2 was expressed in *E. coli* strain BL21 (DE3) and grown at 37^{o}C under normoxic or anaerobic growth conditions, or treated with 1 mM NAC (2 h), 400 μM t-BuOOH (15 h), or 1 mM DA (10 min), as described in the Methods. **B,** Wild type HO-2 was expressed in HEK293 cells and grown at 37 ^{o}C under normoxic conditions or treated with 1 mM NAC (2 h) or 200 μM t-BuOOH (12-15 h), as described in the Methods Section.

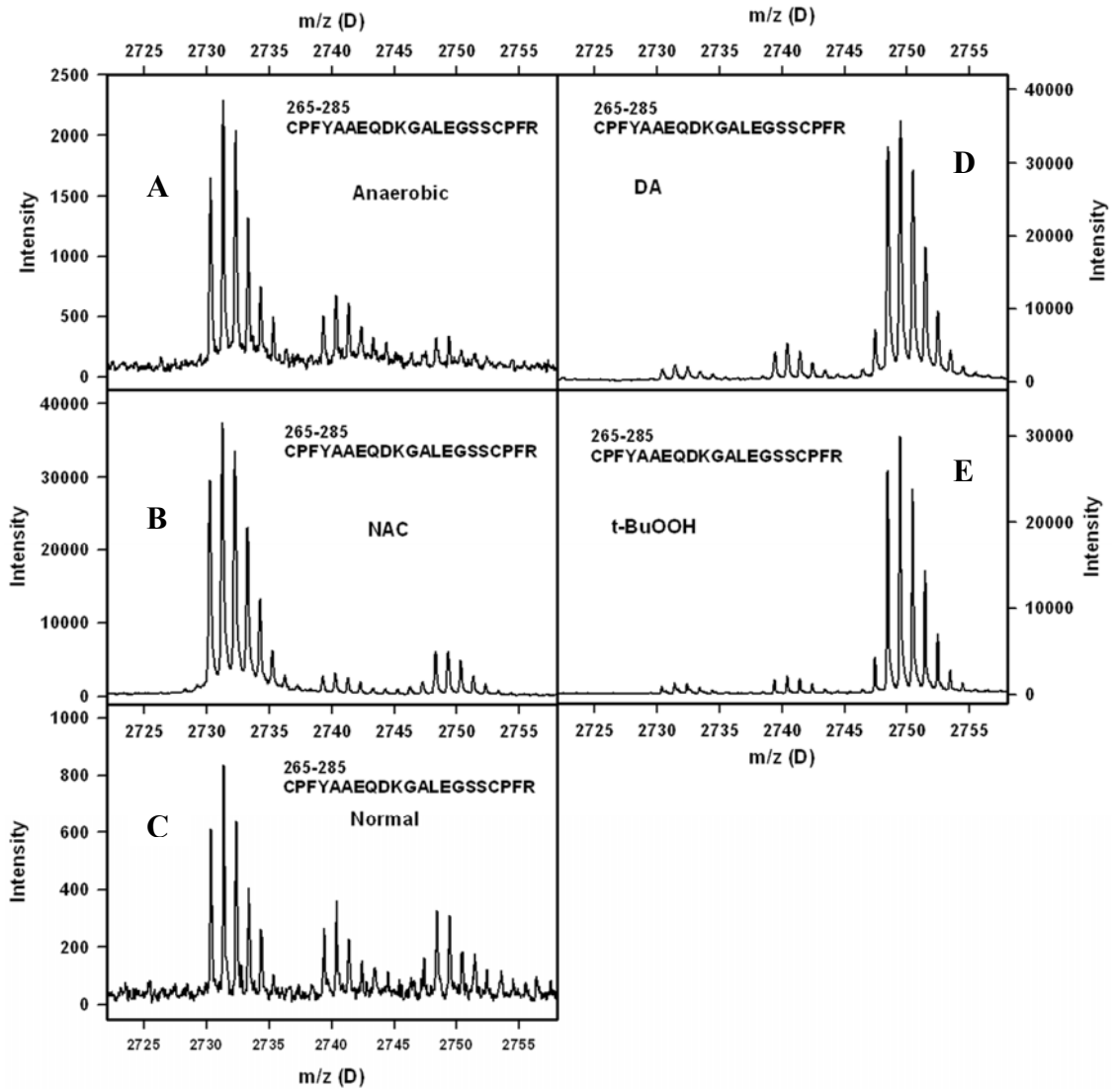

FIGURE 2.7 **Representative mass spectrometric results of the redox states of C-terminal HRMs in HO-2 expressed in *E.coli* strains grown under different conditions**. Full-length HO-2 was stably expressed in a *E.coli* strains as described in "Materials and Methods"). The oxICAT technique was used to investigate the redox states of C-terminal HRMs when cells were treated with **A,** anaerobic growth condition; **B,**1 mM NAC; **C,** normal growth conditions; **D,** 1 mM DA; or **E,** 400 μM t-BuOOH.

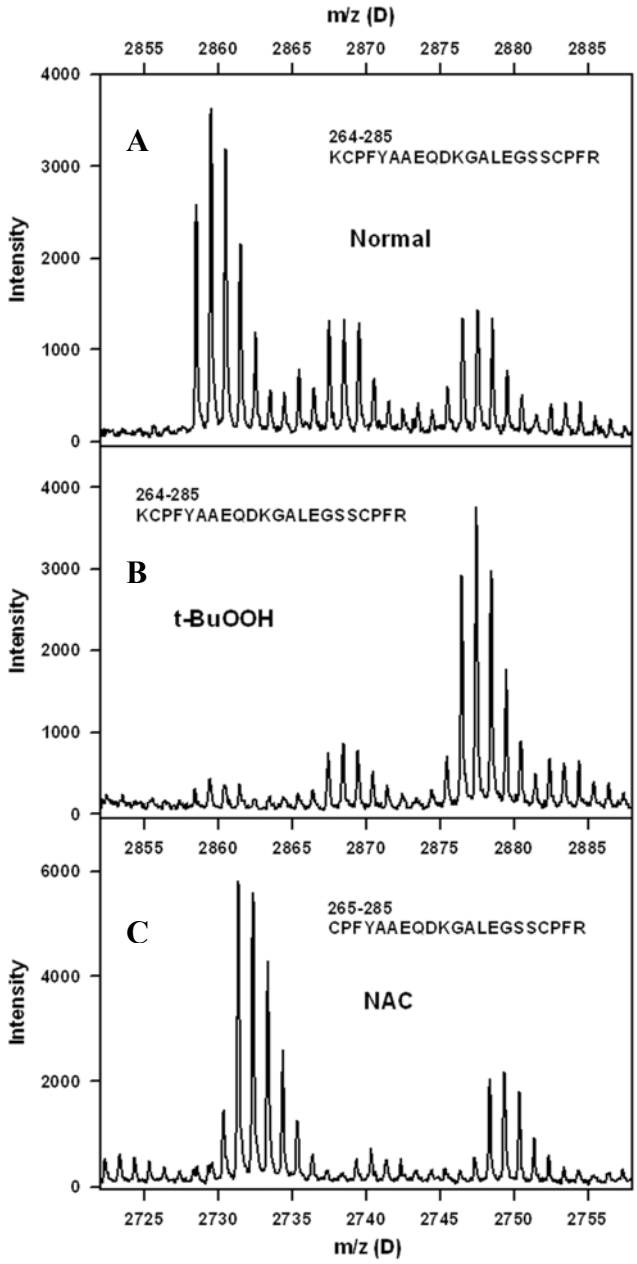

FIGURE 2.8 **Representative mass spectrometric results of the redox states of C-terminal HRMs in HO-2 expressed in HEK293 cells grown under different conditions**. Full-length HO-2 was stably expressed in a HEK293 cell line as described in "Materials and Methods"). The oxICAT technique was used to investigate the redox states of C-terminal HRMs when cells were treated with **A,** normal growth conditions; **B,** 200 μM t-BuOOH for 12-15 h; or **C,** 1 mM NAC, 2h. .

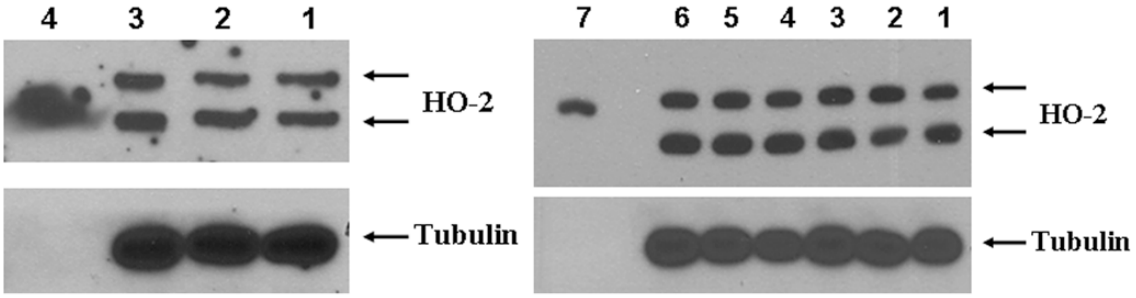

FIGURE 2.9 **Stable expression of HO-2 in HEK293 cells. A,** Cells were cultured under different redox conditions: 1, 1mM NAC (2h); 2, normal conditions; 3, 200 μM t-BuOOH (12 h); 4, purified HO-2_t. **B,** Cells were cultured with different hemin additions.1, normal condition; 2, 100 nM hemin (20 h); 3, 1 μM hemin (20 h); 4, 10 μM hemin (20 h); 5, 50 μM hemin (20 h); 6, 100 μM hemin (20 h); 7, purified HO-2_t.

TABLE 2.1 **Redox states of the thiol/disulfide switch in HO-2 expressed under different cellular redox conditions.**

Expression System	**Reducing environment**				**Oxidative stress**	
E.coli	**NAC**		**Normal**		**t-BuOOH**	
	HO-2^R	**HO-2^O**	**HO-2^R**	**HO-2^O**	**HO-2^R**	**HO-2^O**
	87.0 ± 1.3 %	13.0 ± 1.3 %	62.6 ± 7.0 %	37.4 ± 7.0 %	11.0 ± 6.5 %	89.0 ± 6.5 %
	Anaerobic				**Diamide**	
	HO-2^R	**HO-2^O**			**HO-2^R**	**HO-2^O**
	75.0 ± 1.7 %	25.0 ± 1.7 %			12.2 ± 3.6 %	86.7 ± 5.2 %
HEK293	**NAC**		**Normal**		**t-BuOOH**	
	HO-2^R	**HO-2^O**	**HO-2^R**	**HO-2^O**	**HO-2^R**	**HO-2^O**
	81.5 ± 5.0 %	18.5 ± 5.0 %	70.2 ± 1.8 %	30.3 ± 2.3 %	13.7 ± 3.7 %	86.3 ± 3.7 %

HO-2^R: reduced HO-2; HO-2^O: oxidized HO-2

2.5 Discussion

The binding and redox properties of HO-2 allow it to interlink cellular redox status and heme homeostasis, given that the midpoint reduction potential of the thiol/disulfide redox switch is poised near the ambient intracellular redox potential and that the K_d for heme (0.03 μM) is near the free cellular heme pool (0.03-1 μM) (34). We found that HO-2 expression levels are unaffected by alteration in the cellular redox state (or growth in excess heme); however, the thiol/disulfide switch does exhibit a robust response to redox conditions. When cells are exposed to oxidative conditions, the Cys residues in the C-terminal HRMs in HO-2 are in the disulfide state, which favors heme binding; however, under reducing conditions, the lower affinity dithiol state predominates. Thus, these HRMs of HO-2 act as a redox rheostat, which regulates the binding of heme and, thus, HO-2 activity as a Nernstian function of the redox state of the cell. Under oxidative stress conditions, HO-2 can rapidly degrade heme, increasing the levels of CO and biliverdin; however, under hypoxic (or otherwise reduced) conditions, where the HRMs are in the dithiol state, the K_d (0.35 μM) rises well above the free heme pool (14). This redox switching mechanism could potentially connect the many physiological processes regulated by heme homeostasis and CO signaling to the cellular redox state. Such processes include oxygen sensing by the carotid body (the oxygen chemosensor in mammals), regulation of T cell function, blockade of oxidant formation in neurons where HO-2 appears to be the sole source of CO biogenesis (35), and control of heme homeostasis (9,36,37). Our results also suggest that the myriad proposed functions ascribed to HRM-heme interactions in various proteins might actually be mediated by thiol/disulfide redox reactions. Thus, HO-2 may represent a paradigm for how HRMs can integrate heme, CO, and redox regulation of metabolism (**Figure 2.10**).

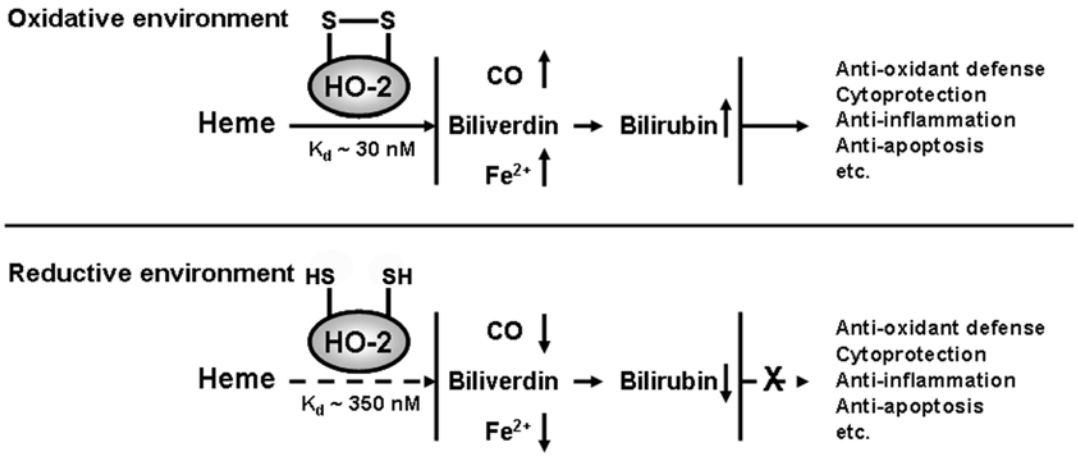

FIGURE 2.10 **Proposed model for the HRM mediated regulatory mechanism of HO-2 in cells.** Under oxidative environments, the redox active thiols of HO-2 would be in oxidized states, with HO-2 having high affinity for Fe^{3+}-heme (K_d = 30 nM). This high heme affinity would stimulate HO-2 activity to generate CO, biliverdin/bilirubin, and Fe^{2+}, which would activate a number of cellular signaling pathways, leading to cytoprotective effect. However, under reducing environments, in which the cells do not face severe oxidative stress, the thiol/disulfide redox switches in HO-2 would exist in the dithiol states, with HO-2 having low affinity for Fe^{3+}-heme (K_d = 350 nM). The low heme affinity would decrease HO-2 activity, resulting in the resting state of HO-2 mediated cytoprotective effect.

2.6 Conclusion

Here, we demonstrate that the C-terminal HRMs, which form a thiol-disulfide redox switch between Cys265 and Cys282, exhibit a redox potential that falls well within the ambient cellular redox potential. By expressing HO-2 in bacterial and human cells and trapping the thiols using the isotope coded affinity tag technique, it was shown that the redox state of the C-terminal HRMs in growing cells responds to the cellular redox state. The disulfide state is favored under oxidative and the dithiol state is predominant under reducing conditions. Thus, the HRMs act as a molecular rheostat that responds to the ambient intracellular redox potential and, based on earlier studies (14), controls activity of HO-2 by regulating heme binding to the enzyme.

2.7 References

1. Maines, M. D. (2004) *Antioxid Redox Signal* **6**, 797-801
2. Ragsdale, S. W. (2008) Heme oxygenase. in *Redox Biochemistry* (Banerjee, R. ed.), John Wiley & Sons, Hoboken, N.J. pp 131-134
3. Bauer, M., Huse, K., Settmacher, U., and Claus, R. A. (2008) *Intensive Care Med* **34**, 640-648
4. Rivera, M., and Zeng, Y. (2005) *J Inorg Biochem* **99**, 337-354
5. Unno, M., Matsui, T., and Ikeda-Saito, M. (2007) *Nat Prod Rep* **24**, 553-570
6. Maines, M. D. (2005) *Physiology (Bethesda)* **20**, 382-389
7. Maines, M. D., and Gibbs, P. E. (2005) *Biochem. Biophys. Res. Commun.* **338**, 568-577
8. Maines, M. D. (1997) *Annu Rev Pharmacol Toxicol* **37**, 517-554
9. Parfenova, H., and Leffler, C. W. (2008) *Curr Pharm Des* **14**, 443-453
10. Otterbein, L. E., Soares, M. P., Yamashita, K., and Bach, F. H. (2003) *Trends Immunol* **24**, 449-455
11. Mense, S. M., and Zhang, L. (2006) *Cell Res* **16**, 681-692
12. Bianchetti, C. M., Yi, L., Ragsdale, S. W., and Phillips, G. N., Jr. (2007) *J Biol Chem* **282**, 37624-37631
13. Schuller, D. J., Wilks, A., Ortiz de Montellano, P. R., and Poulos, T. L. (1999) *Nat Struct Biol* **6**, 860-867
14. Yi, L., and Ragsdale, S. W. (2007) *J Biol Chem* **282**, 21056-21067
15. Jones, D. P. (2002) *Methods Enzymol* **348**, 93-112
16. Huang, T. J., McCoubrey, W. K., Jr., and Maines, M. D. (2001) *Antioxid Redox Signal* **3**, 685-696
17. Qi, Z., Hamza, I., and O'Brian, M. R. (1999) *Proc. Natl. Acad. Sci. U S A* **96**, 13056-13061
18. Hon, T., Hach, A., Lee, H. C., Cheng, T., and Zhang, L. (2000) *Biochem. Biophys. Res. Commun.* **273**, 584-591
19. Lee, H. C., Hon, T., Lan, C., and Zhang, L. (2003) *Mol. Cell Biol.* **23**, 5857-5866
20. Uma, S., Matts, R. L., Guo, Y., White, S., and Chen, J. J. (2000) *Eur. J. Biochem.* **267**, 498-506
21. Chen, J. J., and London, I. M. (1995) *Trends Biochem Sci* **20**, 105-108
22. Yang, J., Panek, H. R., and O'Brian, M. R. (2006) *Mol Microbiol* **60**, 209-218
23. Eisenstein, R. S., and Blemings, K. P. (1998) *J Nutr* **128**, 2295-2298
24. Munakata, H., Sun, J. Y., Yoshida, K., Nakatani, T., Honda, E., Hayakawa, S., Furuyama, K., and Hayashi, N. (2004) *J Biochem (Tokyo)* **136**, 233-238

25. Yoshino, K., Munakata, H., Kuge, O., Ito, A., and Ogishima, T. (2007) *J Biochem* **142**, 453-458
26. McCoubrey, W. K., Jr., Huang, T. J., and Maines, M. D. (1997) *J. Biol. Chem.* **272**, 12568-12574
27. Schafer, F. Q., and Buettner, G. R. (2001) *Free Radic Biol Med* **30**, 1191-1212
28. Leichert, L. I., Gehrke, F., Gudiseva, H. V., Blackwell, T., Ilbert, M., Walker, A. K., Strahler, J. R., Andrews, P. C., and Jakob, U. (2008) *Proc Natl Acad Sci U S A* **105**, 8197-8202
29. Qiu, W., Wang, L., Lu, W., Boechler, A., Sanders, D. A., and Zhong, D. (2007) *Proc. Natl. Acad. Sci. U S A* **104**, 5366-5371
30. Huber-Wunderlich, M., and Glockshuber, R. (1998) *Fold Des* **3**, 161-171
31. Krause, G., Lundstrom, J., Barea, J. L., Pueyo de la Cuesta, C., and Holmgren, A. (1991) *J. Biol. Chem.* **266**, 9494-9500
32. Dooley, C. T., Dore, T. M., Hanson, G. T., Jackson, W. C., Remington, S. J., and Tsien, R. Y. (2004) *J. Biol. Chem.* **279**, 22284-22293
33. Gygi, S. P., Rist, B., Gerber, S. A., Turecek, F., Gelb, M. H., and Aebersold, R. (1999) *Nat Biotechnol* **17**, 994-999
34. Sassa, S. (2004) *Antioxid Redox Signal* **6**, 819-824
35. Boehning, D., and Snyder, S. H. (2002) *Science* **298**, 2339-2340
36. Ryter, S. W., Alam, J., and Choi, A. M. (2006) *Physiol Rev* **86**, 583-650
37. Wu, L., and Wang, R. (2005) *Pharmacol Rev* **57**, 585-630

Chapter 3

Comparison of Apo- and Heme-bound Crystal Structures of a Truncated Human Heme Oxygenase-2

This project was a collaboration with Dr. George N. Phillips's research group at the University of Wisconsin-Madison. The results in this chapter were published in *J. Biol. Chem.*(2007, 282, 37624-37631): **Bianchetti, C. M., Yi, L., Ragsdale, S. W., and Philips, G. N., Jr.** "Comparison of apo- and heme-bound crystal structures of a truncated human heme oxygenase-2".

In this chapter, Li Yi performed the sample preparation. Christopher M. Bianchetti and Li Yi both did the crystal preparation. Christopher M. Bianchetti collected the X-ray diffraction data and preformed the structure determination. Christopher M. Bianchetti and Li Yi both did the structure analysis.

3.1 Abstract

Heme oxygenase (HO) catalyzes the first step in the heme degradation pathway. The crystal structures of apo and heme-bound truncated human heme oxygenase-2 (HO-2) reveal a primarily α-helical architecture similar to that of human heme oxygenase-1 (HO-1), and other known HOs. Proper orientation of heme in HO-2 is required for the regioselective oxidation of the α-meso carbon. This is accomplished by interactions within the heme binding pocket which is made up of two helices. The iron coordinating residue, His45 resides on the proximal helix. The distal helix contains highly conserved glycine residues that allow the helix to flex and interact with the bound heme. Tyr154, Lys199, and Arg203 orient the heme through direct interactions with the heme propionates. The rearrangements of sidechains in heme-bound HO-2 compared to apo HO-2 further elucidate HO-2 heme interactions.

3.2 Introduction

Heme oxygenase (HO) catalyzes the degradation of heme to free iron, carbon monoxide and biliverdin in the presence of NADPH-dependent cytochrome P450 reductase. Seven electrons are transferred and three molecules of oxygen are consumed in the degradation of one molecule of heme to biliverdin (**Figure 1.1**). Subsequently, biliverdin reductase reduces biliverdin to bilirubin (1). Present in both bacteria and eukaryotes, HO is the only known enzyme that can degrade heme. HO not only plays a critical role in heme and iron homeostasis, but the products of heme degradation have important physiological functions (1,2). Iron is the essential catalytic center for heme and many nonheme metalloenzymes and has crucial effects on cytoprotection (3,4). Although CO is toxic at levels above approximately 500 ppm, it also is a signaling molecule (5,6). CO has anti-apoptotic, anti-inflammation, and anti-proliferation properties (7-9). Bilirubin is an antioxidant that is involved in resistance to oxidative stress (10,11).

Two HO isoforms have been reported in mammalian cells, heme oxygenase-1 (HO-1) and heme oxygenase-2 (HO-2) (12). The mammalian HO-1 and HO-2 exhibit similar catalytic activities and share 55% identity and 76% similarity in humans (13,14). Another isoform, HO-3, was recently reported in rat; however, no activity was detected for this isoform and it is considered a pseudogene (15). Plants contain several HOs, including one named HO-2, but these lack the C-terminal membrane spanning region seen in mammalian HOs and are more closely related to the bacterial and insect HO-1 than to the mammalian HO-2 (13,16).

Although they are both membrane-bound proteins and their catalytic activities are similar, HO-1 and HO-2 are expressed in discrete tissues and exhibit very different patterns of expression (17). While human HO-1 is an inducible protein whose expression is induced by heat shock and oxidative stress conditions, HO-2 is constitutively expressed (17-22). HO-1 has been found in most tissues, with particularly high expression levels in liver and spleen; however, HO-2 is mainly found in the brain, testes and carotid body (23-26).

HO-1 and HO-2 exhibit two regions of sequence divergence: one is around residue 127 and the other is near the C-terminus between residues 240 and 295 (HO-2 numbering throughout unless otherwise stated). In both HO-1 and HO-2, the C-termini appear to

play regulatory roles, albeit of quite different natures. Cleavage of the 52 amino acids at the C-terminus of HO-1 affects nuclear import, leading to the activation of genes associated with protection against oxidative stress (27). In HO-2, the C-terminal region between residues 255 and 287 contains two heme regulatory motifs (HRMs), which form a thiol/disulfide redox switch that regulates heme binding affinity (28).

As full-length HO-1 and HO-2 are relatively unstable, most structure-function studies have used truncated proteins in which the membrane region has been removed. The truncated mammalian HO-2 can be expressed at high levels in *Escherichia coli* and, as was first shown for HO-1, has a specific activity that is identical to that of the full-length protein (29). The first three-dimensional structure of human HO-1 was determined for the truncated protein in 1999 (30). Subsequently, many HO-1 crystal structures have been reported, including rat HO-1, biliverdin associated HO-1, ferrous/ferrous-NO bound HO-1 and some HO-1 variants (31-33). These structures led to significant advances in the study of the HO-1 catalytic mechanism (34). The HO-2 used in this study is the soluble portion of HO-2 with a mutation of Cys127 to an alanine and is missing residues 264 – 316, and will be referred to as HO-2 in this paper. Here we report the first apo and heme-bound HO-2 crystal structures at 2.4 Å and 2.6 Å resolution, respectively.

3.3 Materials and methods

3.3.1 Cloning, overexpression, and purification of human HO-2

The full-length human HO-2 cDNA in a pGEX-4T-2 (Amersham GE Healthcare, Piscataway, NJ) GST gene fusion vector was kindly provided by Dr. Mahin D. Maines (University of Rochester, School of Medicine). The truncated HO-2 lacking the three HRMs and the membrane binding region was generated by replacing Cys127 with Ala127 and putting the "TAA" stop codon right before Cys265, which will be referred to as HO-2 in this paper. The QuikChange site-directed mutagenesis protocol from Stratagene (La Jolla, CA) was used for variant generation. A glutathione affinity column was used to help purify HO-2 since the human HO-2 fragment was fused to glutathione S-transferase (GST) in this construct.

HO-2 purification was performed as previously described with slight modifications (28). The newly generated construct was transformed into *E.coli* strain BL21(DE3) for protein overexpression. Cells were grown in LB medium containing 100 μg/ml ampicillin at 37 °C and induced with 0.3mM isopropyl-beta-D-thiogalactopyranoside (IPTG, Gold Biotechnology, Inc, St. Louis, MO). 5-Aminolevulinic acid hydrochloride (Sigma-Aldrich, St. Louis, MO) was added to help the induction of HO-2. After cell harvest, the pellet was resuspended in 5 volumes of lysis buffer (50 mM KCl, 50 mM Tris-HCl pH 7.5), containing 0.04% (v/v) Triton X-100 (Sigma-Aldrich), protease inhibitor (1 tablet/50mL extraction solution, Roche Applied Science, Indianapolis, IN), lysozyme (0.5 mg/ml, Sigma-Aldrich) and DnaseI (5 units/ml, Sigma-Aldrich) at 4 °C.

Cells were lysed by sonication, and the supernatant was loaded onto a glutathione sepharose 4B column (Amersham GE Healthcare). After washing the resin with a buffer containing 50 mM KCl, 50 mM Tris-HCl, pH 7.5, the HO-2-GST fusion protein was eluted with the same buffer containing 10 mM reduced glutathione. Then the glutathione in the fractions was removed through dialysis, and the GST domain was cleaved by limited proteolysis using thrombin. The HO-2 was separated from the GST tag with another glutathione sepharose 4B column. The protein was then concentrated to 5 mg/ml for crystallization. To make heme-bound HO-2, aliquots of a freshly prepared heme solution (0.1 M NaOH solution containing 10% dimethyl sulfoxide (DMSO)) were slowly diluted into a purified apo HO-2 protein solution to give a 2:1 molar ratio of heme

to protein. Less than 5% (volume ratio) of the heme solution was added to prevent any noticeable change in pH of the final heme-protein solution. All purification steps were carried out at 4°C.

3.3.2 HO-2 crystal preparation

Crystals of the apo HO-2 were grown using the hanging drop method with 1.5 μl of a 5 mg/ml protein solution (50mM KCl, 50 mM Tris-HCl pH 7.5) mixed with 1.0 μl of well solution containing 40% polyethylene glycol 1.5K (Fluka, St. Louis, MO), 200 mM potassium glutamate, and 100 mM triethanolamine pH 8.5 at 277 K. The heme-bound HO-2 crystals were grown using the hanging drop method with 1.5 μl of 5 mg/ml^{-1} protein solution in a (50mM KCl, 50mM Tris-HCL pH 7.5) mixed with 1.0 μl of well solution containing 33% polyethylene glycol dimethly ether 500 (Sigma-Aldrich), 20 mM $MgCl_2$, and 100 mM 4-(2-Hydroxyethyl)-1-Piperazine-Propane-Sulfonic Acid (HEPPS) pH 8.5 at 277 K

3.3.3 X-ray data collection and structure solution

X-ray diffraction data for the apo HO-2 structure was collected at a wavelength of 0.97933 Å at The General Medicine and Cancer Institutes Collaborative Access Team (GM/CA-CAT) beamline 23-ID-D located at the Advanced Photon Source (APS) at Argonne National Laboratory. The diffraction data for the heme HO-2 structure was also collected at the GM/CA-CAT beamline 23-ID-B utilizing a wavelength of 0.97946 Å. Both data sets were indexed and scaled using HKL2000 (35). Molecular replacement was carried out with MOLREP using human heme oxygenase-1 (PDB ID 1N45) as the initial model (36). An initial apo HO-2 model was partially built with ARP/wARP resulting in a structure with 54.7% of the possible residues positioned (37). The apo HO-2 structure was completed with several rounds of manual building with Coot and restrained refinement in REFMAC (38,39). The refined apo HO-2 structure was used as the molecular replacement model for the heme-bound HO-2 structure. The heme-bound HO-2 model was then completed as described for apo HO-2. The refinement process for apo HO-2 was monitored using an R_{free} value based on 5.1% of all the independent reflections. The same set of reflections was used to calculate R_{free} in the heme-bound HO-2 structure.

The quality of the final structures was assessed using MOLPROBITY and PROCHECK (40,41). The final model of apo HO-2 was refined to a resolution of 2.40 Å

with an R factor of 0.205 and an R_{free} of 0.253. Heme-bound HO-2 was refined to a resolution of 2.61 Å with an R factor of 0.195 and an R_{free} of 0.256. The 16-conformer heme-bound HO-2 structure had a R factor of 0.156 and an R_{free} of 0.244. All pertinent information on data collection, refinement, and model statistics of apo and heme-bound HO-2 are summarized in **Table 3.1**. Figures were generated using PyMOL and Chimera (42).

TABLE 3.1 **Crystal parameters, X-ray data collection, and refinement statistics.**

	Apo Human HO-2	**Heme Human HO-2**
Space group	$P2_12_12_1$	$P2_12_12_1$
Unit cell parameters (Å)	A = 75.769, B = 86.017, C = 97.753	A = 74.977, B = 85.094, C = 97.846
Data collection statistics		
Wavelength (Å)	0.97933	0.97946
Resolution range (Å)	50.0-2.3 (2.38-2.30)	40.96-2.32 (2.4-2.32)
Number of reflections (measured / unique)	203168 / 28128	278069 / 24030
Completeness (%)	95.9 (78.2)	85.6 (27.4)
R_{merge}	0.08200	0.08300
Redundancy	7.3 (3.9)	11.6 (1.8)
Mean I/σ(I)	21.89 (1.93)	19.2 (0.776)
Refinement and model statistics		
Resolution range	49.15-2.40 (2.46-2.40)	40.96–2.61 (2.68–2.61)
No. of reflections (work / test)	25217	19515
R_{cryst}	0.201	0.205
R_{free}	0.253	0.256
r.m.s.d. bonds (Å)	0.011	0.006
r.m.s.d. angles (˚)	1.255	0.951
ESU from R_{free} (Å)[e]	0.249	0.305
B factor		
Wilson plot (Å)	59.62	65.96
No. of protein molecules / atoms	2 / 3621	2 / 3563
No. of waters	154	86
No. of ions	0	0
No. of auxiliary molecules	2 Triton X-100	2 Hemin
Ramachandran plot (%)		
Most favorable region	93.2	94.7
Additional allowed region	6.8	5.3
Generously allowed region	0.0	0.0
Disallowed region	0.0	0.0
PDB code	2Q32	2QPP

3.4 Experimental results

3.4.1 HO-2 overall structure

The HO-2 that was used in this study lacked the two C-terminal HRM domains (265-316), and had Cys 127 mutated to Ala. These alterations to HO-2 were done to increase the likelihood of crystallization. Two molecules of HO-2 were observed in the asymmetric unit of both apo HO-2 and heme-bound HO-2. Out of the 264 residues in the truncated apoprotein, 212 residues were observed in molecule A, and 217 residues were observed in molecule B. Molecule A of apo HO-2 was lacking electron density in both the N-terminal (Met1 – Met28), and the C-terminal (Ser242 – Lys264) regions. The B molecule of apo HO-2 was lacking density for several N-terminus (Met1 – Met30), and C-terminus (Leu249 – Lys264) residues. There were two partially resolved molecules of Triton X-100 observed near the heme-binding site in both apo HO-2 molecules. Similarly, in the heme-bound HO-2 structure, 213 residues were observed in molecule A and 218 residues were observed in molecule B. The A molecule of heme-bound HO-2 was lacking electron density for Met1 – Met28, and Thr243 – Lys264. The B molecule of heme-bound HO-2 was missing density for Met1 – Arg29, and Leu249 – Lys264. In all previous HO-1 structures, the C-terminal residues also have not been observed.

In the B molecule of heme-bound HO-2, the heme was modeled at 75% occupancy. Elongated positive electron density was observed near the heme in both molecules of the heme-bound HO-2 structure. Compared to the A molecule the heme pocket of the B molecule was more disordered. The four pyrrole rings of the heme in the B molecule were restrained during refinement to form a plane. There was no need to restrain the heme in molecule A beyond the default REFMAC parameters. In addition to REFMAC restrained refinement the heme-bound HO-2 was also modeled using ensemble refinement using CNS (PDB id 2RGZ) (43,44). The disorder of the heme in the heme pocket of the B molecule can be seen in the 16-conformer ensemble refinement (**Figure 3.1**).

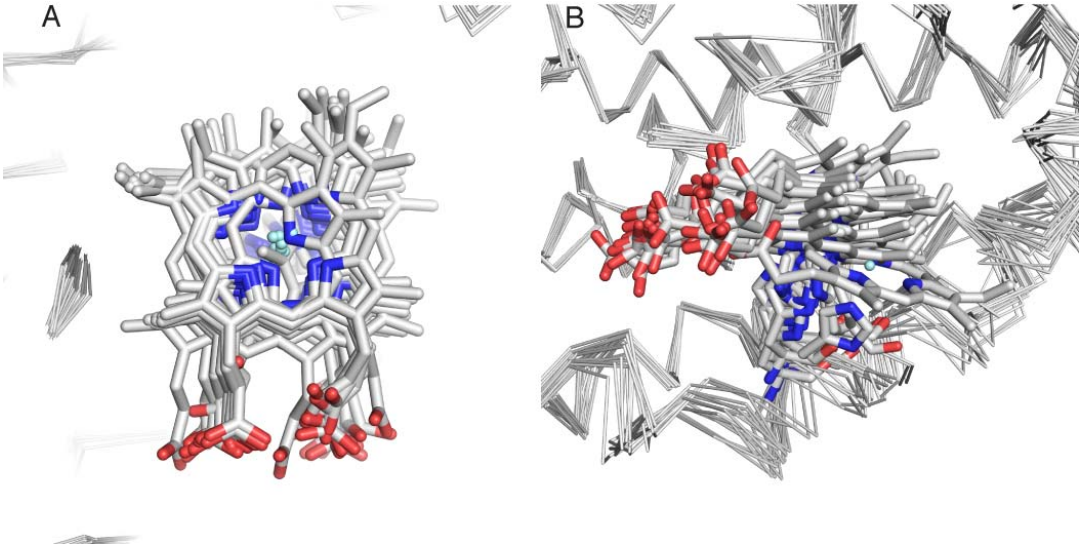

FIGURE 3.1 **Results from the ensemble refinement of heme-bound HO-2.** The spatial distribution of the heme molecule can be seen in the **A,** top view and the **B,** side view of the 16-conformer model of the heme-bound HO-2 B molecule.

The secondary structural elements of HO-2 are almost exclusively α-helical, with short loop segments that connect adjoining α-helixes (**Figure 3.2**). The overall structure of HO-2 is nearly identical to those of human (30) and rat HO-1 (45) (**Figure 3.3A, 3.3B**), the bacterial HOs (*N. meningitidis* HmuO (46), *C. diphtheriae* HemO (47), and *P. aeruginosa* PigA (48)), as well as the Synechocystis HOs (49,50). These similarities include the kinked distal helix and heme binding site. Like HO-1 (45,51)and HmuO (34), the overall fold is maintained even in the absence of substrate heme.

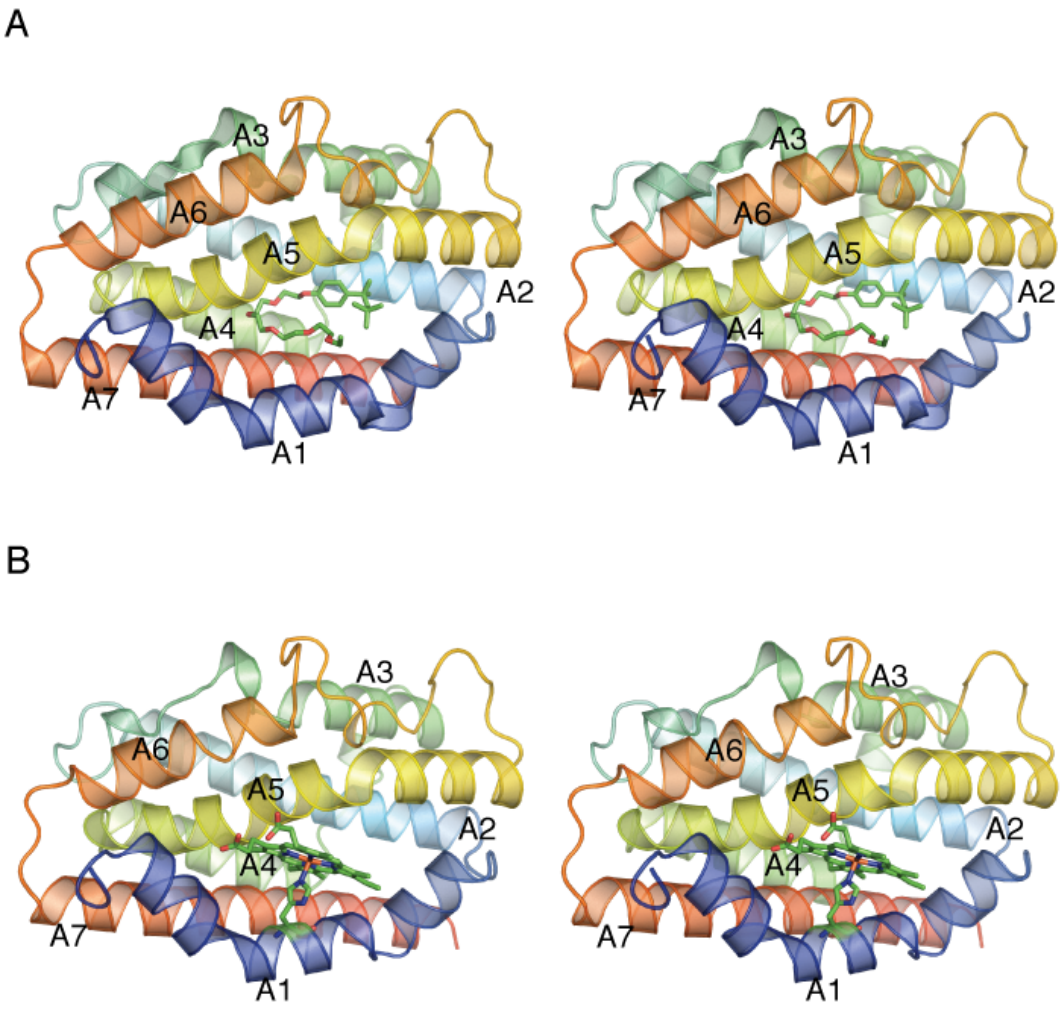

FIGURE 3.2 **The secondary structure of HO-2.** The secondary structure of HO-2 is shown with the N terminus in ***blue*** and the C terminus in ***red.*** The proximal helix is marked A1 and the distal helix is marked A5. **A,** Stereo view of human apo HO-2 secondary structure. Triton X- 100 is shown, with Carbon in green and oxygen in red, positioned in the hydrophobic cavity of HO-2. **B**, Stereo view of heme HO-2 secondary structure. Heme is shown, carbon in green, oxygen in red, nitrogen in blue, and iron in orange, attached to His45.

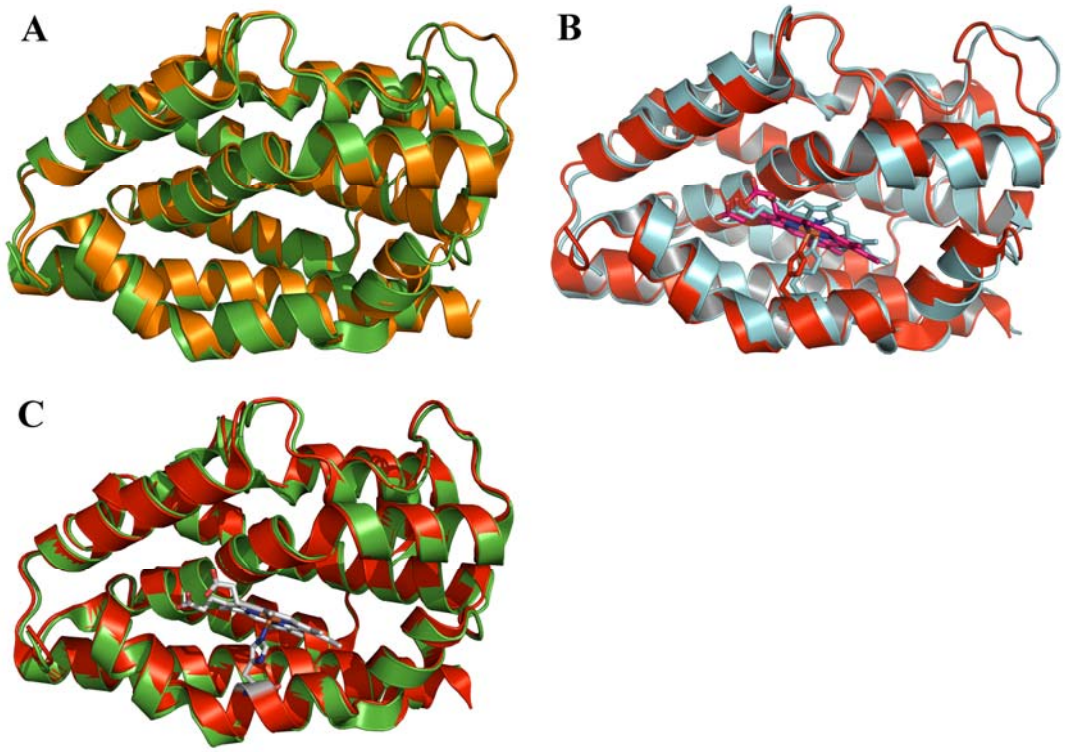

FIGURE 3.3 **Structure comparison between human HO-1 and HO-2. A,** structure comparison between apo-HO-1 (orange) and apo-HO-2 (green). **B,** structure comparison between heme-HO-1 (cyan) and heme-HO-2 (red). **C,** structure comparison between apo-HO-2 (green) and heme-HO-2 (red).

3.4.2 Distal helix in HO-2 structure

A flexible, highly conserved sequence (Gly159–Asp-Leu-Ser-Gly-Gly164), which is an integral part of the heme binding pocket, allows the distal helix to bend and come close to the heme (30,32,45,46,51-54). This glycine-rich flexible region in heme-bound HO-2 allows the backbone atoms of Gly159 to interact with the heme iron through a water molecule. Gly159 in apo HO-2 is in the same position as observed in heme-bound HO-2. The catalytically important Asp160 that resides on the distal helix is relatively unchanged in both apo and heme-bound HO-2 (55,56). The most striking differences between the distal helix in apo HO-2 and heme-bound HO-2 are found in the amino acids near the bound heme. In heme-bound HO-2, Tyr154 repositions to form a hydrogen bond with the propionate located in the heme pocket. The side chains of Thr155 and Arg156 in heme-bound HO-2 move away from the heme allowing more room in the heme pocket

(**Figure 3.4**). The expansion of the heme pocket caused by the movement of Thr155 and Arg156 is not observed in apo HO-2.

In the previously solved heme-bound human HO-1 structure, the two HO-1 monomers in the asymmetric unit were observed in slightly different conformations (30). Molecule A of the heme-bound HO-1 was considered to be in a closed conformation while molecule B was in an open conformation, which was proposed to be important in binding heme and/or releasing products (30). The difference between the open and closed conformation is the position of the distal helix with respect to the heme pocket. In the open conformation, the distal helix has moved away from the heme pocket, causing a slightly larger heme pocket compared to the closed conformation. In the HO-2 structures the movement of the distal helix occurs at Gly163. Gly163 moves away form the heme causing the heme pocket to adopt the open conformation. By comparing the overall r.m.s. deviation of the heme-bound HO-1 and HO-2 alpha-carbons it is apparent that both apo HO-2 and heme-bound HO-2 are in the open conformation (**Figure 3.3C, Table 3.2**). The movement of the distal helix at Gly163 is seen when the apo and heme-bound HO-2 structure is compared to the closed heme-bound HO-1 structure (**Figure 3.5**). All other significant backbone atom deviations between HO-2 and HO-1 are located in the loops between helices.

TABLE 3.2 **r.m.s. deviation of carbon-α atoms between apo and heme-bound molecules of HO-1 and apo and heme-bound molecules of HO-2**

	r.m.s deviation	
	Closed HO-1	Open HO-1
Apo HO-2 Molecule A	0.897	0.786
Apo HO-2 Molecule B	0.881	0.770
Heme HO-2 Molecule A	0.862	0.731
Heme HO-2 Molecule B	0.842	0.697

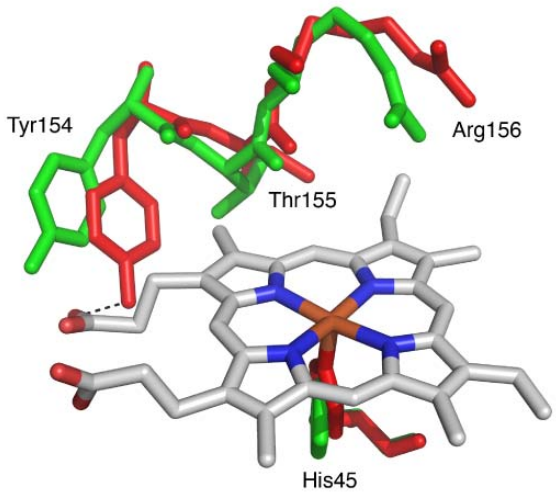

FIGURE 3.4 **Proximal helix side-chain rearrangement observed in heme-bound HO-2 caused by heme binding.** The amino acids in red are from heme HO-2, whereas the amino acids in green are from apo HO-2. The coordinated heme is shown with carbon in white, nitrogen in blue, oxygen in red, and iron in orange.

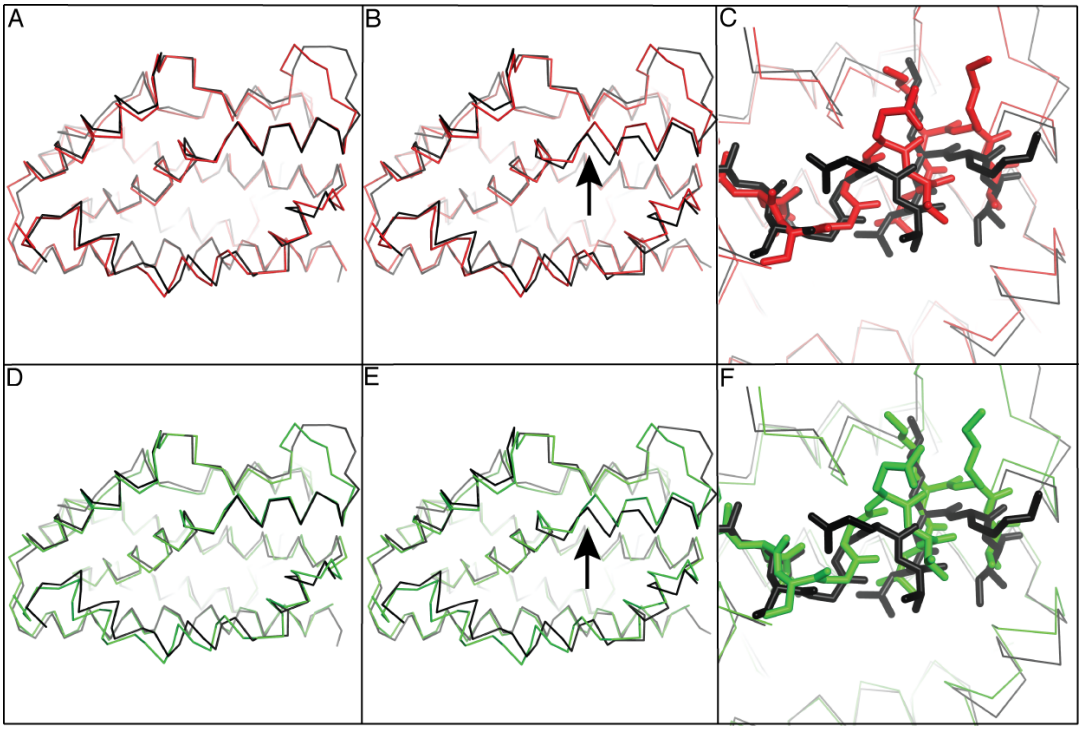

FIGURE 3.5 **Comparison of apo and heme-bound HO-2 to the open and closed conformations of the previously solved heme bound HO-1 structure. A,** Heme-bound HO-2 ribbon diagram in red superimposed over the open conformation of heme-bound HO-1 in black. **B,** Heme-bound HO-2 ribbon diagram superimposed over a ribbon diagram of the closed conformation of heme-bound HO-1. The black arrow shows the position in the distal helix where heme HO-2 deviates from heme HO-1. **C,** Sticks representation of the distal helix (160-170) of heme-bound HO-2 in red superimposed over the closed form of heme-bound HO-1 in black. **D,** Apo HO-2 ribbon diagram in green superimposed over the open conformation of heme HO-1 in black. **E,** Apo HO-2 ribbon diagram superimposed over a ribbon diagram of the open conformation of heme-HO-1. The arrow shows the position were apo HO-2 deviates from the closed conformation of heme HO-1. Both apo and heme-bound HO-2 start to deviate from closed heme HO-1 at similar positions along the distal helix. F, Sticks representation of distal helix (160-170) of apo HO-2 in green superimposed over the closed form of heme-bound HO-1 in black.

3.4.3 Proximal helix in HO-2 structure

Unlike the distal helix, the proximal helix lacks any flexible region that would allow the helix to translocate during heme binding. The heme iron coordinating histidine, His45, resides on the proximal helix (**Figure 3.6**). His45 of heme-bound HO-2 coordinates the heme iron through an imidazole nitrogen with a bonding distance of 2.1 Å in the A molecule. The distance between the imidazole nitrogen of His45 and the heme iron was

restrained during refinement to a distance of 2.1 Å. A hydrogen bonding interaction with Glu49 serves to stabilize the iron coordinating histidine. A carboxyl oxygen from Glu49 forms a hydrogen bond with the imidazole nitrogen of His45 that is not coordinating the heme iron at a distance of 3.5 Å in molecule A and 3.8 Å in molecule B. The interaction between His45 and Glu49 is not present in the apo HO-2 structure. Without a bound heme, the imidazole ring of His45 of apo HO-2 is no longer restrained and adopts a different conformation than the one that is observed in heme-bound HO-2 (**Figure 3.6**). There is little change in the proximal helix with the exception of the movements of His45 and Glu49.

3.4.4 Hydrophobic region in HO-2 structure

The residues that make up the hydrophobic pocket, Val54, Phe53, Phe57, and Phe234 remain unchanged in both apo and heme-bound HO-2. In the heme-bound HO-2, the heme α-meso edge is positioned so that it is directed toward the residues that make up the hydrophobic region of the heme pocket. Unexplained positive electron density was observed between the hydrophobic region and the α-meso edge of the heme in the heme-bound HO-2 structure. We were unable to identify the compound giving rise to the density and the density was left un-modeled (**Figure 3.7A**). In the same region that the unexplained density was found in heme-bound HO-2, a molecule of Triton X-100 was observed in apo HO-2. The Triton X-100 molecule occupied a position near the hydrophobic region of the heme pocket where the heme α-meso edge would occupy (**Figure 3.7B**). The tetramethylbutyl group of the Triton X-100 was in the same position as the unexplained density in heme-bound HO-2.

3.4.5 Heme protein interactions

In HO-2 and other known HOs, the α, β, and γ-meso edges of the heme group are positioned in the interior of the heme pocket with the δ-meso edge exposed to the solvent. In order for the hydroperoxo form of HO-2 to specifically catalyze electrophilic attack on the heme α-meso carbon, the heme group needs to be properly oriented in relation to the heme pocket. The way that HO-2 seems to orientate the bound heme is through interaction with the propionate groups. One of the heme propionate groups is buried in the heme pocket while the other is exposed to solvent. In the heme-bound HO-2 structure, there are three residues that play crucial roles in heme coordination (Tyr154, Lys199, and

Arg203). Tyr154 is located on the distal helix with its OH group 2.7 Å in molecule A and 2.9 Å in molecule B from one of the carboxyl oxygens of the buried propionate (**Figure 3.6**). Located on the A6 helix, Arg203 coordinates the a carboxyl oxygen of the buried propionate at a distance of 2.4 Å in b the A molecule and 2.6 Å the B molecules. The solvent exposed propionate is coordinated to Lys199 and could transiently hydrogen bond with Lys38. Like Arg203, Lys199 is located on the A6 helix and interacts with the solvent exposed propionate at a distance of 3.0 Å in both the A and B molecules. While Lys38 is too distant to form a hydrogen bond with the solvent exposed propionate in the crystal structure, a shift in the position of the propionate could cause the formation of a hydrogen bond. These hydrogen bonds correctly orient the heme and place the α-meso edge carbon in position for hydroxylation (**Figure 3.6**).

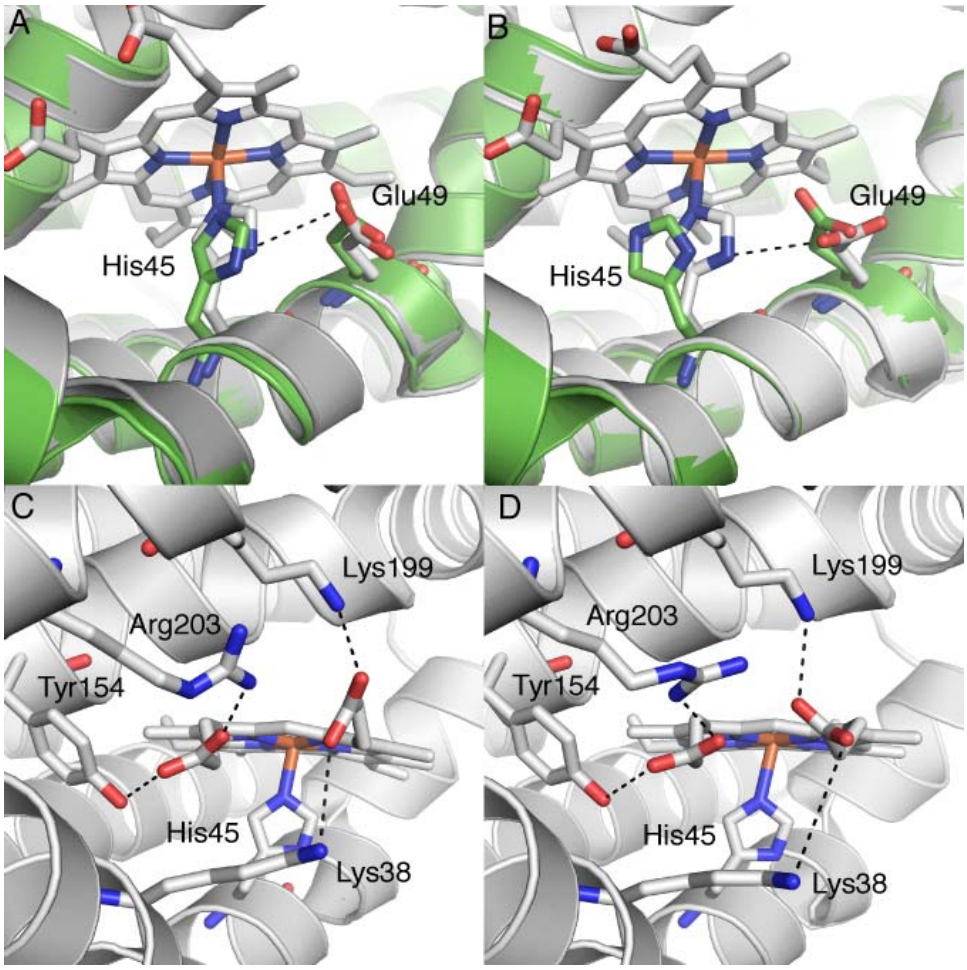

FIGUR E 3.6 **Movement of the distal histidine in apoHO-2 compared with the distal histidine of heme-bound HO-2. A,** molecule A of heme-bound HO-2 shown in gray, compared with the A molecule of apoHO-2 in green. The dashed line represents a hydrogen bond between His45 and Glu49 in the heme-bound HO-2. **B,** molecule B of heme-bound HO-2 in gray compared with the B molecule of apoHO-2 in green. The dashed line represents a hydrogen bond between His45 and Glu49 in the heme-bound HO-2. **C,** protein heme interactions in the A molecule of heme-bound HO-2. The hydrogen bonding amino acids that position the heme are shown in gray. The hydrogen bonds are shown with dashed black lines. **D,** protein heme interactions in the B molecule of heme-bound HO-2. The hydrogen-bonding amino acids that position the heme are shown in gray. The hydrogen bonds are shown with dashed black lines.

3.5 Discussion

The two structures we present are of the core domain of human HO-2. These truncated human HO-2 structures contain the region responsible for heme recognition, binding, and degradation, elucidating the important structural features of HO-2 and improving our understanding of the catalytic mechanism of HO-2. The structures indicate that the catalytic cores of HO-1 and HO-2 are structurally conserved, and the major differences underlying the diverse physiological functions of HO-1 and HO-2 may lie in the C-terminus of the two proteins.

3.5.1 Hydrophobic cavity

The conformation of the HO-2 heme pocket can be directly affected by the hydrophobic cavity. One possible reason that both HO-2 structures were observed in an open conformation could be due to the Triton X-100 in apo HO-2 and the un-modeled electron density in heme-bound HO-2. The Triton X-100, which occupies a position near the hydrophobic cavity, might hinder the heme pocket from assuming a closed conformation. Though there is no definitive evidence, it seems likely that the extra electron density that was observed adjacent to the heme in the heme-bound HO-2 structure is a DMPEG 500 molecule from the crystallization solution. The DMPEG 500 of heme-bound HO-2 could act in a similar way as the Triton X-100 in apo HO-2, and force the distal helix into the open conformation.

This is not the first time that something has been found in proximity to the hydrophobic region. A crystal structure of HO-1 in complex with biliverdin shows that the biliverdin binding site is adjacent to the hydrophobic pocket, and, compared to the heme binding site of HO-1, it has moved further into the interior of the heme pocket (52). A portion of the biliverdin molecule in HO-1 occupies the same position as Triton X-100 in apo HO-2 and unaccounted electron density in heme-bound HO-2. It appears that this large cavity in HOs plays a role in hydrophobic substrate binding.

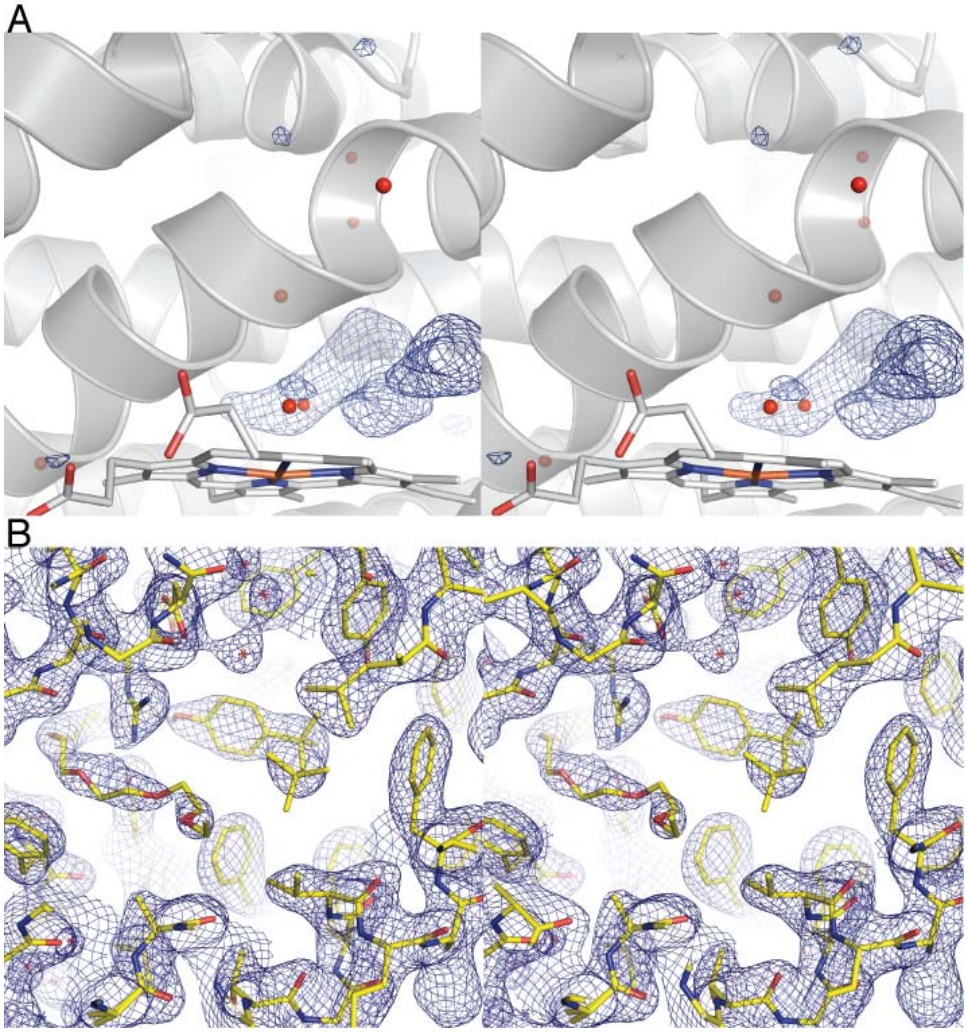

FIGURE 3.7 **Electron density maps of apo- and heme-bound HO-2. A,** stereo view of the F_o - F_c map of the heme-bound HO-2 heme pocket contoured at 3σ. The heme group is shown with carbon in gray, oxygen in red, and iron in orange. The red spheres represent water molecules. **B,** stereo view of the 2 F_o - F_c of the hydrophobic region in the heme pocket of apoHO-2 shown at 1 σ. The Triton X-100 is shown with carbon in yellow and oxygen in red.

3.5.2 Comparison of HO-1 and HO-2

There is a high level (45%) of sequence identity between full-length HO-1 and HO-2 (**Figure 1.3**), with 55% identity in the conserved core regions of HO-1 and HO-2. The heme pocket regions in HO-1 and HO-2 are highly conserved. With such a high level of identity, it is not surprising that the core domains of HO-1 and HO-2, which are responsible for the heme binding and degradation, share a similar fold. Both HO-1 and

HO-2 structures consist mostly of alpha helices (**Figure 3.3**). Overall the secondary structure of HO-2 closely resembles apo-HO-1 and heme-bound HO-1.

It has been shown that mutating Asp140 to an Ala converts HO-1 into a peroxidase (56). It is proposed that the Asp140 to Ala mutant can not stabilize the peroxide bond and therefore forms an Fe^{+4}-O oxyferryl center instead of the Fe^{+3}-OOH reactive intermediate (57). Asp140 stabilizes the Fe^{+3}-OOH intermediate through a hydrogen bonding network with water molecule located near the heme and the Fe^{+3}-OOH intermediate. In the high-resolution heme-bound HO-1 structure, the water molecules thought to be involved in this hydrogen bond network were observed in the closed conformation (51). The open conformation of heme-bound HO-1 has a much less ordered solvent structure with some water thought to be at a partial occupancy. This disorder in the open confirmation may explain why the solvent structure is not seen in the heme-bound HO-2 structure. Even though the entire hydrogen network is not resolved in the heme-bound HO-2 structure, Asp160 still adopts the same conformation as Asp140 in the heme-bound HO-1 model, and is thought to act in a similar fashion.

Although the C-terminal HRM region shows the most significant sequence divergence between HO-1 and HO-2, most of the key amino acids involved in heme binding, Lys38, His45, Glu49, Tyr154, G159, Asp160, Gly163, Lys199, and Arg203 are observed in similar positions in the heme-bound HO-2 structure when compared to heme-bound HO-1. The major differences in the crystal structure of apo HO-2 and heme-bound HO-1 are seen in the helices that directly interact with the heme. The proximal helix of apo HO-2 moves slightly downward and the distal helix moves upward relative to heme-bound HO-1. In heme-bound HO-2, the same displacement of the distal helix is observed when compared to heme-bound HO-1.

3.5.3 Regioselectivity

When free heme is oxidized by ascorbate in an aerobic environment, all four of the heme meso carbons are oxidized with equal frequency (58). The oxidation of heme by HO-1 can also be driven with ascorbate without cytochrome P450 reductase, but the reaction only results in the oxidation of the heme α-meso carbon, just as in the reaction performed in the presence of the reductase (59). Spectroscopic, crystallographic and enzymatic studies have provided important information on the steric and electronic

factors that control regioselectivity in the bacterial and mammalian HOs (34,59,60). The crystal structure described here provides additional insight into how the oxidation of the heme in HO-2 is limited to the α-meso carbon. The distal helix is positioned so that the helix is in close proximity across the entire width of the heme. This sterically hinders access to the β- γ- and δ-meso carbons. In order for the distal helix to restrict access to the β- γ- and δ-meso carbons the heme has to be properly positioned in the heme pocket. As seen in other α-hydroxylating HOs, the interactions between Tyr154, Lys199, Arg203, and to a lesser extent Lys38, and the heme propionates are responsible for positioning the heme in the heme pocket. Disrupting these sidechain-heme interactions can result in the loss of regioselectivity (59-62). Heme oxygenase from *Pseudomonas aeruginosa* (pa-HO or PigA), unlike mammalian HOs, oxidizes the heme at the δ-meso carbon (61,63). Asn19, Phe117, Lys132 and Trp158 of pa-HO interact with the heme instead of Tyr154, Lys199, and Arg203 in heme-bound HO-2. The position of the heme in pa-HO is rotated by ~100° counterclockwise, placing the δ-meso carbon in the same position as the α-meso in HO-2 (48,61). Lys13 coordinates the heme propionate in pa-HO, and the distal helix restricts access to all but the δ-meso carbon. It is apparent that the position of the heme in relation to the heme pocket is the cause of the regioselectivity of HO-2.

3.5.4 An implication for catalysis

HO-2, unlike globins, does not have a distal histidine or any other polar residues that stabilize the iron bound ligand. The only moiety that is in position to stabilize the distal water ligand is the carbonyl oxygen of Gly159. Asp160, which interacts indirectly with the iron hydroperoxy intermediate through a hydrogen bonded water molecule, is hydrogen bonded to a water molecule in a similar position to a water molecule seen in heme-bound HO-1. Both molecules of heme-bound HO-2 were in the open conformation when compared to heme-bound HO-1. The open confirmation of heme-bound HO-1 did not have a fully resolved solvent structure (51). It is likely that the open conformation of heme-bound HO-2 would act in a similar manner to the open confirmation of heme-bound HO-1 and the entire solvent structure would not be observed. It is likely that when HO-2 binds heme, the heme pocket closes, trapping the necessary water molecules that then form a hydrogen bonding network with Asp160. The water molecule network could act as a proton transport system required to form the Fe^{+3}-OOH intermediate, which

subsequently attacks the α-meso carbon. This H-bonding network also appears to be involved in promoting conformational dynamics associated with catalysis (64).

3.6 Conclusion

In this chapter, we report the first apo and heme-bound HO-2 crystal structures using a truncated HO-2 that contains the residues 1-264 with a mutation of Cys127 to Ala. The apo and heme-bound HO-2 crystal structures are solved at 2.4 Å and 2.6 Å resolution, respectively. Both the apo and heme-bound HO-2 crystal structures consist of seven α-helixes, with α-helix 1 and α-helix 5 as proximal and distal helixes, respectively. The His45 residue, which is located at the proximal helix, is confirmed as the iron coordinating residue in our structures. A conserved glycine-rich, flexible segment (G_{159}DLSGG_{164}) exists in the distal helix, facilitating the distal helix to bend and interact with the heme in the active site. Gly159 interacts with the heme iron through a water molecule. This water ligation is supported by a hydrogen bond network, in which Asp160 and Gly163 are involved. Furthermore, the orientation of bound heme is cooperatively maintained by Tyr154, Lys199, and Arg203, which can interact with the heme propionates through hydrogen bonds directly. The translocation of the sidechains, which is composed of Tyr154, Thr155, and Agr156, happens when the heme binds to the active site. This rearrangement further elucidates HO-2 heme interactions and heme degradation mechanism.

3.7 References

1. Maines, M. D. (2005) *Antioxidants & redox signaling* **7**(11-12), 1761-1766
2. Farombi, E. O., and Surh, Y. J. (2006) *Journal of biochemistry and molecular biology* **39**(5), 479-491
3. Grosser, N., Oberle, S., Berndt, G., Erdmann, K., Hemmerle, A., and Schroder, H. (2004) *Biochemical and biophysical research communications* **314**(2), 351-355
4. Ragsdale, S. W. (2006) *Chemical reviews* **106**(8), 3317-3337
5. Kim, H. P., Ryter, S. W., and Choi, A. M. (2006) *Annual review of pharmacology and toxicology* **46**, 411-449
6. Ryter, S. W., Morse, D., and Choi, A. M. (2004) *Sci STKE* **2004**(230), RE6
7. Moore, B. A., Overhaus, M., Whitcomb, J., Ifedigbo, E., Choi, A. M., Otterbein, L. E., and Bauer, A. J. (2005) *Critical care medicine* **33**(6), 1317-1326
8. Otterbein, L. E., Soares, M. P., Yamashita, K., and Bach, F. H. (2003) *Trends in immunology* **24**(8), 449-455
9. Yachie, A., Niida, Y., Wada, T., Igarashi, N., Kaneda, H., Toma, T., Ohta, K., Kasahara, Y., and Koizumi, S. (1999) *The Journal of clinical investigation* **103**(1), 129-135
10. Baranano, D. E., Rao, M., Ferris, C. D., and Snyder, S. H. (2002) *Proceedings of the National Academy of Sciences of the United States of America* **99**(25), 16093-16098
11. Fondevila, C., Shen, X. D., Tsuchiyashi, S., Yamashita, K., Csizmadia, E., Lassman, C., Busuttil, R. W., Kupiec-Weglinski, J. W., and Bach, F. H. (2004) *Hepatology (Baltimore, Md* **40**(6), 1333-1341
12. Maines, M. D., and Gibbs, P. E. M. (2005) *Biochemical and biophysical research communications* **338**(1), 568-577
13. Terry, M. J., Linley, P. J., and Kohchi, T. (2002) *Biochemical Society Transactions* **30**, 604-609
14. Watanabe, T., Kikuchi, M., Hatakeyama, D., Shiga, T., Yamamoto, T., Aonuma, H., Takahata, M., Suzuki, N., and Ito, E. (2007) *Developmental Neurobiology* **67**(4), 456-473
15. McCoubrey, W. K., Huang, T. J., and Maines, M. D. (1997) *European Journal of Biochemistry* **247**(2), 725-732
16. Davis, S. J., Bhoo, S. H., Durski, A. M., Walker, J. M., and Vierstra, R. D. (2001) *Plant physiology* **126**(2), 656-669
17. Maines, M. D. (1997) *Annual review of pharmacology and toxicology* **37**, 517-554
18. Alam, J., Shibahara, S., and Smith, A. (1989) *J Biol Chem* **264**(11), 6371-6375

19. Keyse, S. M., Applegate, L. A., Tromvoukis, Y., and Tyrrell, R. M. (1990) *Molecular and Cellular Biology* **10**(9), 4967-4969
20. Lin, J. H., Villalon, P., Martasek, P., and Abraham, N. G. (1990) *European journal of biochemistry / FEBS* **192**(3), 577-582
21. Rizzardini, M., Terao, M., Falciani, F., and Cantoni, L. (1993) *The Biochemical journal* **290 (Pt 2)**, 343-347
22. Wu, W. T., Chi, K. H., Ho, F. M., Tsao, W. C., and Lin, W. W. (2004) *The Biochemical journal* **379**(Pt 3), 587-593
23. Maines, M. D., Eke, B. C., and Zhao, X. (1996) *Brain research* **722**(1-2), 83-94
24. Pimstone, N. R., Engel, P., Tenhunen, R., Seitz, P. T., Marver, H. S., and Schmid, R. (1971) *The Journal of clinical investigation* **50**(10), 2042-2050
25. Tenhunen, R., Marver, H. S., and Schmid, R. (1970) *The Journal of laboratory and clinical medicine* **75**(3), 410-421
26. Trakshel, G. M., Kutty, R. K., and Maines, M. D. (1986) *J Biol Chem* **261**(24), 11131-11137
27. Lin, Q., Weis, S., Yang, G., Weng, Y. H., Helston, R., Rish, K., Smith, A., Bordner, J., Polte, T., Gaunitz, F., and Dennery, P. A. (2007) *J Biol Chem* **282**(28), 20621-20633
28. Yi, L., and Ragsdale, S. W. (2007) *J Biol Chem* **282**(29), 21056-21067
29. Wilks, A., and Ortiz de Montellano, P. R. (1993) *J Biol Chem* **268**(30), 22357-22362
30. Schuller, D. J., Angela Wilks, Paul R. Ortiz de Montellano and Thomas L. Poulos. (1999) *Nature Structural Biology* **6**, 860-867
31. Lad, L., Wang, J., Li, H., Friedman, J., Bhaskar, B., Ortiz de Montellano, P. R., and Poulos, T. L. (2003) *Journal of molecular biology* **330**(3), 527-538
32. Sugishima, M., Sakamoto, H., Higashimoto, Y., Noguchi, M., and Fukuyama, K. (2003) *J Biol Chem* **278**(34), 32352-32358
33. Sugishima, M., Sakamoto, H., Noguchi, M., and Fukuyama, K. (2003) *Biochemistry* **42**(33), 9898-9905
34. Masaki Unno, Toshitaka. Matsui, and Masao Ikeda-Saito. (2007) *Natural Product Reports* **24**, 553-570
35. Otwinowski, Z. M., Wladek (1997) *Macromolecular Crystallography, Part A*, 307-326
36. A.Vagin, A. T. (1997) *Journal of Biological Chemistry* **30**, 1022-1025
37. Perrakis A, M. R., Lamzin VS. (1999) *Nature Structural Biology* **5**, 458-463
38. Cowtan, P. E. a. K. (2004) *Acta Crystallographica Section D - Biological Crystallography* **60**, 2126 - 2132

39. Murshudov, G. N., Vagin, A.A. & Dodson, E.J. (1997) *Acta Crystallographica Section D - Biological Crystallography* **53**, 240-255
40. R. A. Laskowski, M. W. M., D. S. Moss and J. M. Thornton. (1993) *Journal of Applied Crystallography* **26**, 283-291
41. Simon C. Lovell, I. W. D., W. Bryan Arendall III, Paul I. W. de Bakker, J. Michael Word, Michael G. Prisant, Jane S. Richardson, David C. Richardson. (2003) *Proteins: Structure, Function, and Genetics* **50**, 437-450
42. DeLano, W. L. (2002) The PyMOL Molecular Graphics System. In., DeLano Scientific LLC, San Carlos, CA, USA
43. Levin, E. J., Kondrashov, D. A., Wesenberg, G. E., and Phillips, G. N., Jr. (2007) *Structure* **15**(9), 1040-1052
44. Brunger, A. T., Adams, P. D., Clore, G. M., DeLano, W. L., Gros, P., Grosse-Kunstleve, R. W., Jiang, J. S., Kuszewski, J., Nilges, M., Pannu, N. S., Read, R. J., Rice, L. M., Simonson, T., and Warren, G. L. (1998) *Acta crystallographica* **54**(Pt 5), 905-921
45. Sugishima, M., Omata, Y., Kakuta, Y., Sakamoto, H., Noguchi, M., and Fukuyama, K. (2000) *FEBS Lett* **471**(1), 61-66
46. Schuller, D. J., Zhu, W., Stojiljkovic, I., Wilks, A., and Poulos, T. L. (2001) *Biochemistry* **40**(38), 11552-11558
47. Hirotsu, S., Chu, G. C., Unno, M., Lee, D. S., Yoshida, T., Park, S. Y., Shiro, Y., and Ikeda-Saito, M. (2004) *J Biol Chem* **279**(12), 11937-11947
48. Friedman, J., Lad, L., Li, H., Wilks, A., and Poulos, T. L. (2004) *Biochemistry* **43**(18), 5239-5245
49. Sugishima, M., Hagiwara, Y., Zhang, X., Yoshida, T., Migita, C. T., and Fukuyama, K. (2005) *Biochemistry* **44**(11), 4257-4266
50. Sugishima, M., Migita, C. T., Zhang, X., Yoshida, T., and Fukuyama, K. (2004) *European journal of biochemistry / FEBS* **271**(22), 4517-4525
51. Lad, L., Schuller, D. J., Shimizu, H., Friedman, J., Li, H., Ortiz de Montellano, P. R., and Poulos, T. L. (2003) *J Biol Chem* **278**(10), 7834-7843
52. Lad, L., Friedman, J., Li, H., Bhaskar, B., Ortiz de Montellano, P. R., and Poulos, T. L. (2004) *Biochemistry* **43**(13), 3793-3801
53. Lad, L., Ortiz de Montellano, P. R., and Poulos, T. L. (2004) *Journal of inorganic biochemistry* **98**(11), 1686-1695
54. Sugishima, M., Sakamoto, H., Kakuta, Y., Omata, Y., Hayashi, S., Noguchi, M., and Fukuyama, K. (2002) *Biochemistry* **41**(23), 7293-7300
55. Fujii, H., Zhang, X., Tomita, T., Ikeda-Saito, M., and Yoshida, T. (2001) *Journal of the American Chemical Society* **123**(27), 6475-6484

56. Lightning, L. K., Huang, H., Moenne-Loccoz, P., Loehr, T. M., Schuller, D. J., Poulos, T. L., and de Montellano, P. R. (2001) *J Biol Chem* **276**(14), 10612-10619
57. De Montellano, P. R. O. (1998) *Accounts of Chemical Research* **31**(9), 543-549
58. Sano, S., Sano, T., Morishima, I., Shiro, Y., and Maeda, Y. (1986) *Proceedings of the National Academy of Sciences of the United States of America* **83**(3), 531-535
59. Wang, J., Evans, J. P., Ogura, H., La Mar, G. N., and Ortiz de Montellano, P. R. (2006) *Biochemistry* **45**(1), 61-73
60. Deshmukh, R., Zeng, Y., Furci, L. M., Huang, H. W., Morgan, B. N., Sander, S., Alontaga, A. Y., Bunce, R. A., Moenne-Loccoz, P., Rivera, M., and Wilks, A. (2005) *Biochemistry* **44**(42), 13713-13723
61. Caignan, G. A., Deshmukh, R., Wilks, A., Zeng, Y., Huang, H. W., Moenne-Loccoz, P., Bunce, R. A., Eastman, M. A., and Rivera, M. (2002) *Journal of the American Chemical Society* **124**(50), 14879-14892
62. Wang, J., Lad, L., Poulos, T. L., and Ortiz de Montellano, P. R. (2005) *J Biol Chem* **280**(4), 2797-2806
63. Ratliff, M., Zhu, W., Deshmukh, R., Wilks, A., and Stojiljkovic, I. (2001) *Journal of bacteriology* **183**(21), 6394-6403
64. Rodriguez, J. C., Zeng, Y., Wilks, A., and Rivera, M. (2007) *Journal of the American Chemical Society* **129**(38), 11730-11742

Chapter 4

Spectroscopic Insights into Axial Ligation and Active-Site H-Bonding in Substrate-Bound Human Heme Oxygenase-2

This project was a collaboration with Dr. Thomas C Brunold's research group at the University of Wisconsin-Madison. The results from this chapter has been submitted for publication: **Gardner, J. D., Yi, L., Ragsdale, S. W., and Brunold, T.C.** "Spectroscopic Insights into Axial Ligation and Active-site H-bonding in Substrate-Bound Human Heme Oxygenase-2".

In this chapter, Jessica D. Gardner performed the magnetic circular dichroism (MCD) and resonance Raman (rR) experiments. Li Yi performed the sample preparation and the EPR and UV-visible spectroscopic experiements. Jessica D. Gardner and Thomas C Brunold analyzed the MCD and rR data. Li Yi and Stephen W. Ragsdale analyzed the EPR and UV-visible spectroscopic data.

4.1 Abstract

Heme oxygenases (HOs) are monooxygenases that catalyze the first step in heme degradation, converting heme to biliverdin with concomitant release of Fe(II) and CO from the porphyrin macrocycle. Two heme oxygenase isoforms, HO-1 and HO-2, exist that differ in several ways, including a complete lack of Cys residues in HO-1 and the presence of three Cys residues as part of heme regulatory motifs (HRMs) in HO-2. HRMs in other heme proteins are thought to directly bind heme, or to otherwise regulate protein stability or activity; however, it is not currently known how the HRMs exert these effects on HO-2 function. To better understand the properties of this vital enzyme and to elucidate possible roles of its HRMs, various forms of HO-2 possessing distinct alterations to the HRMs were prepared. In this study, variants with Cys265 in a thiol form are compared to those with this residue in an oxidized (part of a disulfide bond or existing as a sulfenate moiety) form. Absorption and magnetic circular dichroism spectroscopic data of these HO-2 variants clearly demonstrate that a new low-spin Fe(III)-heme species characteristic of thiolate ligation is formed when Cys265 is reduced. Additionally, absorption, magnetic circular dichroism, and resonance Raman data collected at different temperatures reveal an intriguing temperature dependence of the Fe spin state in the heme-HO-2 complex. These findings are consistent with the presence of a hydrogen-bonding network at the heme's distal side within the active site of HO-2 with potentially significant differences from that observed in HO-1.

4.2. Introduction

Heme is an Fe-containing cofactor necessary for a variety of biological processes (1). It is an integral component of the O_2 transport and storage proteins hemoglobin and myoglobin (2). Heme is also found in the cytochromes involved in the electron transport chain used for ATP synthesis. Additionally, heme serves as a cofactor in many enzymes, such as cytochromes P450, which are monooxygenases that insert oxygen into a variety of biological substrates, and peroxidases that catalyze oxidation-reduction reactions involving peroxides (3). Heme also plays a regulatory role as a small molecule sensor in proteins such as FixL, in which O_2 binding to heme ultimately regulates gene expression, and soluble guanylate cyclase, which is activated by binding of NO to heme (4-6). In spite of its importance, heme is toxic when it is free in the body. Free heme is a lipophilic molecule that can intercalate in, and thus destabilize, lipid bilayers of cell and organelle membranes (7,8). It also generates reactive oxygen species that can damage lipids, proteins, and DNA (8,9). A heme degradation pathway exists to prevent such damage. Heme is first oxidized by heme oxygenase (HO) to produce biliverdin, along with CO and Fe (10,11). The biliverdin is subsequently reduced by biliverdin reductase to bilirubin, which is less lipophilic and thus more readily excreted.

By catalyzing the first step in heme degradation, HO plays a vital role in maintaining proper heme homeostasis. Crystal structures of human forms of the enzymes have revealed that heme binds to HO in a highly conserved pocket of hydrophobic amino-acid residues (12-14). Several residues contribute to H-bonding interactions with peripheral substituents of the heme macrocycle to correctly orient the substrate within the active site. Additionally, the heme is ligated axially by a His residue from the protein and a solvent molecule. The reaction catalyzed by HO is intriguing in that heme serves as both cofactor and substrate, essentially catalyzing its own degradation (15). Catalytic mechanisms have been proposed wherein O_2 coordinates axially to Fe, replacing solvent in the distal position, and subsequently attacks the α-methine carbon of the heme macrocycle (11).

Two heme oxygenase isoforms, HO-1 and HO-2, exist that catalyze the same reaction but differ in several notable ways (16). HO-1 exhibits inducible expression, whereas HO-2 is expressed constitutively. Also, while HO-1 is localized predominantly

in the liver and spleen where it serves to break down excess heme, HO-2 is present at high levels in the brain where it is thought to contribute to cell signaling by formation of CO (16-18). Structurally, the two isoforms have very similar, though not entirely identical, heme-binding regions but otherwise exhibit a number of significant differences, including a complete lack of Cys residues in HO-1 and the presence of three Cys residues as part of heme regulatory motifs (HRMs) in HO-2 (19). HRMs are also found in a few other heme proteins and are thought to bind heme or to otherwise regulate protein stability and/or activity (20-27). For instance, the yeast gene transcriptional activator HAP1 is activated by heme binding to the Cys residue in its HRM, which blocks repressor binding (20). Also, binding of heme to an HRM in α-aminolevulinic acid synthase, the first enzyme in heme biosynthesis, inhibits transport of this enzyme into the mitochondria (21).

At present, the roles that HRMs play with respect to HO-2 function are incompletely understood; however, it has been shown through mutagenesis studies that the HRMs are not necessary for catalysis (19). Recently, it was proposed that the HRMs act as a so-called redox switch to regulate HO-2 heme binding affinity (28). Studies of various forms of HO-2 possessing distinct alterations (truncations or Cys to Ala mutations) to the HRMs provided evidence that a disulfide bond exists between the Cys residues of the two C-terminal HRMs (Cys265 and Cys282) that can be reduced to provide a free thiol(ate) group (Cys265) capable of coordinating to the heme iron. The disulfide-reduced HO-2 species were shown to have significantly lower binding affinities for Fe(III)-heme than their counterparts containing intact disulfide bonds. Further characterization of these species by absorption (Abs), magnetic circular dichroism (MCD), and resonance Raman (rR) spectroscopies presented herein confirms the presence of a Cys-ligated heme species. Additionally, these spectroscopic studies reveal an intriguing temperature dependence of the spin state of the Fe(III) ion in the heme-HO-2 complex, consistent with the possibility that, as observed in HO-1, a hydrogen-bonding network exists at the heme's distal site in HO-2, which could play an important role in the catalytic mechanism employed by this enzyme. Moreover, because this temperature-dependent behavior has only been observed in HO-2, our data suggest that small, but potentially significant, differences exist between the active sites of these two HO isoforms.

4.3 Materials and methods

4.3.1 HO-2 and its variants experimental samples preparation

Samples of three HO-2 variants were used for the experiments described below. Each variant was truncated to remove the membrane-binding region (amino-acid residues 289-316) because the full-length protein is less stable and cannot be prepared at sufficiently high concentrations for these spectroscopic experiments; this truncated protein is hereafter referred to as HO-2_t. The variants studied include HO-2_t, C127A/C282A HO-2_t, and C127A HO-2_t^*, where HO-2_t^* indicates the removal of amino acid residues 265-316, which contain the C-terminal HRMs. Each species was characterized in the as-isolated (i.e., containing Fe(III)-heme and a disulfide bond between C265 and C282 in the case of HO-2_t) and dithiothreitol (DTT)-reduced (wherein Cys residues are reduced to the thiol form but the Fe remains in the Fe(III) state) forms. The HO-2_t and C127A HO-2_t^* variants were also studied in the Fe(II)-heme form. To prepare these samples, the protein was suspended in buffer containing 50 mM Tris-HCl and 50 mM KCl (pH 7.5). DTT-reduced protein was prepared by incubating 150 μM as-isolated protein with 10 mM DTT on ice for 1 h. then extensively dialyzing with buffer in an anaerobic chamber (Vacuum Atmospheres Company, Hawthorne, CA). The number of free thiol groups in the DTT-reduced HO-2^{Δ} variants was determined using 5,5'-dithiobis(2-nitrobenzoate) (DTNB) as described previously (28). The protein-heme complexes were prepared by incubating purified HO-2_t or its variants with a 1.5-fold molar excess of a freshly prepared Fe(III)-heme stock solution containing 5-10% dimethyl sulfoxide (DMSO) and 100 mM NaOH to prevent heme aggregation. This stock solution was passed through a 0.22 μm filter prior to addition to HO-2 to ensure that no heme aggregates were present. Excess heme was immediately removed from the reconstituted protein samples by two cycles of chromatography with a Bio-Spin6 column (Bio-Rad, Hercules, CA). During a previous optimization of this method it was found that the final heme/protein ratio is approximately 1:1, as verified by the pyridine hemochrome assay (29). All samples were examined spectroscopically after chromatography to verify the absence of unbound heme, the presence of which would give rise to a characteristic broad Abs band at 385 nm. Addition of Fe(III)-heme was carried out in an anaerobic chamber in the case of the DTT-reduced HO-2 variants. Fe(II)-heme was prepared by

adding freshly prepared sodium dithionite (2 mM final concentration) to a stock solution of 200 μM Fe(III)-heme in 20% DMSO in the anaerobic chamber. This was then added to protein anaerobically as described above. Protein concentrations were determined using the Rose-Bengal method (30). Samples contained 15-20 μM heme-bound protein, and all samples used for low temperature (LT) absorption (Abs) and magnetic circular dichroism (MCD) experiments also contained approximately 60% (v/v) glycerol. In preparation for spectroscopic experiments, the samples were thawed on ice, transferred into MCD sample cells or NMR tubes, and frozen in liquid N_2. All DTT-reduced and Fe(II)-heme-containing samples were handled under an atmosphere of N_2 (g).

4.3.2 Absorption, magnetic circular dichroism, and resonance Raman spectroscopic studies

Room temperature (RT) Abs spectra were obtained using a Varian Cary 5e spectrophotometer. The sample compartment was purged with N_2 (g) when collecting data for the DTT-reduced and Fe(II)-heme-containing samples. LT (4.5 K) Abs and MCD and 277 K MCD spectra were obtained using a Jasco J-715 spectropolarimeter in conjunction with an Oxford Instruments SM4000-8T magnetocryostat. The MCD spectra presented herein were obtained by subtracting the –7 T data from the +7 T data.

Resonance Raman (rR) data were obtained by exciting the samples with 406.7 or 413.1 nm light from a Kr^+ ion laser (Coherent I-302C). The power of the incident light was approximately 25 and 15 mW for LT (77 K) and 277 K experiments, respectively. Light scattered at approximately 135^o from the sample was dispersed by a triple monochromator (Acton Research SpectraPro) with a 2400 g/mm grating and detected with a liquid-N_2-cooled back-illuminated CCD camera (Princeton Instruments Spec-10 100BR, 1340 x 100 pixels). The NMR tubes containing the samples were immersed in liquid N_2 or an ice/H_2O bath during data collection.

4.4. Experimental results

4.4.1 Redox changes in the HRMs affect the spin state of Fe^{3+}-heme

EPR measurements were performed to characterize the axial ligand for the Fe^{3+}-heme in oxidized and reduced HO-2 (**Figure 4.1**). All the EPR measurements were performed at 10 K, since the low-spin heme relaxes very fast. The spectra of oxidized HO-2 indicate a predominantly six-coordinate high-spin state with g-values for the high spin component at 5.80 and 1.99. These values are indicative of ligation by His and water (31), like in HO-1 (32) (**Figure 4.1A**). A small portion of the low-spin component at 2.87, 2.26, and 1.64 was also exist in the spectra, which indicates a His/N ligation of heme (**Figure 4.1A**). Compared with the EPR spectra of oxidized HO-2, the EPR spectra of reduced HO-2 exhibit a mixture of high spin (5.78) and low spin heme (g-values at 2.41, 2.26, and 1.91). These values are indicative of thiolate/water ligation (31).

Compared with the EPR spectra of oxidized/reduced HO-2, the EPR spectra of oxidized and reduced C265A are nearly identical, indicating a predominantly high-spin state (**Figure 4.1B**). The low spin heme components (g-values at 2.41, 2.26, and 1.91) are present neither in oxidized nor reduced C265A, which suggests that Cys265 is responsible for the thiolate/water ligation. Thus, when the HRMs are in the disulfide state, the low- and high-spin ferric heme appears to have His and water (or OH, or N) ligands (g values of 5.80 and 1.99, or 2.87, 2.26, and 1.64, respectively). It is only upon reduction of the HRM that the EPR spectra of the low-spin heme switch to the values characteristic of Cys and water (or OH) ligation (2.41, 2.26, and 1.91).

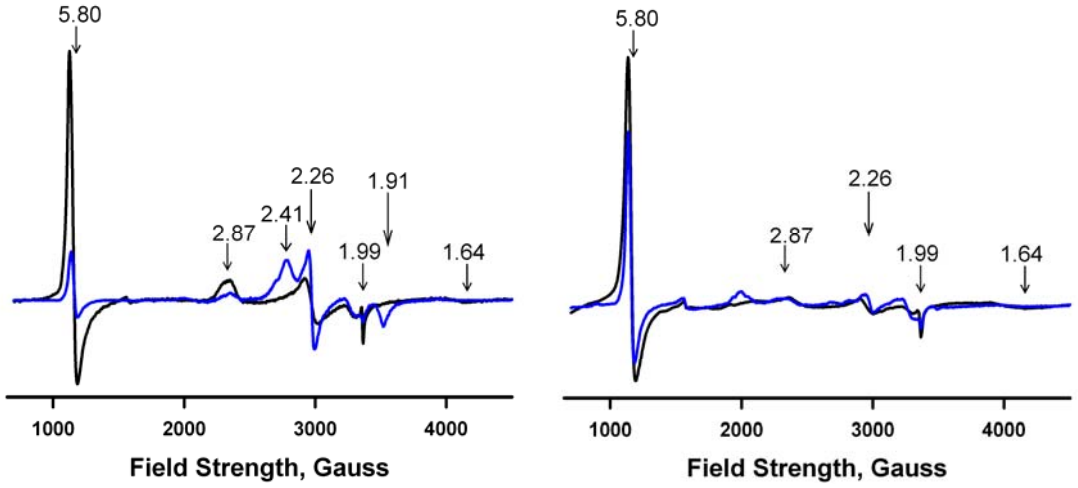

A **B**

FIGURE 4.1 **EPR spectra of ferric heme complexed with oxidized and reduced HO-2 and C265A variant.** Samples were prepared with 1:1 ratio of Fe^{3+}-heme and HO-2. EPR measurements were performed at 10 K with microwave frequency of 9.39 GHz, microwave power of 1 mW, field modulation amplitude of 10.15 G at 100 kHz. **A**, Fe^{3+}-heme plus oxidized HO-2 (black); Fe^{3+}-heme plus reduced HO-2 (blue). **B,** Fe^{3+}-heme plus oxidized C265A (black); Fe^{3+}-heme plus reduced C265A (blue)

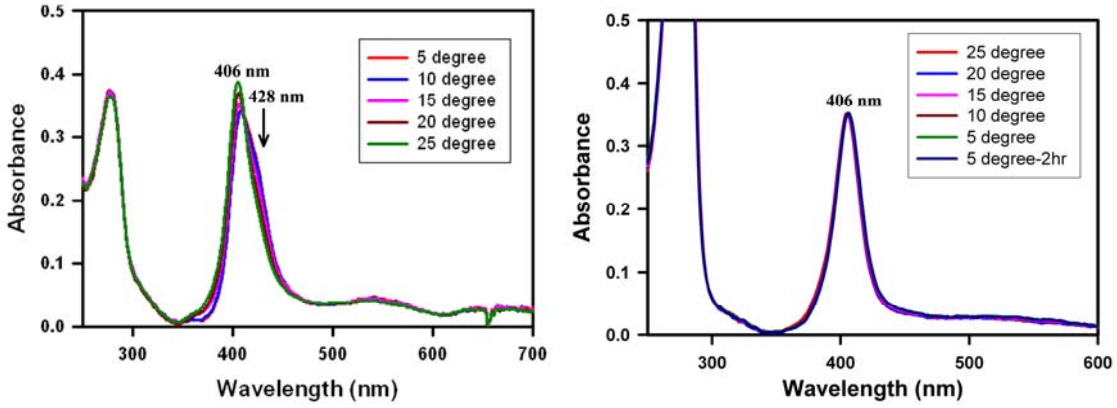

A **B**

FIGURE 4.2 **UV-visible spectra of Fe^{3+}-heme-reduced HO-2 and Fe^{3+}-heme-reduced C265A variant at different temperatures.** UV-visible spectra were recorded in the temperature range of 25 °C to 5 °C. Samples were prepared with 1:1 ratio of Fe^{3+}-heme and DTT-reduced protein. DTT was removed before heme constitution. A, Fe^{3+}-heme plus reduced HO-2. B, Fe^{3+}-heme plus reduced C265A

4.4.2 Cys265 in HO-2 can ligate to Fe^{3+}-heme to form a low-spin Fe^{3+}-heme species

4.4.2.1 Abs and MCD data

The replacement of His ligation (His45) by thiol ligation (Cys265), which is apparent in the EPR measurements (**Figure 4.1**), is also indicated by low-temperature UV-visible spectroscopic analysis (**Figure 4.2**). For the Fe^{3+}-heme bound reduced HO-2, (**Figure 4.2A**), as the temperature decreased from 25 °C to 5 °C, the peak intensity at 406 nm decreased accompanied by an increase in absorbance at 428 nm, indicating a conversion from His/water to Cys/water ligation. This spectral change is not observed with Fe^{3+}-heme bound reduced C265A variant, which may be due to the lack of thiol ligand in C265A variant (**Figure 4.2B**).

In order to further elucidate this Cys265 mediate ligand switch, RT Abs spectra were obtained for the as-isolated (i.e., Fe(III)-heme-bound) truncated form of heme oxygenase-2 (HO-2_t) and two variants (C127A/C282A HO-2_t, containing only Cys265 that is at least partially oxidized to its sulfenate form, and C127A HO-2_t^*, lacking all three Cys residues) that possess changes to the C-terminal heme-regulatory motifs (HRMs) (28). The Abs spectrum of each of these species exhibits the Soret feature at approximately 403 nm and distinct charge transfer (CT) bands at approximately 500 and 631 nm (**Figure 4.3A**, dotted lines), typical of high-spin Fe(III)-heme complexes (33). These data are consistent with the results obtained in previous studies of HO-2_t at neutral pH (28,34,35). On the basis of the close resemblance of their Abs spectra, it can be concluded that at RT all three variant species investigated feature similar heme environments. However, significant spectral changes were observed for all three samples upon cooling to LT. In each case the Abs spectrum at 4.5 K (**Figure 4.3A**, solid lines) consists of a Soret band red-shifted to 411 nm and α and β bands at approximately 560 and 533 nm, respectively, indicative of a six-coordinate low-spin Fe(III)-heme complex (33).

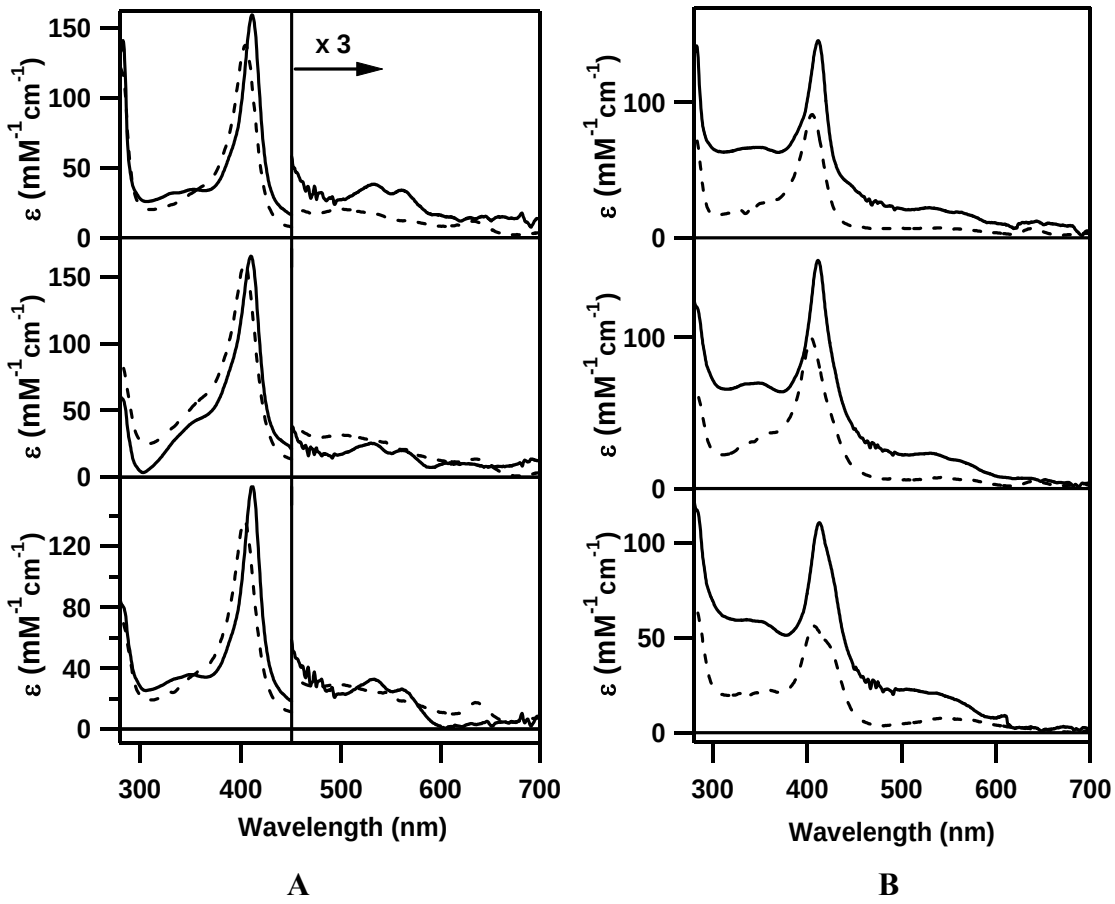

FIGURE 4.3 **Abs spectra of Fe^{3+}-heme-bound HO-2 and its variants.** A, RT (---) and 4.5 K (—) Abs spectra of as-isolated Fe^{3+}-heme-bound C127A HO-2_t^* (top), C127A/C282A HO-2_t (middle), and HO-2_t (bottom). B, RT (---) and 4.5 K (—) Abs spectra of DTT-reduced Fe^{3+}-heme-bound C127A HO-2_t* (top), C127A/C282A HO-2_t (middle), and HO-2_t (bottom). Conditions: 15 μM (HO-2, C127A HO-2_t^*) or 20 μM (C127A/C282A HO-2) protein, 50 mM Tris-HCl, 50 mM KCl (pH 7.5), 60% (v/v) glycerol.

A curious difference between our Abs spectra and those published previously for a low-spin form Fe(III)-HO-2 obtained at pH 9.5 (34) is the position of the α-band, which is blue-shifted by about 15 nm in our spectra. This up-shift of the α-band is consistent with of a neutral N-donor molecule (such as a His residue) serving as a second axial ligand to the Fe(III)-heme. We do not yet have definitive evidence for the identity of the sixth ligand in our HO-2 species, so it is possible that OH^- is in fact still bound and the change in the Abs spectrum bears no real significance. However, it seems likely that our data reflect the presence of a neutral (perhaps N-donor) ligand instead of the hydroxide

ion observed for the HO-2-bound low spin Fe(III)-heme. This latter possibility is also supported by EPR data obtained for this species (**Figure 4.1**, which clearly reveal the presence of a low spin Fe(III)-heme species that exhibits g-values characteristic of a His/N-donor axial ligand set (g = 2.87, 2.25, 1.64).

To explore the effects of reducing the disulfide bond between the Cys residues of the C-terminal HRMs (C265 and C282), Abs spectra were also collected for the DTT-reduced counterparts of the samples described above (**Figure 4.3B**). All three species still contain Fe(III)-heme, but the disulfide bond and sulfenate moiety have been reduced to thiol groups in HO-2_t and C127A/C282A HO-2_t, respectively. After reduction, these samples contained approximately 3.00 and 0.82 thiols/protein, respectively, as determined by the DTNB assay (compared to 0.09 thiol/protein for the as-isolated C127A/C282A species). Like the data for the as-isolated samples, the Abs spectra of the DTT-reduced samples are characteristic of high-spin Fe(III)-heme species at RT and a low-spin Fe(III)-heme species at LT However, while the Abs spectra for the as-isolated samples are virtually identical to one another, some small differences are observed in the spectra of these DTT-reduced samples. Specifically, a shoulder in the Soret region (approximately 428 nm) is observed in the spectra of the DTT-reduced HO-2_t and C127A/C282A HO-2_t samples. The position of this new feature does not change as a function of temperature. These results suggest the presence of a second heme species in the DTT-reduced samples that remains low spin at all temperatures (see **Figure 4.4**, top).

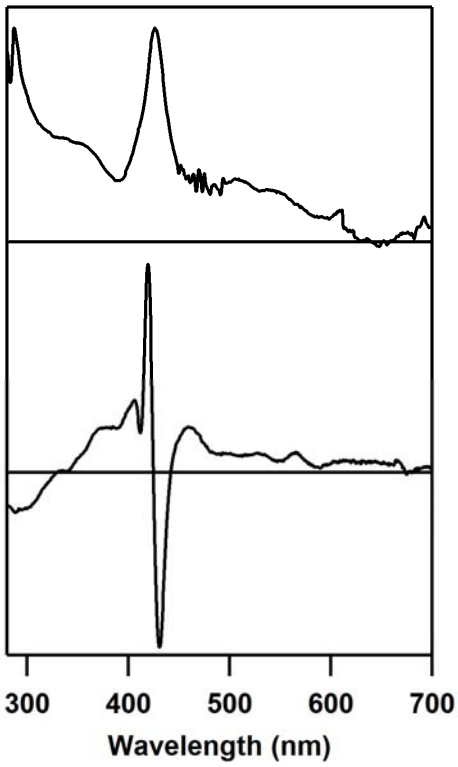

FIGURE 4.4. **Abs (top) and MCD (bottom) spectra representing the spectral contributions of the putative Cys265-ligated Fe^{3+}-HO-2 species.** Spectra were obtained by subtracting data for the DTT-reduced Fe(III)-bound C127A HO-2_t^* species from those for the analogous HO-2_t species.

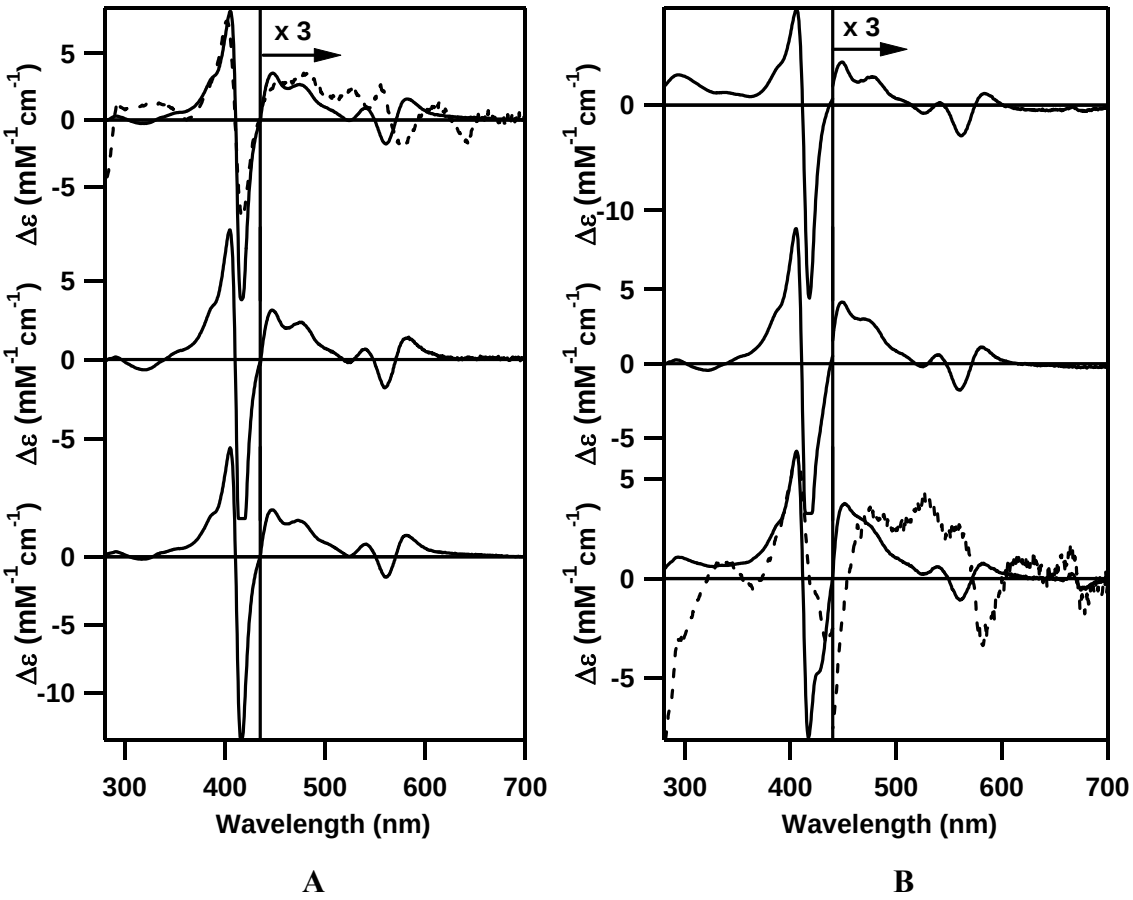

FIGURE 4.5 **MCD spectra of Fe^{3+}-heme-bound HO-2 and its variants.** A, MCD spectra of 277 K (---; x 30 for comparison) and 8 K (—) MCD spectra of as-isolated Fe^{3+}-heme-bound C127A HO-2_t* (top), C127A/C282A HO-2_t (middle), and HO-2_t (bottom). B, 277 K (---; x 30 for comparison) and 4.5 K (—) MCD spectra of DTT-reduced Fe^{3+}-heme-bound C127A HO-2_t* (top), C127A/C282A HO-2_t (middle), and HO-2_t (bottom). Conditions: 15 μM (HO-2_t, C127A HO-2_t^*) or 20 μM (C127A/C282A HO-2_t) protein, 50 mM Tris-HCl, 50 mM KCl (pH 7.5), 60% (v/v) glycerol.

In agreement with the Abs data described above, LT MCD spectra indicate the presence of predominantly low-spin Fe(III)-heme at cryogenic temperatures in all of the as-isolated and DTT-reduced Fe(III)-heme-bound samples studied (see **Figure 4.5A** and **Figure 4.5B**, respectively). This is particularly evident from the peak position of the intense derivative-shaped Soret feature centered at approximately 411 nm and the presence of several weaker features in the spectral region between 430 and 600 nm (36). While the MCD spectra of all of the as-isolated and DTT-reduced C127A HO-2_t^* samples

are identical, spectral differences are observed for the DTT-reduced HO-2_t and C127A/C282A HO-2_t samples. Although these latter spectra are quite similar to those of the analogous as-isolated samples, an additional shoulder is present at approximately 428 nm, corresponding to the shoulder seen in the Abs spectra, and subtle changes are also apparent in the α/β region. These data suggest that while the DTT-reduced samples still primarily contain the same Fe(III)-heme species observed in the as-isolated samples, an additional species is present that exhibits distinct spectroscopic signatures (see **Figure 4.4**, bottom). Note that on the basis of the close resemblance of the Abs and MCD data obtained for the DTT-reduced C127A/C282A HO-2_t and C127A HO-2_t^* samples (**Figure 4.3B** and **4.5B**) it may appear that, as proposed previously (28), the redox state of the HRMs has no effect on the optical spectra of these species. However, a more careful inspection of these data clearly reveals that the C127A/C282A HO-2_t spectra differ from those of the C127A HO-2_t^* variant by the presence of an additional Soret feature approximately 428 nm, which is particularly obvious in the LT MCD spectrum (**Figure 4.5B**). Consequently, the former sample is spectroscopically more similar to the HO-2_t sample, each containing two distinct heme species (**Figure 4.6**). However, the relative concentration of the second, unique heme species is considerably lower in the C127A/C282A HO-2_t sample than in the HO-2_t sample. This difference can be seen quite clearly by comparing the Abs and MCD data of these and additional, independently prepared samples (**Figure 4.6**). Thus, our RT Abs spectra are, in fact, qualitatively similar to those reported previously (28), with small quantitative differences arising from a currently unknown variation in sample preparations. However, our current data clearly demonstrate that the redox state of the HRMs affects the HO-2 species present and that this change can be observed easily via Abs and MCD spectroscopies.

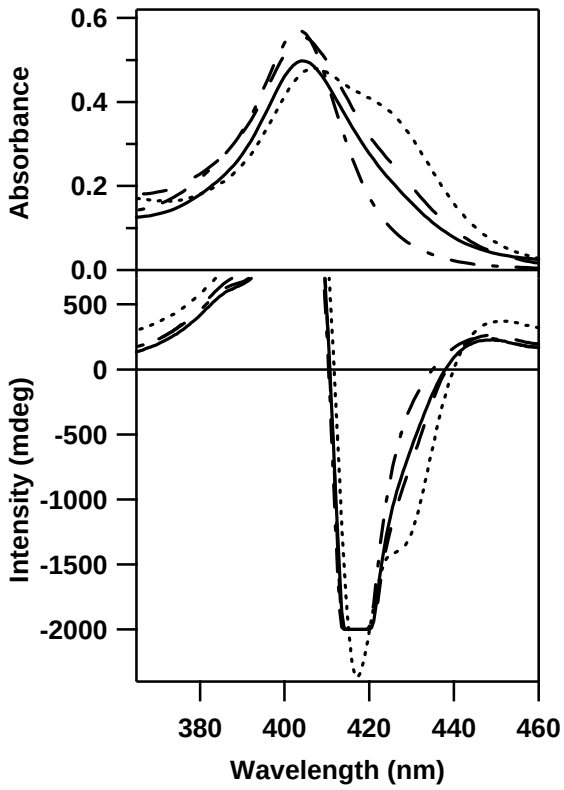

FIGURE 4.6. **273 K Abs (top) and 4.5 K MCD (bottom) spectra of HO-2 and its variants.** oxidized (— -) and reduced (···, —) HO-2_t and reduced C127A/C282A HO-2_t (- --). The reduced C127A/C282A HO-2_t sample and the second reduced HO-2_t sample (—) were prepared at a different time and have considerably less of the second heme species observed in the first reduced HO-2_t sample (···).

For the as-isolated C127A HO-2_t * and DTT-reduced HO-2_t samples, MCD spectra were also collected at 277 K (**Figure 4.5**, broken lines). On the basis of the marked decrease in intensity of the negatively-signed Soret feature and several spectral changes in the α/β region, it is reasonable to conclude that at 277 K the major heme species in as-isolated C127A HO-2_t^* contains a high-spin Fe(III) ion (36). Alternatively, the 277 K MCD spectrum of DTT-reduced HO-2_t exhibits two Soret features instead of just one, suggesting that two distinct heme species are present at this temperature. One species exhibits spectral features similar to those of as-isolated C127A HO-2_t^*, signifying the presence of high-spin Fe(III)-heme. The spectral features due to the second species are nearly identical to those displayed by the second heme species observed at LT for this sample and C127A/C282A HO-2_t. Thus, these results confirm the conclusions drawn

from the Abs data; namely, (i) the major heme species in all samples undergoes a spin-state conversion from high-spin at RT to low-spin at LT, and (ii) a second heme species is present in the DTT-reduced HO-2_t and C127A/C282A HO-2_t samples that exhibits red-shifted Soret features and remains low spin at all temperatures.

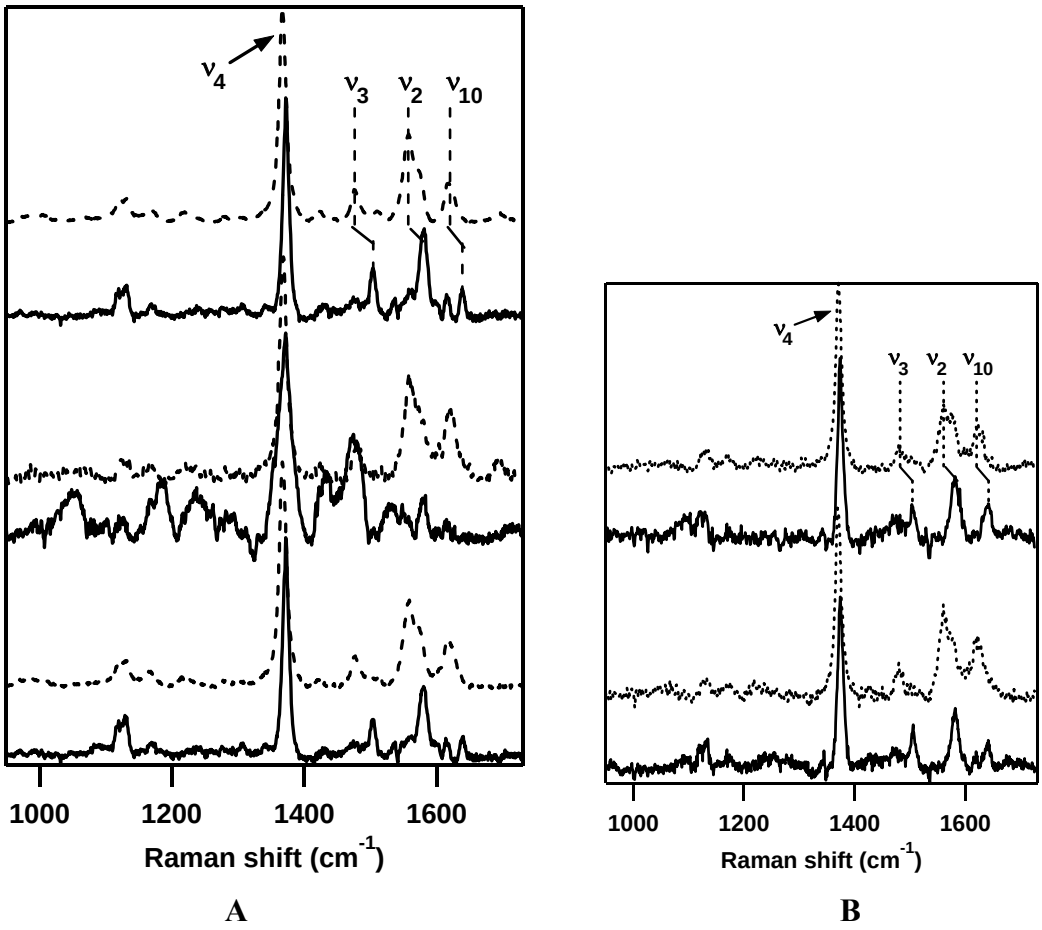

FIGURE 4.7 **rR spectra of as-isolated and reduced HO-2 and its variants**. A, 273 K (---) and 77 K (—) rR spectra of as-isolated Fe^{3+}-heme-bound C127A HO-2_t * (top), C127A/C282A HO-2_t (middle), and HO-2_t (bottom), obtained with λ_{ex} = 413.1 nm. B, 273 K (---) and 77 K (—) rR spectra of reduced Fe^{3+}-heme-bound C127A/C282A HO-2_t (top) and HO-2_t (bottom), obtained with λ_{ex} = 413.1 nm. Conditions: 20 μM HO-2_t, 50 mM Tris-HCl, 50 mM KCl (pH 7.5).

4.4.2.2 rR data

The rR spectra of the as-isolated and DTT-reduced HO-2 variants are presented in **Figure 4.7A and 4.7B**, respectively. The spectra of all of these samples are virtually identical. The oxidation-state (ν_4 = 1371 cm^{-1}) and spin-state (ν_2 = 1580 cm^{-1}, ν_3 = 1504 cm^{-1}, ν_{10} = 1637 cm^{-1}) marker bands observed for these species at LT are characteristic of six-coordinate low-spin Fe(III)-heme (37-39). At 273 K these bands are observed at lower frequencies (ν_4 = 1368 cm^{-1}, ν_2 = 1560 cm^{-1}, ν_3 = 1480 cm^{-1}, ν_{10} = 1617 cm^{-1}) that are typical of six-coordinate high-spin Fe(III)-heme complexes (37-39). These results are consistent with the Abs and MCD data presented above and provide further evidence that the spin state of the HO-2-bound Fe(III)-heme is temperature dependent. Additional rR data were collected for otherwise identical samples in the presence and absence of 60% (v/v) glycerol to determine if the temperature dependence of the Fe(III)-heme spin state is due to differential freezing in the absence and presence of the glassing agent necessary for LT Abs and MCD experiments. It is evident from the similarity between these spectra (**Figure 4.8**) that this is not the case.

4.4.3 HRMs in HO-2 are not involved in ligation of the Fe^{2+}-heme

Because Fe(II)-heme species are also involved in the reaction catalyzed by HOs, it is equally important to explore how the HRMs affect the Fe(II)-heme-bound form of HO-2. In previous studies of the HO-2 variants investigated here only Abs and EPR spectroscopies were employed; thus, the Fe(II)-heme-bound forms of these species remained poorly characterized (28). To address this issue, we have also performed Abs and MCD spectroscopic studies of the Fe(II)-heme-bound HO-2 species. The Abs spectra of the Fe(II)-heme-bound HO-2_t and C127A HO-2_t^* samples are presented in **Figure 4.9**. At RT the two species give rise to nearly identical spectra, each containing a broad Soret feature at approximately 430 nm consisting of two distinct components, as well as noticeable but broad and indistinct α and β bands. The presence of two bands in the Soret region suggests that these samples contain contributions from both high-spin and low-spin Fe(II)-heme species (33). At 4.5 K, the two Soret bands are still present, but instead of having nearly equal intensities, the shorter-wavelength feature is now more dominant. Also, the α and β bands are more distinct at LT. These spectral changes are consistent with a higher proportion of low-spin Fe(II)-heme at cryogenic temperature (33). The fact

that both HO-2_t, which contains three reduced Cys residues, and C127A HO-2_t^*, which lacks all of these Cys residues, give rise to virtually identical Abs spectra both at LT and at RT suggests that no significant structural differences, such as Cys ligation to the Fe(II)-heme in the former sample, exist between these samples.

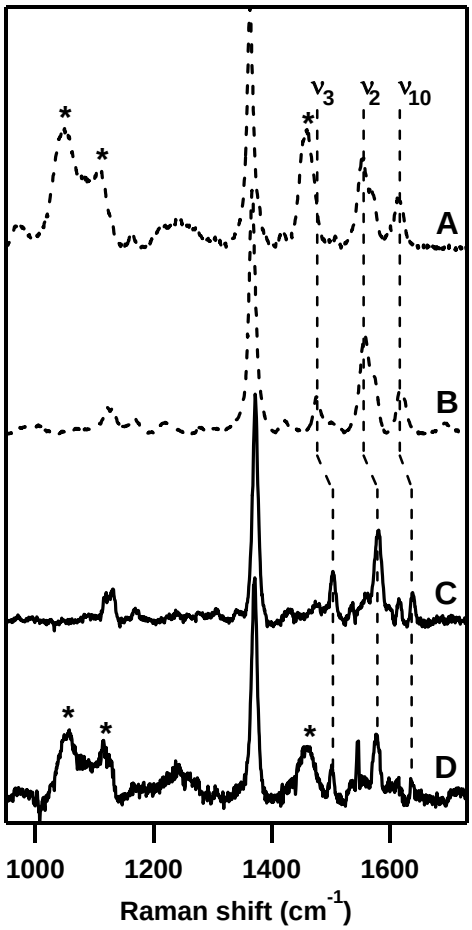

FIFURE 4.8 **Glycerol does not affect rR spectra.** 273 K (---) and 77 K (—) rR spectra of as-isolated Fe^{3+}-heme-bound C127A HO-2_t* in the presence (A, D) and absence (B, C) of glycerol. Features marked by * are due to glycerol vibrations. λ_{ex} = 406.7 nm (A) or 413.1 nm (B-D).

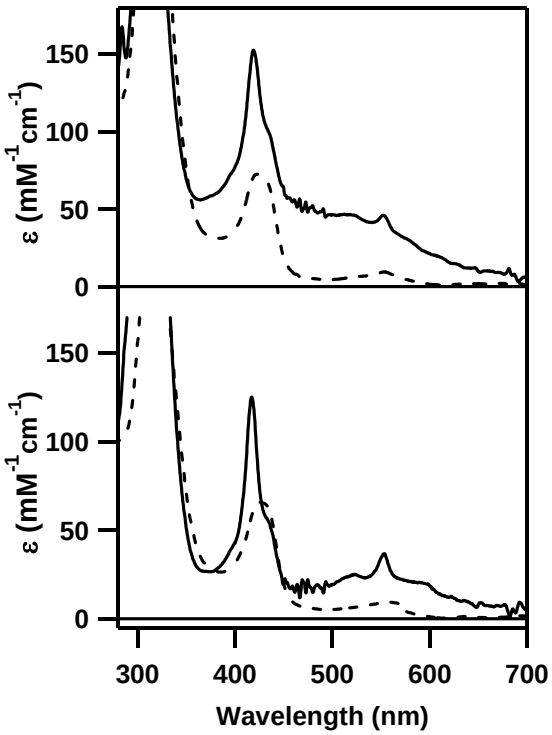

FIGURE 4.9 **Abs spectra of Fe^{2+}-heme-bound HO-2 and its variants.** RT (---) and 4.5 K (—) Abs spectra of Fe^{2+}-heme-bound C127A HO-2_t^* (top) and HO-2_t (bottom). Conditions: 15 μM HO-2_t, 50 mM Tris-HCl, 50 mM KCl (pH 7.5), 60% (v/v) glycerol.

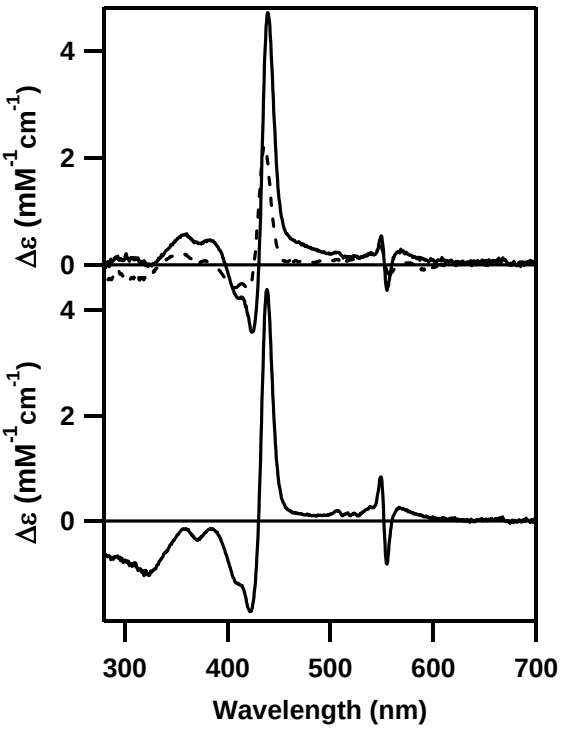

FIGURE 4.10 **MCD spectra of Fe^{2+}-heme-bound HO-2 and its variants.** 277 K (---) and 4.5 K (—) MCD spectra of Fe^{2+}-heme-bound C127A HO-2_t * (top) and HO-2_t (bottom). Conditions: 15 μM HO-2, 50 mM Tris-HCl, 50 mM KCl (pH 7.5), 60% (v/v) glycerol.

The LT MCD data obtained for these two samples (**Figure 4.10**) allow for a more conclusive assignment of the Fe(II)-heme species present. In agreement with the Abs data, the MCD spectra of the two samples are quite similar and exhibit characteristic features of both high- and low-spin Fe(II)-heme species. The temperature-dependent features in the Soret region are due to the high-spin component; alternatively, the sharp derivative-shaped feature at 552 nm is characteristic of low-spin Fe(II)-heme. More specifically, the position of this latter feature is indicative of a low-spin Fe(II)-heme species with His, rather than Cys, axial ligation (40-42). This result provides further evidence against Cys ligation in the Fe(II)-heme-bound HO-2 species. Thus, the HRMs do not appear to have the same influence on the Fe(II)- and Fe(III)-heme-bound HO-2 species.

Because five-coordinate Fe(II) heme proteins tend to be high spin even at LT, it follows that a sixth ligand must be present in the low-spin Fe(II) species we observe.

Thus, it appears that our samples contain a mixture of five- and six-coordinate Fe(II)-heme, with the relative amount of six-coordinate species increasing with decreasing temperature. While it is clear from our data that one axial ligand to the Fe(II) heme is His rather than Cys, the identity of the sixth ligand is not yet established. There does not appear to be a good candidate for this ligand among the amino-acid residues within the enzyme's active site, so the most likely ligand would be solvent (H_2O/OH^-) or a buffer molecule.

4.5 Discussion

4.5.1 Temperature dependence of the Fe-heme spin state

A particularly intriguing aspect of the spectroscopic data obtained in this study is that the Fe(III)-heme spin state of the investigated HO-2 species changes as a function of temperature. This spin-state change is evidenced by the blue shift of the Soret feature as well as a loss of discernible α/β features and the appearance of distinct CT bands in the Abs spectra (**Figures 4.3 and 4.4**) when the temperature is increased. These Abs spectral changes are accompanied by a loss of negative intensity in the Soret region and several changes in the 450-700 nm region in the corresponding MCD spectra (**Figure 4.5**) and marked shifts of the spin-state marker bands in the rR spectra (**Figure 4.7**). Collectively, the data obtained using these three complementary spectroscopic techniques provide compelling evidence that the ferric ion in the Fe(III)-heme-HO-2 complex adopts a high-spin configuration at RT and a low-spin configuration at LT (33,36-39). Although glycerol could in principle affect the protein structure in the frozen state, its presence in these HO-2 samples is not the cause of the observed spin-state change since rR spectra obtained in the presence and absence of glycerol are virtually identical (**Figure 4.8**). Alternatively, a temperature-dependant pK_a change or some other buffer effect could be responsible for the spin-state change upon freezing. However, EPR data collected for samples prepared in different buffers appear virtually identical (not shown), strongly suggesting that the temperature dependence of the spin state of the Fe(III)-heme-HO-2 complex is in fact intrinsic to this species.

Likewise, a comparison of RT Abs with LT Abs and MCD data for the Fe(II)-heme-containing HO-2 samples leads to the conclusion that the spin state of the ferrous ion exhibits a similar temperature dependence. As was seen with the Fe(III)-heme-bound HO-2 species, a higher proportion of low-spin Fe(II)-heme is present at LT while high-spin Fe(II)-heme predominates at RT (**Figure 4.9** and **Figure 4.10**).

Clues as to what may cause this spin-state change come from a comparison to other heme proteins with active-site environments similar to that of HO-2. For instance, a similar change in spin state is observed in both heme oxygenase isoforms and other heme proteins such as metmyoglobin (metMb) and methemoglobin (metHb) as a function of pH (2,34,43). This change is thought to be the result of a change in the protonation state

of the axial solvent ligand, from H_2O at low pH to OH^- at high pH. The acidity of the solvent ligand appears to be modulated by a H-bonding interaction with a distal amino-acid residue, often a His as seen in metMb and metHb. However, HOs lack a distal His residue, and instead possesses a H-bonding network to a nearby Asp residue (see below). Additionally, some heme proteins, including the O_2-sensing heme kinase FixL and the ring-cleaving enzyme indoleamine 2,3-dioxygenase, exhibit a temperature-dependent spin state that is thought to be the result of a thermal equilibrium between high- and low-spin Fe(II)- or Fe(III)-heme, with the high-spin state being more favored at higher temperatures (4,44-46). This phenomenon has been attributed to H-bonding interactions involving the axially bound solvent molecule (OH^-) of the heme moiety and nearby amino-acid residues (2). It has been suggested that a stronger H-bond donation to the axial OH^- ligand at high temperature makes this ligand more H_2O-like, resulting in a weaker ligand field experienced by the Fe ion and, thus, favoring a high-spin configuration.

Although there is no obvious H-bonding amino-acid residue adjacent to the distal solvent molecule in HOs, an examination of structural data for heme-bound human HO-1 reveals a short chain of H_2O molecules that link the Fe ion to Asp and Arg residues (47). Mutational studies of HO-1 provided evidence that this particular Asp residue (Asp140) and the precisely structured H-bonding network it supports are critical for proper HO function (47,48). A similar H-bonding network has been identified in rat HO-1 and a HO from *Corynebacterium diphtheriae* (HmuO) (49-51). Additionally, a recent X-ray crystallographic study has revealed that human HO-2 possesses an active site similar to that of HO-1 (12). Although the crystal structure was obtained for a significantly truncated HO-2 variant, this form of the enzyme is catalytically active. Furthermore, most crystal structures available for HO-1 were obtained for proteins with similar truncations. Thus, it is reasonable to assume that the truncation leaves the active site intact, and that meaningful comparisons can be made to known structures of HO-1. To this end, it is intriguing to note that human HO-2 possesses an Asp residue whose position is similar to the Asp140 anchoring the active-site H-bonding network in HO-1 (see above).

While the X-ray crystal structure of human HO-2 did not provide direct evidence for the existence of a H-bonding network between the Asp residue and a solvent bound to the heme moiety, the many similarities between HO-1 and HO-2 suggest that this is likely the case. Our data are also consistent with this conclusion. Specifically, the observed temperature dependence of the Fe spin state in HO-2_t can be explained in terms of small changes in H-bonding interactions, presumably involving a weakening of the H-bond donation to an axial ligand such as a solvent molecule or another H-bond accepting ligand at LT so as to strengthen the Fe-ligand bond and stabilize low-spin Fe. Although the low temperatures used in the experiments described above are not physiologically relevant and future studies of HO-2 species containing mutations of distal site residues are needed to provide more conclusive evidence, this spin-state change clearly supports the possibility that a H-bonding network exists at the distal heme site, where O_2 is thought to bind during catalysis (11,28). Presumably, a H-bonding interaction similar to the one with the axial ligand in the resting enzyme will serve to stabilize and activate an Fe-heme-bound O_2 moiety in the early intermediates formed during the catalytic cycle of HO-2 in analogy to its proposed role in HO-1.

Despite these similarities between HO-1 and HO-2, however, the former does not exhibit a temperature-dependent spin-state change. LT EPR data of Fe(III)-heme-HO-1 at neutral pH appear indicative of a high-spin species (43), and no evidence for a low-spin species at any temperature has been obtained under these conditions (note, however, that HO-1 does in fact also form a low spin species, but its relative population is dependent only on pH and not on temperature). Because of the close similarity in structures of HO-1 and HO-2 and the presence of this H-bonding network in HO-1, the mere existence of such a network in HO-2 is not sufficient to explain the temperature-dependent behavior we observe for HO-2. However, HO-1 and HO-2 are not completely identical. They are reported to have different pK_a values (7.6 for HO-1, 8.5 for HO-2), and small structural differences are apparent even within their active sites (12-14,34,43,47). Instead of a mere deprotonation of, or an alteration of a H-bonding interaction with, an axial solvent ligand causing the observed spin-state change, our HO-2 species appear capable of undergoing a ligand exchange (perhaps involving an N-donor) upon conversion to their low spin Fe(III)-heme-bound form. The identity of this new ligand is not yet known, nor is its

relevance, if any, to the catalytic mechanism of HO-2. However, this observation does bring to light new differences between the two HO isoforms. On the basis of these results, we conclude that small but important differences exist between the active sites of HO-1 and HO-2, which result in distinct temperature behaviors of the heme spin states.

4.5.2 Evidence for Cys ligation to Fe^{3+}-heme

Although the necessity of heme oxygenases is undisputed, questions arise as to why two distinct forms of this enzyme are required. HO-1 appears well suited to fulfill its obvious role in heme degradation. It is localized primarily in liver and spleen tissue where much of the heme catabolism occurs, and its transcription is regulated in part by cellular markers for free heme, such as the presence of a heme/hemopexin complex that serves to transport heme to hepatocytes, as well as oxidative stress, which can result from free heme (17). In contrast, HO-2 is expressed constitutively and is found in high concentrations in other areas of the body, such as the brain (18). It has been proposed that although HO-2 effectively degrades heme like HO-1 does, its primary role may be to generate CO, which can act as a cellular signaling molecule (17). Understanding the differences between the two heme oxygenase isoforms may help to more clearly elucidate the need for two forms of this enzyme and the distinct roles they may have.

One noticeable difference between the two heme oxygenase isoforms is the presence of three Cys residues as part of HRMs in HO-2 and the complete lack of Cys residues in HO-1 (19). A few hemoproteins are known to contain HRMs that appear to play important roles in regulation or enzyme activity (20-27). It is thought that these proteins, as well as HO-2, bind heme at the HRMs and that a Cys residue within the HRM serves as an axial ligand to the heme. For HO-2, it has been proposed that heme can bind to the HRMs as well as to His45 in the active site, resulting in a protein complex containing multiple heme molecules (19). However, recent experiments have led to the suggestion that only one heme binds to each HO-2 protein, either coordinating to His45 in the active site or to Cys265 within one of the HRMs of DTT-reduced HO-2 species (28). However, though, mutational studies of HO-2 have revealed that the HRMs are not necessary for enzyme activity or stability (19,28). Nonetheless, recent studies have provided evidence that two of the three HRMs of HO-2 may constitute a redox switch that regulates the

heme binding affinity of HO-2 in response to the reducing nature of the protein environment (28).

The spectroscopic data obtained in our studies of various HO-2 species provide further support for the proposed Cys ligation to Fe(III)-heme. The Abs and MCD spectra of as-isolated HO-2_t and C127A HO-2_t^* are identical (**Figure 4.5A**); thus, the presence of Cys residues in HO-2_t and C127A/C282A HO-2_t does not affect the binding of heme to the catalytic site (via His45). However, some spectral differences are observed among the DTT-reduced forms of the Fe(III)-heme-bound HO-2 species investigated, most notably the appearance of additional features for the samples that contain Cys265. Specifically, a low-energy shoulder at approximately 428 nm appears on the Soret feature in both the Abs and MCD spectra (**Figure 4.3B** and **Figure 4.5B**) and small changes are discernible in the α/β region of the MCD spectra, signifying the presence of two distinct heme-bound protein species. The majority species gives rise to spectra identical to those of the as-isolated HO-2 samples, indicating that it contains His-ligated Fe(III)-heme. Alternatively, because the second (i.e., minority) species is observed exclusively in samples with free thiolate groups, which are known to coordinate to Fe(III)-hemes (3), it likely possesses Cys-ligated Fe(III)-heme.

Strong support for this assignment of the minority species in the DTT-reduced HO-2 samples investigated comes from a comparison to other spectroscopically characterized hemoproteins that are known to have Cys coordination (33,40,52-58). As shown in **Table 4.1**, a characteristic feature defining Cys-bound Fe(III)-heme species is a noticeably red-shifted Soret band. Consistent with this trend, the Soret band of the minority HO-2 species (**Figure 4.4**), which we propose to contain six-coordinate, Cys265-ligated low-spin Fe(III)-heme, is red-shifted by 17 nm relative to that of the majority, His45-ligated Fe(III)-heme species. Interestingly, the appearance of the spectral features due to this minority Fe(III)-heme species is concurrent with a marked decrease in the intensity of those associated with the His45-ligated form of HO-2. This observation suggests that the formation of the Cys-ligated Fe(III)-heme species occurs at the expense of the His-bound form, corroborating a previous proposal that a single heme binds to each protein molecule (28).

TABLE 4.1 **Position of the Soret band (nm) in the Abs and MCD spectra of various Fe^{3+}-heme-bound proteins with and without thiolate ligation**.

Protein	Soret band position Abs	MCD	Axial ligands	reference
thiolate ligation (low spin)				
P450cam	417	418	Cys, H_2O	50, 51
CooA	423	*n.a.*[a]	Cys, Pro	38
Cystathionine β Synthase	428	425	His, Cys	52
H93G Myoglobin	425	425	Ethanethiol, imidazole	53, 31
H66C Cytochrome b_2	423	423	Cys, ?	54
HO-2 (minority)	***428***		***Cys, H_2O***	*This work*
thiolate ligation (h.s.)				
P450cam	391	397	Cys	51
no thiolate ligation				
C75S(A) CooA	415 (411)	*n.a.*	Pro, ?	55, 56
Cytochrome b_2	413	413	His, His	54
HO-2 (majority)	***411***	***411***	***His, ?***	*This work*

n.a.[a] = not available

In contrast, no differences are observed between the spectra of the various Fe(II)-heme-bound HO-2 species investigated, indicating that the presence of Cys residues does not affect the heme environment in the ferrous state. Consistent with this finding, the position of the MCD A-term feature associated with the low-spin Fe(II)-heme fraction is characteristic of His rather than Cys ligation (41,53,54,59,60). Thus, it appears that Cys265 competes with His45 as an axial ligand to ferric but not ferrous heme bound to HO-2.

It has recently been reported that the EPR spectra exhibited by the as-isolated HO-2 variants investigated here are all identical and that an additional species, with EPR signatures characteristic of thiolate-ligated low-spin Fe(III)-heme, is present in the DTT-reduced HO-2_t and C127A/C282A HO-2_t species (28). These findings are in excellent

agreement with the conclusions drawn from the spectroscopic data obtained in the present study. One noticeable difference between the EPR spectra and our Abs, MCD, and rR data is that the former EPR spectra seem to suggest that the His-ligated heme bound to HO-2 contains predominantly high-spin Fe(III) at LT while the latter data are consistent with mostly low-spin His-ligated Fe(III)-heme. However, the EPR data clearly show that both high-spin and low-spin Fe(III)-heme species are present in HO-2 at LT, though no quantitation of the relative amounts of each has been reported.

4.6 Conclusion

My previous studies have demonstrated that an intramolecular disulfide bond exists between the Cys residues of the two C-terminal HRMs (Cys265 and Cys282), forming a redox switch to control the affinity of HO-2 for heme. In addition, Cys265 is capable of coordinating to the heme iron when it is in the free thiol state. Further characterization of these species by absorption (Abs), magnetic circular dichroism (MCD), and resonance Raman (rR) spectroscopies presented herein confirms the presence of a Cys-ligated heme species. Additionally, these spectroscopic studies reveal an intriguing temperature dependence of the spin state of the Fe^{3+} ion in the heme-HO-2 complex, hinting at the possibility that, as observed in HO-1, a hydrogen-bonding network exists at the distal site of the heme in HO-2, which could play an important role in the catalytic mechanism employed by this enzyme.

4.7 References

1. Ponka, P. (1999) *Am. J. Med. Sci.* **318**, 241-256
2. Antonini, E., and Brunori, M. (1971) Hemoglobin and Myoglobin in their Reactions with Ligands. in *Frontiers of Biology* (Neuberger, A., and Tatum, E. L. eds.), North-Holland Publishing Company, Amsterdam. pp 43-47
3. Dawson, J. H., and Sono, M. (1987) *Chem. Rev.* **87**, 1255-1276
4. Lukat-Rodgers, G. S., and Rodgers, K. R. (1998) *J. Biol. Inorg. Chem.* **3**, 274-281
5. Craven, P. A., and DeRubertis, F. R. (1983) *Biochim. Biophys. Acta* **745**, 310-321
6. Ignarro, L. J., Degnan, J. N., Baricos, W. H., Kadowitz, P. J., and Wolin, M. S. (1982) *Biochim. Biophys. Acta* **718**, 49-59
7. Sassa, S. (2006) *J. Clin. Biochem. Nutr.* **38**, 138-155
8. Kumar, S., and Bandyopadhyay, U. (2005) *Toxicol. Lett.* **157**, 175-188
9. Imlay, J. A. (2003) *Annu. Rev. Microbiol.* **57**, 395-418
10. Tenhunen, R., Marver, H. S., and Schmid, R. (1969) *J. Biol. Chem.* **244**, 6388-6394
11. Ortiz de Montellano, P. R. (1998) *Acc. Chem. Res.* **31**, 543-549
12. Bianchetti, C. M., Yi, L., Ragsdale, S. W., and Phillips, G. N., Jr. (2007) *J. Biol. Chem.* **282**, 37624-37631
13. Schuller, D. J., Wilks, A., Ortiz de Montellano, P. R., and Poulos, T. L. (1999) *Nat. Struct. Biol.* **6**, 860-867
14. Lad, L., Schuller, D. J., Shimizu, H., Friedman, J., Li, H., Ortiz de Montellano, P. R., and Poulos, T. L. (2003) *J. Biol. Chem.* **278**, 7834-7843
15. Yoshida, T., and Kikuchi, G. (1978) *J. Biol. Chem.* **253**, 4230-4236
16. Maines, M. D., Trakshel, G. M., and Kutty, R. K. (1986) *J. Biol. Chem.* **261**, 411-419
17. Maines, M. D. (1997) *Annu. Rev. Pharmacol. Toxicol.* **37**, 517-554
18. Ewing, J. F., and Maines, M. D. (1992) *Mol. Cell. Neurosci.* **3**, 559-570
19. McCoubrey, W. K., Jr., Huang, T. J., and Maines, M. D. (1997) *J. Biol. Chem.* **272**, 12568-12574
20. Zhang, L., and Guarente, L. (1995) *EMBO J.* **14**, 313-320
21. Lathrop, J. T., and Timko, M. P. (1993) *Science* **259**, 522-525
22. Qi, Z., Hamza, I., and O'Brian, M. R. (1999) *Proc. Natl. Acad. Sci. USA* **96**, 13056-13061
23. Ogawa, K., Sun, J., Taketani, S., Nakajima, O., Nishitani, C., Sassa, S., Hayashi, N., Yamamoto, M., Shibahara, S., Fujita, H., and Igarashi, K. (2001) *EMBO J.* **20**, 2835-2843
24. Yang, J., Ishimori, K., and O'Brian, M. R. (2005) *J. Biol. Chem.* **280**, 7671-7676

25. Lee, H. C., Hon, T., Lan, C., and Zhang, L. (2003) *Mol. Cell. Biol.* **23**, 5857-5866
26. Hon, T., Hach, A., Lee, H. C., Cheng, T., and Zhang, L. (2000) *Biochem. Biophys. Res. Commun.* **273**, 584-591
27. Munakata, H., Sun, J.-Y., Yoshida, K., Nakatani, T., Honda, E., Hayakawa, S., Furuyama, K., and Hayashi, N. (2004) *J. Biochem.* **136**, 233-238
28. Yi, L., and Ragsdale, S. W. (2007) *J. Biol. Chem.* **282**, 21056-21067
29. Berry, E. A., and Trumpower, B. L. (1987) *Anal. Biochem.* **161**, 1-15
30. Elliot, J. I., and Brewer, J. M. (1978) *Arch. Biochem. Biophys.* **190**, 351-357
31. Blumberg, W. E., and Peisach, J. (1971) A unified theory for low spin forms of all ferric heme proteins as studied by EPR. in *Probes of Structure and Function of Macromolecules and Membranes: Probes of Enzymes and Hemoproteins* (Chance, B., Yonetani, T., and Mildvan, A. S. eds.), Academic Press, New York. pp 215-229
32. Takahashi, S., Wang, J., Rousseau, D., Ishikawa, K., Yoshida, T., Host, J., and Ikeda-Saito, M. (1995) *J. Biol. Chem.* **270**, 1010-1014
33. Brill, A. S., and Williams, J. P. (1961) *Biochem. J.* **78**, 246-253
34. Ishikawa, K., Takeuchi, N., Takahashi, S., Matera, K. M., Sato, M., Shibahara, S., Rousseau, D. L., Ikeda-Saito, M., and Yoshida, T. (1995) *J. Biol. Chem.* **270**, 6345-6350
35. Ishikawa, K., Mansfield Matera, K., Zhou, H., Fujii, H., Sato, M., Yoshimura, T., Ikeda-Saito, M., and Yoshida, T. (1998) *J. Biol. Chem.* **273**, 4317-4322
36. Cheesman, M. R., Greenwood, C., and Thomson, A. J. (1991) *Adv. Inorg. Chem,* **36**, 201-255
37. Mino, Y., Wariishi, H., Blackburn, N. J., Loehr, T. M., and Gold, M. H. (1988) *J. Biol. Chem.* **263**, 7029-7036
38. Morikis, D., Champion, P. M., Springer, B. A., Egeberg, K. D., and Sligar, S. G. (1990) *J. Biol. Chem.* **265**, 12143-12145
39. Carey, P. R. (1982) *Biochemical Applications of Raman and Resonance Raman Spectroscopies*, Academic Press, New York
40. Dhawan, I. K., Shelver, D., Thorsteinsson, M. V., Roberts, G. P., and Johnson, M. K. (1999) *Biochemistry* **38**, 12805-12813
41. Vickery, L., Salmon, A., and Sauer, K. (1975) *Biochim. Biophys. Acta* **386**, 87-98
42. Vickery, L., Nozawa, T., and Sauer, K. (1976) *J. Am. Chem. Soc.* **98**, 351-357
43. Takahashi, S., Wang, J., Rousseau, D. L., Ishikawa, K., Yoshida, T., Host, J. R., and Ikeda-Saito, M. (1994) *J. Biol. Chem.* **269**, 1010-1014
44. Asher, S. A., and Schuster, T. M. (1979) *Biochemistry* **18**, 5377-5387

45. Feis, A., Marzocchi, M. P., Paoli, M., and Smulevich, G. (1994) *Biochemistry* **33**, 4577-4583
46. Uchida, K., Shimizu, T., Makino, R., Sakaguchi, K., Iizuka, T., and Ishimura, Y. (1983) *J. Biol. Chem.* **258**, 2519-2525
47. Lad, L., Wang, J., Li, H., Friedman, J., Bhaskar, B., Ortiz de Montellano, P. R., and Poulos, T. L. (2003) *J. Mol. Biol.* **330**, 527-538
48. Fujii, H., Zhang, X., Tomita, T., Ikeda-Saito, M., and Yoshida, T. (2001) *J. Am. Chem. Soc.* **123**, 6475-6484
49. Sugishima, M., Sakamoto, H., Higashimoto, Y., Omata, Y., Hayashi, S., Noguchi, M., and Fukuyama, K. (2002) *J. Biol. Chem.* **277**, 45086-45090
50. Sato, H., Sugishima, M., Sakamoto, H., Higashimoto, Y., Shimokawa, C., Fukuyama, K., Palmer, G., and Noguchi, M. (2009) *Biochem. J.* **419**, 339-345
51. Matsui, T., Furukawa, M., Unno, M., Tomita, T., and Ikeda-Saito, M. (2005) *J. Biol. Chem.* **280**, 2981-2989
52. Dawson, J. H., Andersson, L. A., and Sono, M. (1982) *J. Biol. Chem.* **257**, 3606-3617
53. Sono, M., Andersson, L. A., and Dawson, J. H. (1982) *J. Biol. Chem.* **257**, 8308-8320
54. Pazicni, S., Lukat-Rodgers, G. S., Oliveriusová, J., Rees, K. A., Parks, R. B., Clark, R. W., Rodgers, K. R., Kraus, J. P., and Burstyn, J. N. (2004) *Biochemistry* **43**, 14684-14695
55. Roach, M. P., Pond, A. E., Thomas, M. R., Boxer, S. G., and Dawson, J. H. (1999) *J. Am. Chem. Soc.* **121**, 12088-12093
56. Mowat, C. G., Miles, C. S., Munro, A. W., Cheesman, M. R., Quaroni, L. G., Reid, G. A., and Chapman, S. K. (2000) *J. Biol. Inorg. Chem.* **5**, 584-592
57. Shelver, D., Thorsteinsson, M. V., Kerby, R. L., Chung, S.-Y., Roberts, G. P., Reynolds, M. F., Parks, R. B., and Burstyn, J. N. (1999) *Biochemistry* **38**, 2669-2678
58. Aono, S., Ohkubo, K., Matsuo, T., and Nakajima, H. (1998) *J. Biol. Chem.* **273**, 25757-25764
59. Pazicni, S., Cherney, M. M., Lukat-Rodgers, G. S., Oliveriusová, J., Rodgers, K. R., Kraus, J. P., and Burstyn, J. N. (2005) *Biochemistry* **44**, 16785-16795
60. Clark, R. W., Youn, H., Parks, R. B., Cherney, M. M., Roberts, G. P., and Burstyn, J. N. (2004) *Biochemistry* **43**, 14149-14160

Chapter 5

Identification of a Redox Switch That Controls Affinity of the Human BK Channel for Heme and CO

The results from this chapter were submitted to *J. Biol. Chem.* Yi, L., Morgan, J. T., and Ragsdale, S. W. "Identification of a redox switch that controls affinity of the human BK channel for heme and CO".

In this chapter, Jeffrey T. Morgan characterized the C615S variants, and Li Yi participated in the conception and design of the experiments, performed the remaining experiments, analyzed the data, wrote the first draft, and participated in preparing the final draft manuscript.

5.1 Abstract

Heme is a required prosthetic group in many electron transfer proteins and redox enzymes. The human BK channel, which is a large-conductance Ca^{2+} and voltage-activated K^+ channel, is involved in the hypoxic response in the carotid body. The BK channel has been shown to bind and undergo inhibition by heme and activation by CO. Furthermore, evidence suggests that human HO-2 acts as an oxygen sensor and CO donor that can form a protein complex with the BK channel. Here we describe a thiol/disulfide redox switch in the human BK channel and biochemical experiments of heme, CO and HO-2 binding to a 134-residue region within the cytoplasmic domain of the channel. This region, called the heme binding domain (HBD) forms a linker segment between two Ca^{2+}-sensing domains (called RCK1 and RCK2) of the BK channel. The HBD includes a CXXCH motif in which histidine serves as the axial heme ligand and the two cysteine residues can form a reversible thiol/disulfide redox switch that regulates affinity of the HBD for heme. The reduced dithiol state binds heme (K_d = 210 nM) 14-fold more tightly than the oxidized disulfide state. Furthermore, the HBD is shown to tightly bind CO (K_d = 50 nM) with the Cys residues in the CXXCH motif regulating affinity of the HBD for CO. This HBD is also shown to interact with HO-2. We propose that the thiol/disulfide switch in the HBD is a mechanism by which activity of the BK channel can respond quickly and reversibly to changes in the redox state of the cell, especially as it switches between hypoxic and normoxic conditions.

5.2 Introduction

Large-conductance Ca^{2+} and voltage-activated K^+ channels, also known as Slo or BK channels, play important roles in many physiological phenomena, including oxygen sensing, vasodilation, synaptic transmission, and hormone secretion (1,2). In the carotid body, the BK channel was found to be involved in the hypoxic response (3,4). BK channels (for big K^+) have the largest single-channel conductance of all K^+- selective channels and are activated synergistically by intracellular Ca^{2+} and by membrane potential (1,5). When open, K^+ efflux by the BK channel hyperpolarizes the cell membrane potential. Like other voltage-gated K^+ channels, the human BK channel complex is composed of four pore-forming α (Slo1) subunits that contain transmembrane and cytoplasmic regions (6). Each α subunit includes a seven-helix transmembrane segment (S0) and a voltage-sensing domain (S1-S4) and contributes one-fourth of the ion conduction pore (S5-S6) (7). At the C-terminal end of the BK channel, there is a large more than 700-residue cytoplasmic region, which contains two homologous domains termed "regulators of conductance of potassium" (RCK1 and RCK2) that form a gating ring that is essential for Ca^{2+} activation of the channel (8,9). RCK1 also serves as a H^+ sensor (9,10). RCK domains also exist in other potassium channels, such as MthK (*Methanobacterium thermautotrophicum*), KtrAB (*Vibrio alginolyticus*) and EcoliTrkA2 (*Escherichia coli*) K^+ transporters (11-13).

The BK channel has recently been identified as a hemeprotein (14-17). Heme binding under hypoxic conditions strongly inhibits the channel, while under normoxic conditions, CO, which is generated by heme oxygenase-2 (HO-2) during heme degradation, activates the BK channel. Thus, the substrate (heme) and the product (CO) of heme degradation by HO-2 are implied in regulating channel activity. Furthermore, coimmunoprecipitation experiments in HEK293 cells overexpressing the BK channel indicate that HO-2 can form a complex with the BK channel (15). In addition, knocking out HO-2 expression significantly reduces channel activity (15).

One of the aims of this work is to further explore the interactions between the BK channel and HO-2, heme and CO. This is significant because both heme and CO serve as signaling molecules in various physiological processes in cells, including circadian rhythm, oxygen utilization and T cell activation (18,19). Although heme degradation in

mammals is catalyzed by both the inducible HO-1 and the constituitive HO-2 isozymes (20), HO-2 is the major isozyme in neural tissues and is the sole CO source in neurons (21).

The BK channel appears to be unique as a heme-regulated ion channel. A segment that links RCK1 and RCK2 has been implicated in heme binding (14,16). This linker region contains a CXXCH (X is any amino acid) motif that is highly conserved in all BK channels, and the replacement of the Cys or His residues by Ser or Arg, respectively, abolish the sensitivity of the BK channel to heme and CO (14). CO also binds to the complex between heme and a synthetic 23-residue heme binding peptide (HBP), containing residues 601-623 of the BK channel and including the CXXCH motif (17). Mutagenesis studies demonstrate that an Asp and two His residues within the RCK1 domain are required for the stimulatory action of CO on the BK channel, suggesting another layer of regulation (22).

In our work described here, a soluble 134-residue linker region, which we refer to as the heme-binding domain (HBD), between RCK1 and RCK2 was cloned, expressed and purified to address the heme binding properties of the human BK channel. We characterized the HBD using EPR and UV-visible spectroscopy. Our results demonstrate that His616 in the $C_{612}XXC_{615}H$ motif serves as the axial heme ligand. The Cys residues were shown to form a thiol/disulfide redox switch that regulates the affinities of the channel for heme and CO. In this paper, "oxidized" and "reduced" refer to the state of the disulfide bonds between Cys612-Cys615; the redox state of the Fe in the heme will be explicitly identified as Fe^{3+}-heme or Fe^{2+}-heme. Reduction of the disulfide bond in the CXXCH motif enhances the affinity of HBD for heme by ~14-fold. In addition, replacement of the Cys residues by Ser decreases the CO affinity by over 50-fold. We propose that thiol/disulfide redox modulation of the affinity for heme and CO is one way that the BK channel can rapidly respond to the switch between hypoxic and normoxic conditions.

5.3 Materials and methods

5.3.1 Cloning, overexpression and purification of the HBD of human BK channel

Biochemical studies were performed with a construct that contains residues 584 to 717 of the cytoplasmic C-terminal end of the human BK channel (GI:119574985) (23). This HBD consists of the linker segment between the intracellular RCK1 and RCK2 domains. The HBD fragment was cloned into the NdeI and EcoRI restriction sites of the pET28a (Novagen, Gibbstown, NJ) vector, which fuses the HBD to a 6XHis tag.

We attempted, but were unsuccessful, in expressing and purifying the entire cytoplasmic region of the human BK channel in either *Pichia pastoris* or *E. coli* cells because the protein appeared to aggregate in inclusion bodies. We attempted the expression in yeast using a pPICZαA vector and in *E. coli* using either a pGEX4T-2 vector or a pET28-sumo vector to anchor the glutathione-S-transferase (GST) or sumo fusion tags, respectively, to the protein. None of these approaches yielded a soluble protein. Because our primary interests were in the effects of heme and redox on the channel and because the RCK domains can also be found in other non-heme regulated potassium channels, we finally focused on expressing only the HBD, which contains the characteristic CXXCH motif and connects RCK1 and RCK2 in the human BK channel.

BL21 cells carrying the HBD-pET28a plasmid were cultured at 37 °C in 1 L of Luria-Bertani (LB) medium containing 100 μg/ mL kanamycin. When the optical density (OD_{600}) reached 0.8-1.0, 300 μL of 1 M isopropyl-beta-D-thiogalactopyranoside (IPTG) (Gold Biotechnology, Inc, St. Louis, MO) was added to induce HBD expression. The cells were incubated for another 20 hours at 18 °C and harvested by centrifugation at 7,000 rpm for 10 minutes at 4° C in a J2-HS centrifuge (Beckman, Palo Alto, CA).

The cell pellet was resuspended in 5 volumes of lysis buffer (50 mM Tris-HCl, 400 mM NaCl, 50 mM NaH_2PO_4, 3 mM imidazole and 10% glycerol, pH 8.0), containing 0.1% (v/v) Triton X-100 (Sigma-Aldrich, St. Louis, MO), 1 mM phenylmethylsulfonyl fluoride (Sigma-Aldrich), 2 mM 2-mercaptoethanol (Sigma-Aldrich), EDTA-free protease inhibitor (1 tablet/50mL extraction solution, Roche Applied Science, Indianapolis, IN), lysozyme (0.5 mg/mL, Sigma-Aldrich) and DnaseI (5 units/mL, Sigma-Aldrich) at 4 °C. Cells were then lysed by sonication and the suspension was centrifuged at 17,000 rpm for 1 hr at 4 °C. The supernatant was loaded onto a 5 mL Ni-

NTA agarose column (Qiagen, Valencia, CA), which was extensively washed with wash buffer (50 mM Tris-HCl, 400 mM NaCl, 50 mM NaH_2PO_4, 15 mM imidazole and 10% glycerol, pH 8.0), containing 0.1 % (v/v) Triton X-100. The 6XHis tag-HBD fusion protein was then eluted with elution buffer (50 mM Tris-HCl, 400 mM NaCl, 50 mM NaH_2PO_4 and 10% glycerol, pH 8.0) containing a gradient from 20 to 200 mM imidazole according to the manufacturer's instructions. All these steps were carried out in a cold room under aerobic conditions at 4 °C. Densitometry measurements after SDS-PAGE were performed using UN-SCAN-IT software (gel 6.1, Silk Scientific, Inc. Orem, Utah). Protein concentrations were calculated based on the Bradford method using a standard curve generated using known amounts of BSA (bovine serum albumin, Sigma-Aldrich).

A 23-residue heme binding peptide (HBP) containing residues 601-623 of the BK channel and including the CXXCH motif was also used in our studies. The HBP was designed based on previous research (14) and synthesized from EZBiolab (EZBiolab, Carmel, IN).

The HO-2 and its F253W mutant used in our studies is a truncated form (HO-2Δ289-316, denoted as HO-2 and F253W here, respectively) that lacks the C-terminal membrane-binding region. The generation and purification of HO-2 and its F253W variant were performed as previously described (24,25).

5.3.2 Site-directed mutagenesis of HBD

A number of variants were generated to determine the functional role(s) of the CXXCH motif in the human BK channel, including C612S, C615S, H616A, C612S/C615S, C628S/C630S and F610W. All mutations were generated using the QuikChange site-directed mutagenesis protocol from Stratagene (La Jolla, CA). The HBD-pET28a plasmid was the template for the PCR reactions using primers from Integrated DNA Technologies. All these variants were purified by the same procedure as that described above for the wild-type enzyme.

5.3.3 Quantification of heme binding by the pyridine hemochrome assay

HBD–heme complexes were prepared by incubating 50 μM purified HBD with a 10-fold molar excess of Fe^{3+}-heme from a stock that was freshly prepared in 20 % DMSO to prevent aggregation. After incubation at 4 °C for 10 min, excess free heme was removed by chromatography on a Bio-spin 6 column (Bio-Rad, Hercules, CA). The HBD

concentration in the HBD-Fe^{3+}-heme complexes was determined using the Bradford method. Then HBD-heme complexes were diluted to 2.0 μM or 2.5 μM based on the calculated protein concentration. The amount of heme bound to HBD in the diluted HBD-Fe^{3+}-heme complex was calculated using the pyridine hemochrome assay with a difference extinction coefficient at 556 nm of 28.32 mM^{-1} cm^{-1} (26).

5.3.4 Determination of free thiol groups in HBD

Free thiol quantification of HBD was conducted by the 5,5'-dithio-bis (2-nitrobenzoic acid) (DTNB) assay basically as described previously (27). HBD and variants were added to a reaction buffer containing 100 mM Tris·HCl buffer, pH 8.0 and 100 μM DTNB at room temperature for 15 min. Then, the difference absorption spectrum was recorded and the difference absorption value at 412 nm was used to calculate the free thiol concentration in the protein. The DTNB titration was performed in the presence of 8 M urea to expose all the thiol groups. When the thiol groups in DTT-reduced HBD were measured, the DTT in the protein solution was removed using Bio-spin 6 column (Bio-Rad) under anaerobic conditions before reacting with DTNB.

5.3.5 Electron paramagnetic resonance spectroscopic studies

EPR measurements were performed at 10 K on a Bruker EMX spectrometer, operating with microwave frequencies between 9.376 and 9.379 GHz, and equipped with an Oxford ITC4 temperature controller, a Hewlett-Packard Model 5340 automatic frequency counter, and a Bruker gaussmeter (Bruker Biospin Corp., Billerica, MA). The EPR samples were prepared in 50 mM phosphate buffer at pH 7.5. The EPR spectrum of the low-spin heme in HBD-Fe^{3+}-heme complex was simulated using the Bruker SimFonia program (Bruker Biospin Corp., Billerica, MA).

5.3.6 Determination of the affinity of HBD for Fe^{3+}-heme, Fe^{2+}-heme and Fe^{2+}-heme-CO

The heme binding affinity of each of the HBD variants was determined as previously described in an Olis-updated CARY-14 double beam spectrophotometer (24). For measurements with the reduced (dithiol-containing) protein, the as-isolated protein was incubated with a 100-fold molar excess of DTT in the anaerobic chamber (Vacuum Atmospheres Company, Hawthorne, CA) for 30 min and, then, DTT was removed by performing chromatography on a Bio-spin 6 column twice. The titration was performed

under anaerobic conditions in serum-stoppered cuvettes. The Fe^{3+}-heme and Fe^{2+}-heme stock solutions were freshly prepared as previously described (24).

To determine the binding affinity of the HBD-Fe^{2+}-heme complex for CO, the HBD-Fe^{2+}-heme complex was purified using chromatography on a Bio-spin 6 column in an anaerobic chamber. Then, freshly prepared CO solutions were added to the reference and sample (containing the HBD-Fe^{2+}-heme complex) cuvettes and the difference spectra from 350 nm to 750 nm were measured. The CO concentration in the stock solution was calculated by titration against a known amount of myoglobin, using extinction coefficients of 121 $mM^{-1}cm^{-1}$ (deoxyMb) at 435 nm and 207 $mM^{-1}cm^{-1}$ (MbCO) at 423 nm (28). The titration experiments were performed under anaerobic conditions.

5.3.7 Intrinsic fluorescence quenching analysis

Strong intrinsic tryptophan fluorescence is not detectable in the as-isolated HBD; therefore, we engineered a Phe-to-Trp substitution near the CXXCH motif in HBD. This F610W variant exhibits intrinsic tryptophan fluorescence that decreases upon adding HO-2, providing a straightforward and direct measure of the interaction between HBD and HO-2. The excitation wavelength was set at 285 nm. Intensity of the fluorescence emission at 340 nm of the F610W (1 μM) variant of the HBD was measured with a Shimadzu RF-530 1 PC spectrofluorophotometer (Columbia, MD) at 20 °C. Fluorescence quenching experiments were also performed by titrating the HBD containing zinc protoporphyrin (ZnPP) (Sigma-Aldrich) with Fe^{3+}-heme-bound HO-2. For the Zn-PP experiments, the excitation wavelength was set at 415 nm and the emission at 588 nm was recorded.

5.3.8 Data fitting

The heme titration data were plotted and fit to a one-site binding model to determine the dissociation constants (Equations 1 and 2). ΔA is the absorbance difference between sample and reference cuvettes. $\Delta\varepsilon$ is the difference extinction coefficient between bound and free ligand and EL is the concentration of the protein-ligand complex. The EL concentration is determined using the quadratic Equation 2, in which E_O is the total protein concentration, L_O is the total ligand concentration and K_d is the dissociation constant. The quadratic binding equation was used because the K_d value was near the concentration of protein in the assay.

$\Delta A = \Delta\varepsilon \cdot EL$ (Eq.1)

$EL = 0.5\{E_O + L_O + K_d - [(E_O + L_O + K_d)^2 - 4\ E_O \cdot L_O]^{1/2}\}$ (Eq.2)

The intrinsic fluorescence quenching data were plotted and fit using the same basic equation with heme titration data. A one-site binding model was used to determine the dissociation constants (Equations 3-6). ΔEM is the emission intensity difference between sample and reference cuvettes. EM_O is the initial emission intensity cause by unbound analyte. Δε is the difference extinction coefficient between bound and free titrant, and EL is the concentration of the analyte-titrant complex. In intrinsic fluorescence quenching experiments, the EM (emission) intensity was corrected with inner-filter effect correction (29). EL concentration is determined using the quadratic Equation 6, in which E_O is the total analyte concentration, L_O is the total titrant concentration and K_d is the dissociation constant. The quadratic binding equation was used because the K_d value was near the concentration of protein in the assay.

$\Delta EM = -\Delta\varepsilon \cdot EL + EM_O$ (Eq.3)

$b = (E_O + L_O + K_d)$ (Eq.4)

$c = E_O \cdot L_O$ (Eq.5)

$EL = [b - (b^2 - 4 \cdot c)^{1/2}]/2$ (Eq.6)

5.3.9 Determination of the midpoint reduction potential of the thiol/disulfide redox couples in HBD

The midpoint reduction potential of the thiol/disulfide redox couples in HBD was calculated using Mal-PEG 5000 (Laysan Bio, Arab, AL) alkylation as previously described (25). The data was fitted with the Nernst Equation (Eq. 7). In equation 3, *E* is the ambient potential in solution; E^0 is the midpoint reduction potential of the thiol/disulfide couple in the HBD; *R* is the universal gas constant: $R = 8.31\ JK^{-1}mol^{-1}$; *T* is the absolute temperature; *F* is the Faraday constant ($9.65\times10^4\ Cmol^{-1}$); and *z* is the number of electrons transferred in the reaction.

$$E = E^0 - \frac{RT}{zF} \ln \frac{[\text{reduced HBD}]}{[\text{oxidized HBD}]} \qquad \text{(Eq.7)}$$

5.4 Experimental results

5.4.1 Evaluation of heme binding to the CXXCH motif in HBD

Previous *in vivo* electrophysiological studies indicated that the human BK channel binds heme (14); however, quantitative heme binding studies of the channel have not been performed. Because our primary interests were in the effects of heme and redox on the channel, we finally focused on expressing the HBD, which is a soluble and well-behaved protein that contains the characteristic CXXCH motif and connects RCK1 and RCK2 in the human BK channel.

We successfully cloned and expressed the 6XHis tagged HBD in *E. coli* cells and purified the 20 kDa protein to 85% homogeneity, based on densitometry measurements of the bands observed in SDS-PAGE experiments (**Figure 5.1**). The real UV-visible spectra of the Fe^{3+}, Fe^{2+} and Fe^{2+}-CO states of the as-isolated protein, in which cysteines were present in their disulfide states (**Table 5.1**), demonstrate that HBD specifically binds ferric and ferrous heme with a His residue as the axial ligand (**Figure 5.2**). The absorbance maximum for the Soret peak for the Fe^{3+}-heme is at 406 nm. The Fe^{2+}-heme exhibits a Soret peak at 426 nm and two long-wavelength peaks at 530 nm and 560 nm, while the Fe^{2+}-heme-CO adduct shows a Soret peak at 419 nm and two long wavelength peaks at 535 nm and 568 nm.

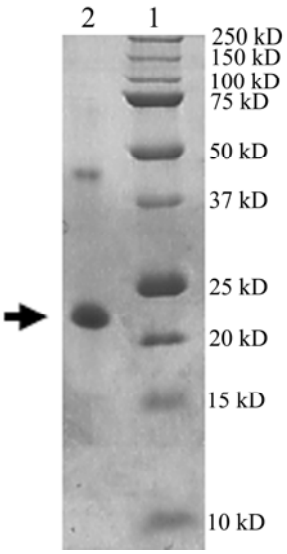

FIGURE 5.1 **SDS-PAGE of purified HBD protein.** Lane 1, molecular mass marker; Lane 2, 15 μg purified HBD.

TABLE 5.1 **Quantification of free thiols in oxidized and reduced HBD by the DTNB assay.** Assays for oxidized proteins were performed in the air. Reduced proteins were generated by treatment with DTT in the anaerobic chamber followed by removal of the excess DTT (see details in "Materials and Methods"). HBD was incubated in the presence of 8 M urea under aerobic or anaerobic conditions. All measurements were performed in triplicate with different amounts of protein. The average number of free thiols (mol/mol protein) are presented.

	- DTT treatment + Urea	+ DTT treatment + Urea
HBD	0.21 ± 0.01	4.1 ± 0.2
H616A	0.20 ± 0.01	4.0 ± 0.2
C612S	0.86 ± 0.01	2.5 ± 0.2
C615S	0.89 ± 0.08	2.7 ± 0.7
C612S/C615S	0.19 ± 0.06	2.2 ± 0.1

The axial EPR spectra of as-isolated HBD indicate a predominantly six-coordinate high-spin Fe^{3+}-heme with *g*-values at 5.92 and 1.99 (**Figure 5.3A**). This spectrum is different from those of five-coordinate high-spin Fe^{3+}-heme systems (30), which generally are rhombic. The *g*-values are indicative of ligation by histidine and water, as observed in myoglobin (30). Interestingly, in addition to the predominantly six-coordinate high-spin Fe^{3+}-heme species, there is a minor low-spin component with *g*-values (g_1 = 2.96, g_2 = 2.25, and g_3 = 1.53) that are characteristic of His/His axial ligation (31) (**Figure 5.3A and insets**). The EPR spectra of the H616A variant are very weak, reflecting the low levels of heme bound to the form of H616A lacking its axial heme ligand; however, this small signal is suggestive of a histidine-bound heme (**Figure 5.3C**). Thus, the UV-visible and EPR spectroscopic analysis indicate that the linker segment between the two RCK domains in human BK channel is the HBD with His616 in the CXXCH motif as the protein-based heme ligand.

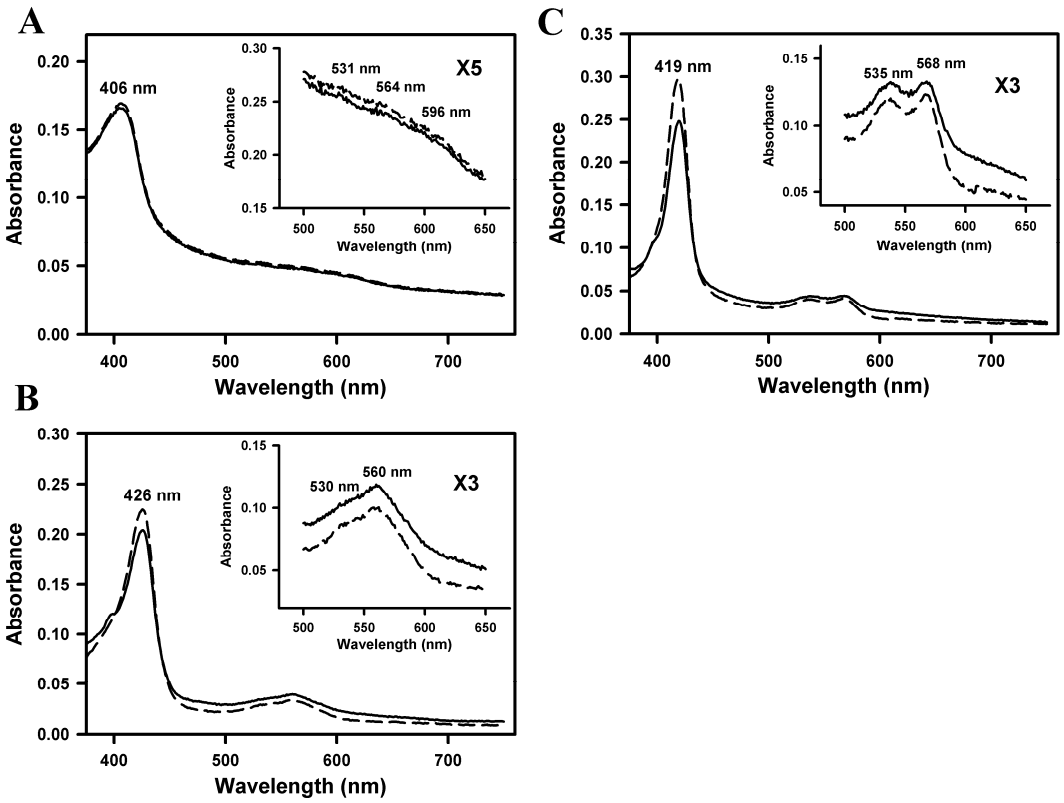

FIGURE 5.2 **Absorption spectra of complexes between heme and HBD.** HBD (1.5 μM) and heme (1.5 μM) were present in the sample cell with only buffer in the reference cell. The insets are expansions of the 500 - 630 nm range. The spectra are obtained from complexes between the oxidized (solid line) and reduced (dashed line) forms of the HBD with: (**A)** Fe^{3+}-heme, (**B)** Fe^{2+}-heme and (**C)** Fe^{2+}-heme–CO.

5.4.2 Cys612 and Cys615 undergo thiol/disulfide redox interconversion

There are four highly conserved Cys residues located in the HBD of the human BK channel; two are in the CXXCH motif (Cys612 and Cys615) and the other two are located at positions 628 and 630. To determine the redox states of these residues, we measured the number of free thiol groups in HBD and variants in their oxidized and DTT-reduced states using the DTNB assay (**Table 5.1**). In all cases, DTT was removed before the DTNB assay. This assay was performed with urea denatured-HBD to ensure that all Cys residues were accessible to the DTNB. Only 0.20 and 0.21 thiol groups were detected for as-isolated the HBD and the H616A variant, respectively; however, four thiols per mol protein were measured for the DTT-reduced HBD (4.1) and the H616A variant (4.0). The C612S and C615S variants contain a single (0.86 and 0.89, respectively)

free thiol group in the oxidized state, while, in the DTT-reduced state, they contain three (2.5 and 2.7, respectively). Correspondingly, the C612S/C615S variant, contains no (0.19) free thiol groups in the oxidized state, but two (2.2) in the DTT-reduced state. Thus, the combined results of the DTNB titrations strongly indicate that as-isolated HBD contains two intramolecular disulfide bonds; one is between Cys612 and Cys615, the other is between Cys628 and Cys630.

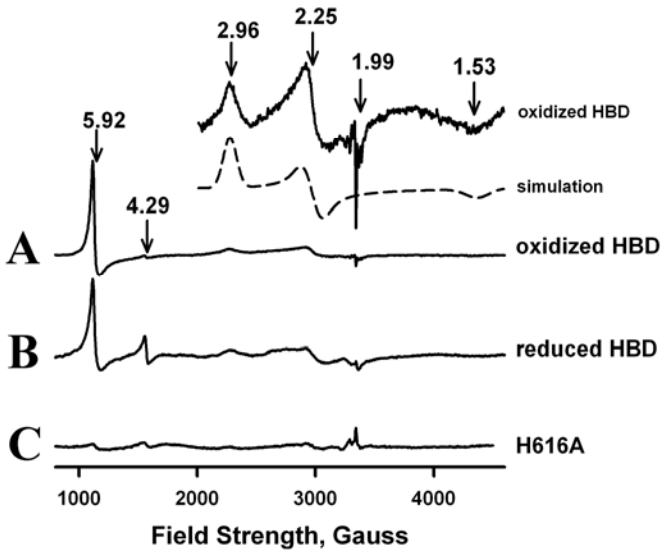

FIGURE 5.3 **EPR spectra of Fe^{3+}-heme complexed with HBDs.** Samples were prepared with a 1:1 ratio of Fe^{3+}-heme and HBD as described in Materials and Methods. EPR measurements were performed at 10 K with microwave frequency of 9.376-9.379 GHz, microwave power of 1mW, field modulation amplitude of 10.15 G at 100 kHz. **A,** 100 μM Fe^{3+}-heme plus oxidized HBD, with samples were prepared in air. **B,** 100 μM Fe^{3+}-heme plus reduced HBD, with samples were prepared under anaerobic conditions. **C.** 100 μM Fe^{3+}-heme plus H616A. The Inset shows an 8-fold vertical expansion of the low-spin region of spectrum A and the best-fit simulation (dashed line).

5.4.3 Stoichiometry of heme binding to the HBD

To measure the heme stoichiometry, a ten-fold molar excess of heme was incubated with the oxidized and reduced HBD. Unbound heme was removed by gel filtration chromatography and the heme content was measured by the pyridine hemochrome assay. Oxidized HBD, at 2.0 μM, was found to bind 1.6 (± 0.1) μM Fe^{3+}-heme and reduced HBD, at 2.5 μM, bound 2.3 (± 0.1) μM Fe^{3+}-heme (**Figure 5.4A and 4B**). The results

indicated that both oxidized and reduced HBD saturate at a 1:1 complex with Fe^{3+}-heme. Furthermore, the EPR spectrum of the reduced HBD is indistinguishable from that of the oxidized protein (**Figure 5.3A and 3B**), indicating a predominantly six-coordinate high-spin state heme. In addition, the absorption spectra of the Fe(III)-, Fe(II)- and Fe(II)-CO states of DTT-reduced HBD, are identical to those of the corresponding states of the oxidized protein (**Figure 5.2**). Thus, the heme ligands in the ferric, ferrous, and ferrous-CO states are independent of the redox state of cysteines in the HBD. There is no evidence for heme binding to any of the four Cys residues in the HBD.

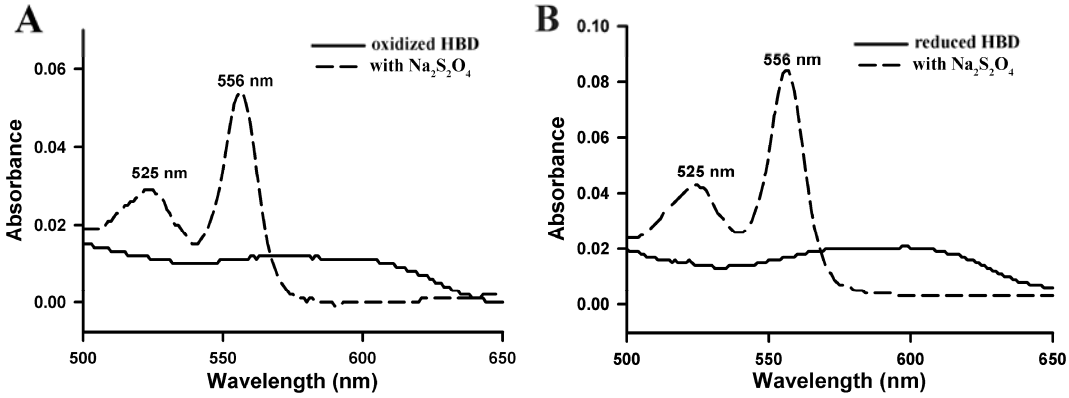

FIGURE 5.4 **Fe^{3+}-heme binding to HBD assayed by the pyridine hemochrome method. A,** 2.0 μM oxidized HBD. **B,** 2.5 μM reduced HBD. Protein concentration was calculated by the Bradford method. The heme concentration was determined by following the absorbance change at 556 nm (See details in "Materials and Methods").

5.4.4 Determination of the redox potential of cysteines in HBD

To test the hypothesis that the redox switch constituted by Cys residues in HBD is physiologically relevant, the midpoint reduction potential of the thiol/disulfide redox couples was determined. Since the Cys628S/Cys630S variant is very unstable, only the overall redox potential of the cysteines in HBD could be determined. After as-isolated HBD samples were equilibrated with solutions having a gradient of ambient redox potentials from -133 mV to -252 mV, the proteins were precipitated and alkylated with MAL-PEG 5000 and run on nonreducing SDS-PAGE. MAL-PEG 5000 traps free thiol residues as an adduct that increases the protein's mass by 5 kDa per thiol modification.

Thus, the oxidized (non-modified disulfide) is the lowest band on the non-reducing gel and the modified proteins are the other bands of increasing size (**Figure 5.5A**). There are four bands besides that of the fully oxidized HBD (the lowest band) existing in the non-reducing gel, which results from the graded alkylation during the reaction with MAL-PEG 5000. Then, the ratio of fully reduced/fully oxidized protein at each ambient redox potential was quantified and fitted to the Nernst equation. The midpoint reduction potential of the thiol/disulfide couples in HBD was determined to be -184 (± 2) mV (**Figure 5.5B**). This midpoint potential represents a cumulative value corresponding to both the Cys612/Cys615 and C6ys28/Cys630 couples. Because the data fit a single titration curve and because bands corresponding to the modification of four Cys residues are observed, we conclude that both thiol/disulfide pairs are redox active and have similar redox potentials. Furthermore, because the intracellular ambient redox potential ranges from -170 mV to -325 mV (32,33), the measured midpoint potential (-184 mV) indicates that both thiol/disulfide redox couples (Cys612/Cys615 and Cys628/Cys630) in the HBD are poised to respond to the redox state within the cell.

5.4.5 Effect of redox state of the Cys612-Cys615 on heme binding

The effect of the redox state of the Cys612-Cys615 thiol/disulfide redox couple on heme binding was determined. As described above, HBD binds only 1 heme per mol protein in both oxidized and reduced states. However, the Fe^{3+}-heme titration curves of the oxidized and reduced HBD are noticeably different, indicating different affinities of the oxidized and reduced HBD for Fe^{3+}-heme (**Figure 5.6A**). Thus, the dissociation constants (K_d) were measured for the oxidized and reduced states of HBD and for the CXXCH variants.

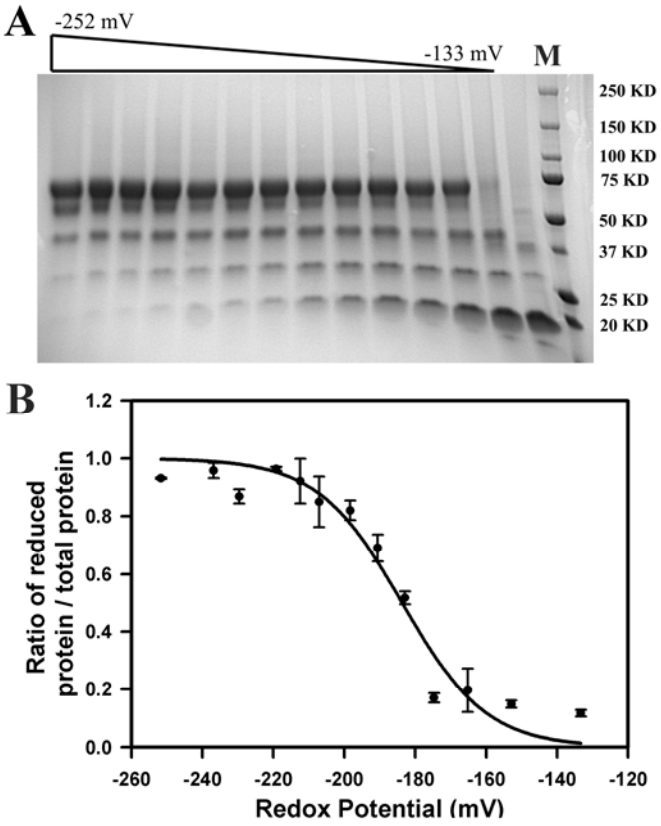

FIGURE 5.5 **Measurement of the midpoint redox potential of the thiol/disulfide couples in HBD**. The ambient redox potential, set by variation of the GSSG/GSH ratio, ranged from -133 mV to -252 mV. (See details in "Materials and Methods"). **A,** SDS-PAGE analysis of the alkylation of HBD by Mal-PEG 5000. M: molecular mass marker. **B,** Nernst analysis of results from non-reducing PAGE shown in A. The redox potential of the thiol/disulfide couples in HBD is $E^0 = -184 \pm 2$ mV.

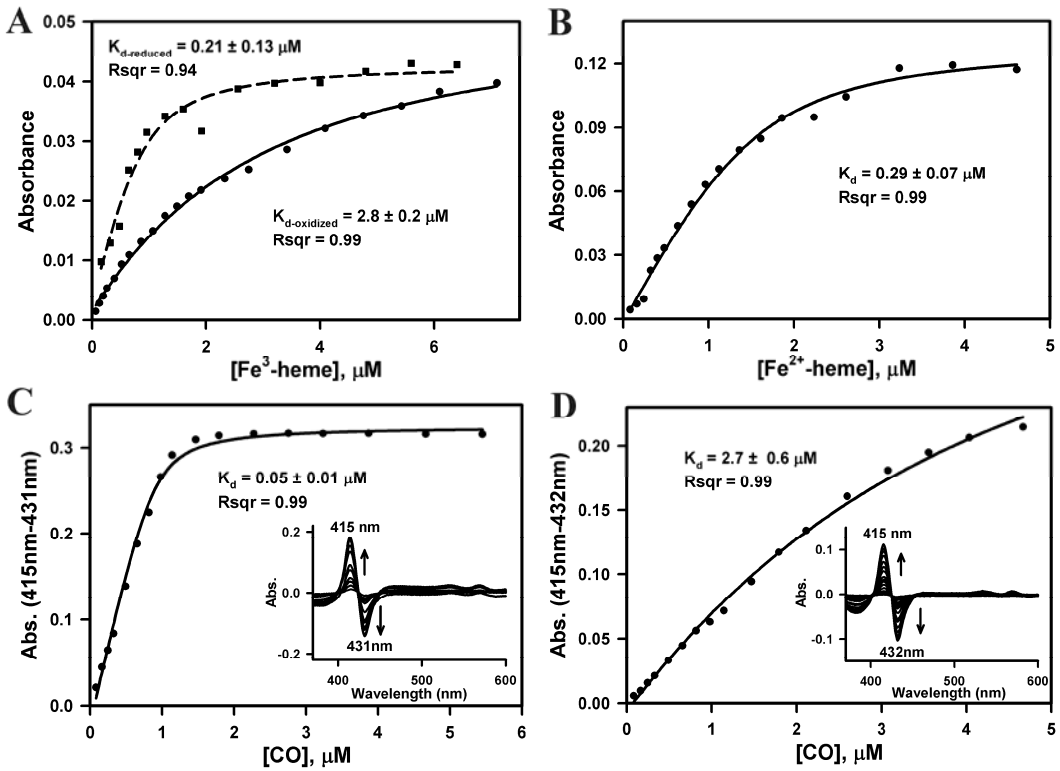

FIGURE 5.6 **Titration of HBD and the C612/C615 HBD variant with Fe^{3+}-heme, Fe^{2+}-heme, and Fe^{2+}-heme-CO.** Titrations were performed by monitoring the absorbance increase at 415 nm (Fe^{3+}-heme), 426 nm (Fe^{2+}-heme) and by subtracting the absorbance at 431/432 nm from that at 415 nm (Fe^{2+}-heme-CO). A, 1 μM oxidized and reduced HBD proteins were titrated with Fe^{3+}-heme. Oxidized HBD (solid line), reduced HBD (dash line). B, 1 μM reduced HBD protein was titrated with Fe^{2+}-heme. C, 1 μM reduced HBD-Fe^{2+}-heme complexes were titrated with CO. D, 1 μM reduced C512S/C615S-Fe^{2+}-heme complexes were titrated with CO. The Insets in C and D are the difference spectra from the CO titration. Dissociation constants (K_d) were calculated by using the quadratic equation with a one-site binding model (see details in "Materials and Methods").

Dissociation constants (K_d values) for the complexes between the HBD (and the HBD variants) and Fe^{3+}-heme were calculated by fitting the data to a quadratic one-site binding model (**Table 5.2**). The K_d values of all the oxidized HBD proteins were very high, varying from 1.50 to 13.5 μM, indicating a very weak Fe^{3+}-heme affinity. However, the Fe^{3+}-heme binding affinity of reduced HBD (K_d = 0.21 μM) was 14-fold higher than that of the oxidized protein (K_d = 2.8 μM) (**Figure 5.6A**). Similar results were observed with the HBP (**Table 5.2 and Figure 5.7**) that contains the CXXCH motif. For the

oxidized HBP (generated by treatment with diamide), the K_d value for the ferric heme is 14.5 ± 4.6 μM, which is 90-fold higher than that of the reduced HBP (K_d = 0.16 ± 0.05 μM). In addition, the oxidized and reduced C612S/C615S variant exhibited a similar weak Fe^{3+}-heme affinity, with K_d values of 1.5 μM and 1.7 μM in the oxidized and reduced states, respectively (**Figure 5.8**). The H616A variant exhibited very large K_d values (K_d = 13.5 μM), as expected if His616 is the heme ligand in HBD (**Figure 5.9**). These results strongly indicate that Cys612 and Cys615 may act as a redox switch that controls ferric heme binding to HBD. Considering the overall midpoint reduction potential of the cysteines in HBD is -184 mV, this switch might have physiological relevance in cells.

TABLE 5.2 **Heme affinity of HBD.** Fe^{3+}-heme and Fe^{2+}-heme titrations were performed with the oxidized and reduced states of HBD (and HBD variants) under aerobic and anaerobic conditions, respectively. A freshly prepared heme solution was titrated into a 1 μM HBD (or HBP) solution, and the absorbance spectra were recorded. The absorbance value at the Soret peak (415 nm for Fe^{3+}-heme titration and 426 nm for Fe^{2+}-heme titration) was plotted versus heme concentration. K_d was calculated by using the quadratic equation with a one-site binding model (see details in "Materials and Methods"). All the measurements were done in triplicate.

	Ferric Heme Titration		Ferrous Heme Titration	Ferrous Heme-CO Titration
	Oxidized Form K_d (μM)	Reduced Form K_d (μM)	Reduced Form K_d (μM)	Reduced Form K_d (μM)
HBD	2.8 ± 0.2	0.21 ± 0.13	0.29 ± 0.07	0.05 ± 0.01
C612S/C615S	1.5 ± 0.1	1.7 ± 0.3	0.49 ± 0.29	2.7 ± 0.6
H616A	13.5 ± 2.0	7.4 ± 0.8	3.3 ± 0.8	13.8 ± 3.7
F610W	2.0 ± 0.2	0.42 ± 0.10	0.18 ± 0.03	0.03 ± 0.01
HBP	14.5 ± 4.6	0.16 ± 0.05	ND	ND

ND: not determined

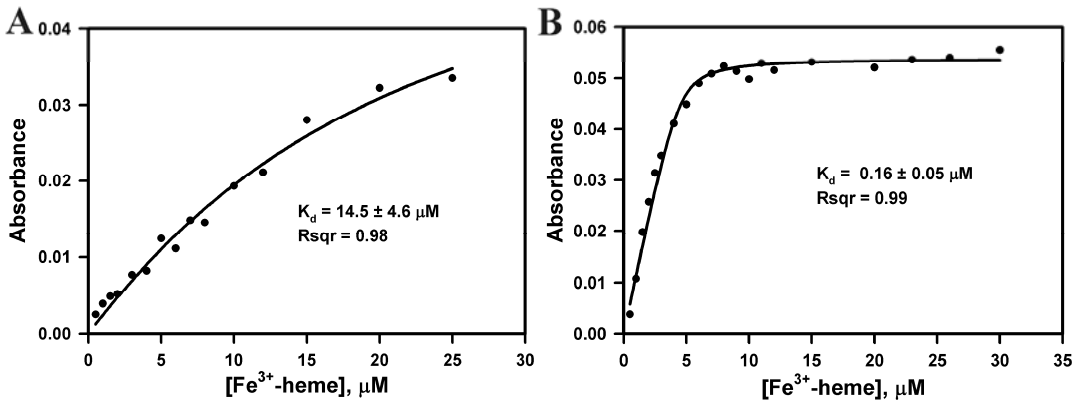

FIGURE 5.7 **Titration of oxidized and reduced HBP with Fe^{3+}-heme.** Titration curves were developed by monitoring the absorbance increase at 415 nm (Fe^{3+}-heme). **A**, 5 μM oxidized HBP peptide (601-623) was titrated with Fe^{3+}-heme. **B**, 5 μM reduced HBP peptide (601-623) was titrated with Fe^{3+}-heme. Dissociation constants (K_d) were calculated by using the quadratic equation with a one-site binding model (see details in "Materials and Methods"). The 23-residue HBP contains residues 601-623 of the BK Channel.

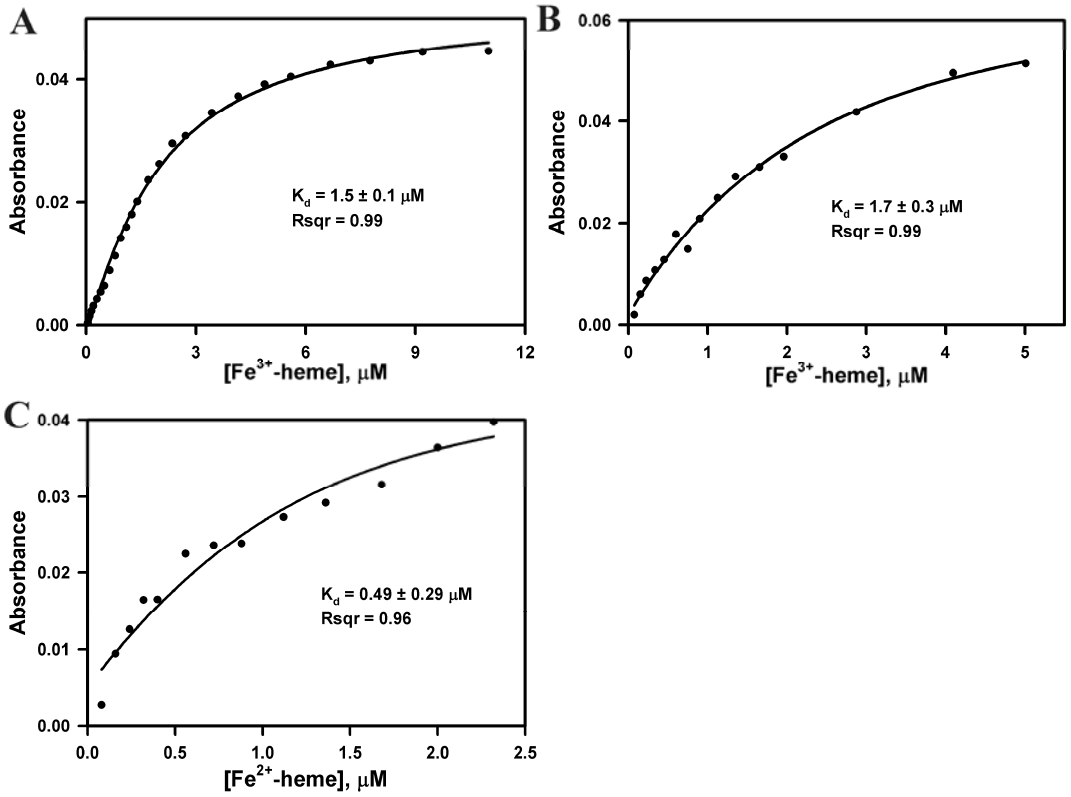

FIGURE 5.8 **Titration of the C612S/C615S HBD variant with Fe^{3+}- and Fe^{2+}-heme.** Titrations were performed by monitoring the absorbance increase at 415 nm (Fe^{3+}-heme) and 426 nm (Fe^{2+}-heme). A, 1 μM oxidized C612S/C615S protein was titrated with Fe^{3+}-heme. B, 1 μM reduced C612S/C615S protein was titrated with Fe^{3+}-heme. C, 1 μM reduced C512S/C615S protein was titrated with Fe^{2+}-heme. Dissociation constants (K_d) were calculated by using the quadratic equation with a one-site binding model (see details in "Materials and Methods").

5.4.6 Effect of substitutions in Cys612 and Cys615 on Fe^{2+}-heme-CO Binding

Heme binding to the BK channel inhibits channel activity, while CO can activate the channel. Thus, we measured how a substitution in the Cys612-Cys615 couple affects CO binding to the Fe^{2+}-heme (**Table 5.2**). We were unable to perform these titrations with both redox states of the HBD because reductants that reduce the Fe^{3+}-heme also reduce the disulfide bonds in HBD. The native HBD and the C612S/C615S variant have similar affinities for Fe^{2+}-heme, with K_d values of 0.29 μM and 0.49 μM, respectively (**Figure 5.6B and Figure 5.8C**). However, the HBD-Fe^{2+}-heme complex has a 50-fold higher affinity for CO (K_d = 0.05 μM) (**Figure 5.6C**) than the C612S/C615S variant (K_d = 2.7

μM) (**Figure 5.6D**). The H616A variant has even weaker affinity for CO (K_d = 13.8 μM), presumably due to loss of the heme ligand (**Figure 5.9D**).

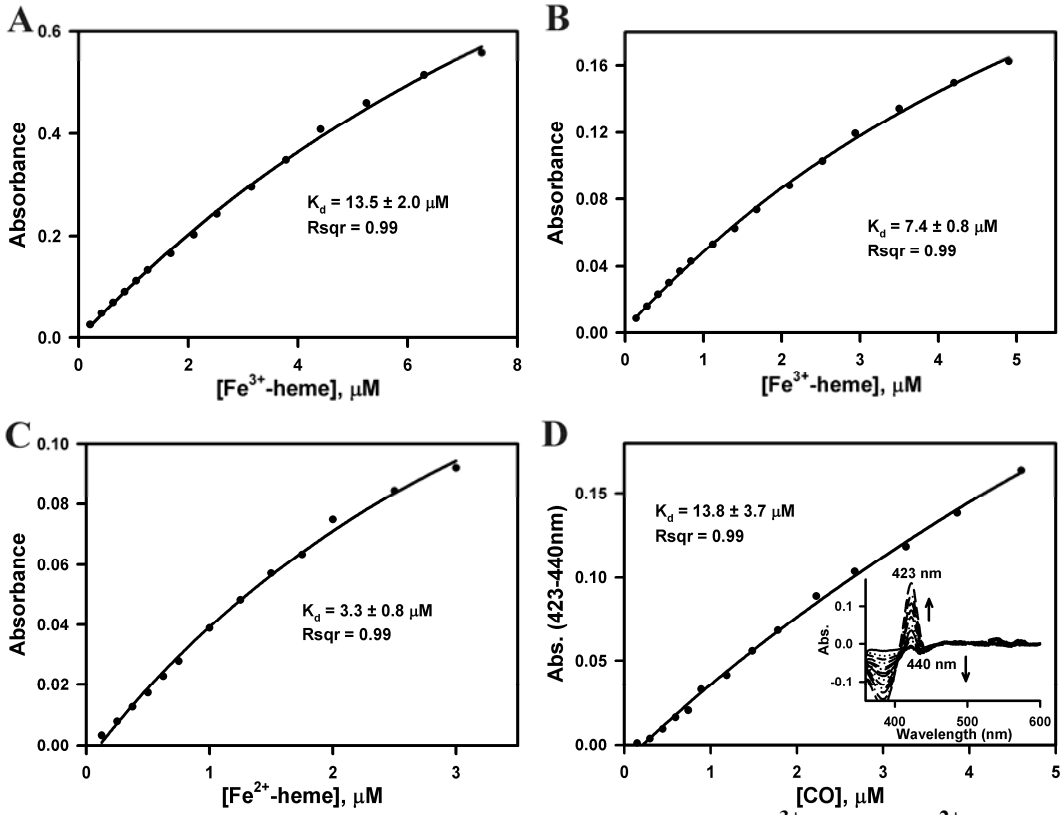

FIGURE 5.9 **Titration of the H616A HBD variant with Fe^{3+}-heme, Fe^{2+}-heme, and Fe^{2+}-heme-CO.** Titrations were performed by monitoring the absorbance increase at 415 nm (Fe^{3+}-heme), 426 nm (Fe^{2+}-heme) and by subtracting the absorbance at 440 nm from that at 423 nm (Fe^{2+}-heme-CO). A, 1 μM oxidized H616A protein was titrated with Fe^{3+}-heme. B, 1 μM reduced H616A protein was titrated with Fe^{3+}-heme. C, 1 μM reduced H161A protein was titrated with Fe^{2+}-heme. D, 1 μM reduced H161A-Fe^{2+}-heme complex was titrated with CO. Dissociation constants (K_d) were calculated by using the quadratic equation with a one-site binding model (see details in "Materials and Methods").

5.4.7 HBD interaction with HO-2

HO is the only heme degradation enzyme identified so far in mammals. *In vivo* studies indicated that HO-2 acts as an oxygen sensor to form a complex with human BK channel, regulating channel activity (15). Since the HBD was identified as the heme regulatory domain in BK channel, we formed the hypothesis that HBD is the key domain

involved in the interaction with HO-2. This hypothesis was addressed using intrinsic tryptophan fluorescence quenching experiments with a F610W HBD variant (**Figure 5.10**). We performed this substitution at position 610 because, if Cys612 and Cys615 are part of a loop or helix, an aromatic residue at position 610 would not be expected to interfere with the disulfide bond. While sequence comparisons reveal that both Trp609 and Tyr610 naturally occur in several organisms, the F610W variant exhibits intense intrinsic fluorescence, but the F609W variant does not. The F610W variant has similar affinities for Fe^{3+}-heme, Fe^{2+}-heme, and Fe^{2+}-heme-CO as does the native HBD (**Table 5.2 and Figure 5.11**), indicating that this Phe-to-Trp replacement does not significantly change the properties of HBD. The Fe^{3+}-heme binding affinity of oxidized F610W (K_d = 2.0 μM) was five-fold lower than that of reduced F610W (K_d = 0.42 μM). Furthermore, the affinities of reduced F610W for Fe^{2+}-heme (K_d = 0.18 μM) and Fe^{2+}-heme-F610W complex for CO (K_d = 0.03 μM) were comparable to those of reduced HBD, indicating that the Phe to Trp mutation does not undermine the binding abilities of protein for Fe^{2+}-heme and CO. When excited at 285 nm, the F610W variant exhibited an emission spectrum centered at 338 nm. Fluorescence quenching was observed when either apo-HO-2 or heme-bound HO-2 was titrated into the F610W variant of HBD, yielding K_d values of 0.25 ± 0.08 μM and 0.43 ± 0.04 μM, respectively (**Figure 5.10A and 5.10B**). The interaction between HO-2 and HBD was further investigated by titrating HBP into the F253W HO-2 variant, which has been shown to exhibit quenching of intrinsic Trp fluorescence in earlier ligand binding and redox titration experiments (25). Fluorescence quenching was also observed when apo-HBP was titrated into F253W, indicating the CXXCH motif and its nearby region may be involved in its interaction with HO-2 (**Figure 5.12**).

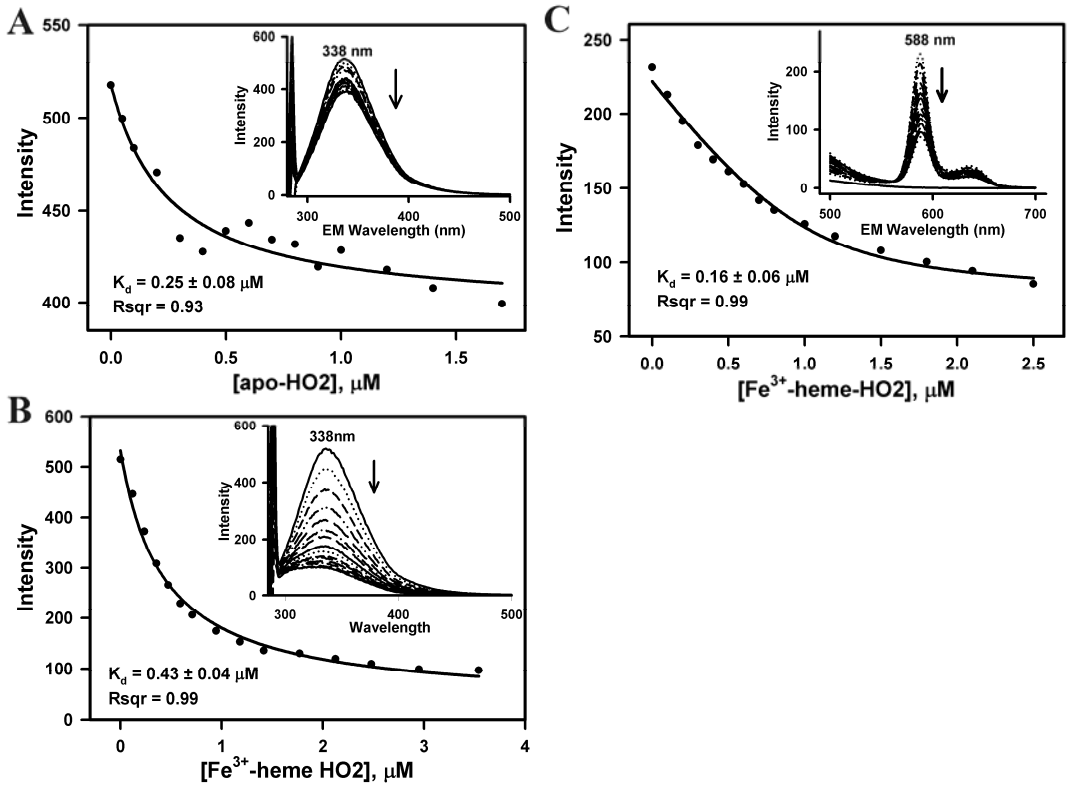

FIGURE 5.10 **Titration of HBD with HO-2.** Fluorescence quenching experiments were performed to examine the interaction between HBD and HO-2. The data was corrected by subtracting the inner-filter effect as described (29). **A,** apo-F610W was titrated with apo-HO-2. The experiments were performed by exciting at 285 nm and following the emission intensity at 338 nm. **B,** apo-F610W was titrated with Fe^{3+}-heme-HO-2, with the excitation wavelength set at 285 nm, and the emission intensity was measured at 338 nm. **C,** ZnPP-HBD was titrated with Fe^{3+}-heme-HO-2, with excitation at 415 nm and emission at 588 nm.

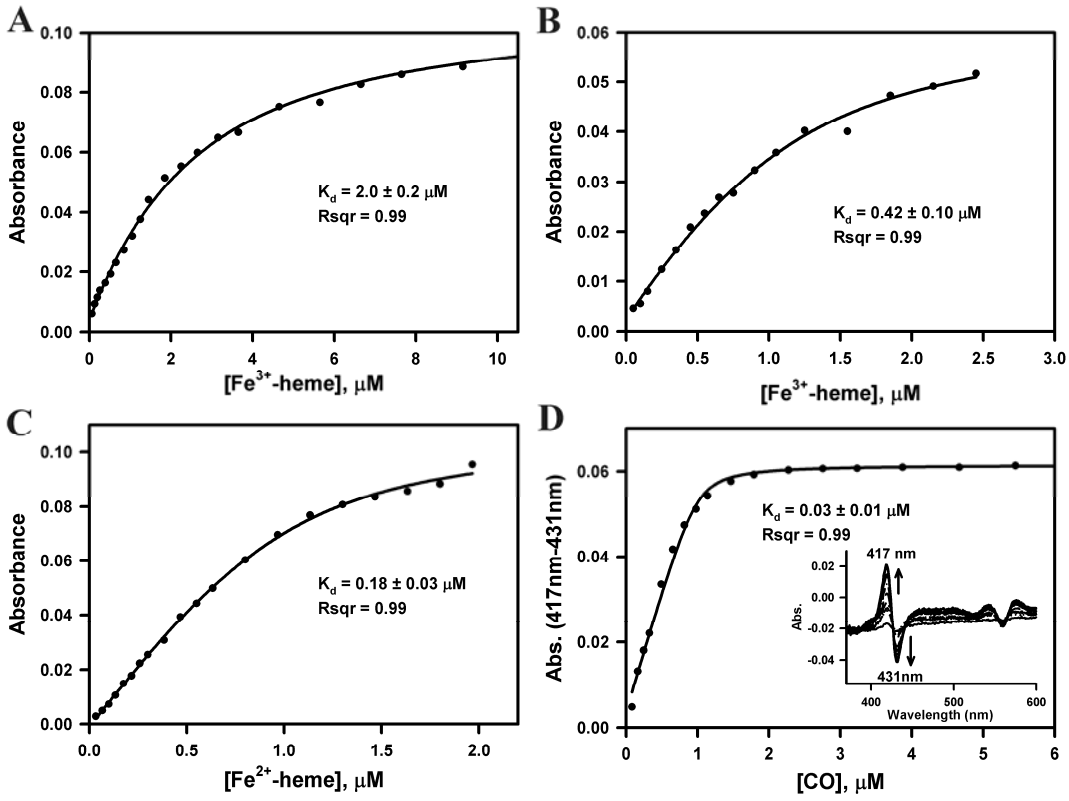

FIGURE 5.11 **Titration of F610W HBD variant with Fe^{3+}-heme, Fe^{2+}-heme, and Fe^{2+}-heme-CO.** Titrations were performed by monitoring the absorbance increase at 415 nm (Fe^{3+}-heme), 426 nm (Fe^{2+}-heme), and by subtracting the absorbance at 431 nm from that at 417 nm (Fe^{2+}-heme-CO). **A,** 1 μM oxidized F610W protein was titrated with Fe^{3+}-heme. **B,** 1 μM reduced F610W protein was titrated with Fe^{3+}-heme. **C,** 1 μM reduced F610W protein was titrated with Fe^{2+}-heme. **D,** 1 μM reduced F610W-Fe^{2+}-heme complexes were titrated with CO. The insets are the difference spectra from the CO titration. Dissociation constants (K_d) were calculated by using the quadratic equation with a one-site binding model (see details in "Materials and Methods").

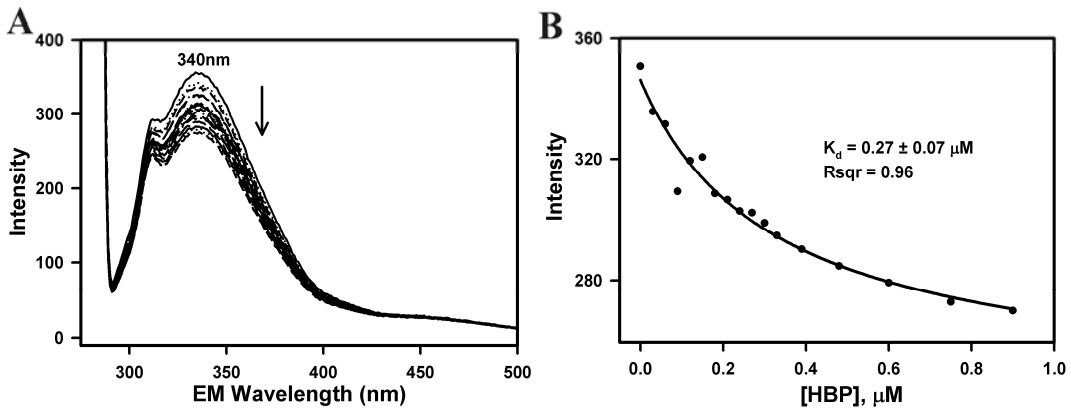

FIGURE 5.12 **Titration of the HBP with HO-2(F253W).** Fluorescence quenching experiments were performed to assess the interaction between HBD and HO-2. The data was corrected by applying inner-filter effect. 300 nM HO-2 (F253W) was titrated with HBD peptide (601-623), The excitation wavelength was 285 nm and the emission was monitored at 340 nm. A, Spectra of F153W being titrated with HBP. B, Dissociation constants (K_d) were calculated by using the quadratic equation with a one-site binding model (see details in "Materials and Methods").

In related experiments, ZnPP was used to monitor interactions between HO-2 and the HBD. In order to ensure that "heme" exchange did not occur during the experiments, it was important to first establish whether HO-2 or the HBD binds ZnPP most tightly. It was established that the oxidized HBD has a significantly higher affinity for ZnPP (K_d = 0.22 μM) than for Fe^{3+}-heme (**Figure 5.13A**). On the other hand, HO-2 binds Fe^{3+}-heme (K_d = 0.03 μM, (24)) 15-fold more tightly than ZnPP (K_d = 0.45 μM, **Figure 5.13B**). Thus, we could monitor quenching of fluorescence from the ZnPP-HBD complex, which has its emission peak at 588 nm when excited at 415 nm. When the ZnPP-HBD complex was titrated with heme-bound HO-2, significant fluorescence quenching was detected (K_d = 0.16 ± 0.06 μM) (**Figure 5.10C**). These fluorescence-quenching studies complement the intrinsic Trp fluorescence quenching experiments and strongly indicate that the HBD not only binds heme, but also is the site in the BK channel that interacts with HO-2. Our results indicate that this interaction can occur in both apo- and heme-bound states.

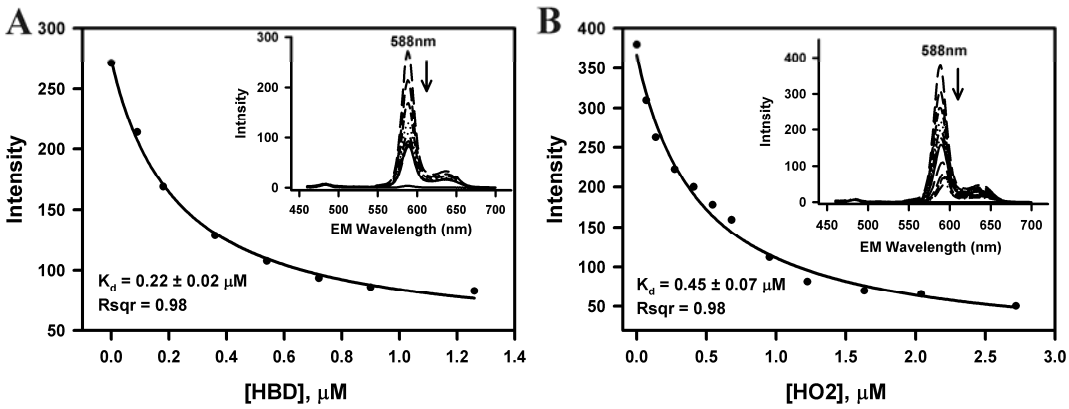

FIGURE 5.13 **Titration of ZnPP with HBD and HO-2. A,** 0.5 μM ZnPP was titrated with HBD. **B,** 1 μM ZnPP was titrated with HO-2. Excitation wavelength is at 415 nm and emission wavelength is at 588 nm. Titrations were performed by monitoring the fluorescence decreasing at 588 nm. The insets are the fluorescent spectra from the HBD titration.

5.5 Discussion

The rapid physiological response to hypoxia is mediated by the carotid body, which is an arterial O_2 chemoreceptor organ (34). The rapid inhibition of ion channel activity in glomus cells of the carotid body by hypoxia was first demonstrated in 1988 (35). Under normoxic conditions, the glomus cell membrane is hyperpolarized due to the pumping of K^+ through the open BK channel, while inhibition of channel activity initiates a wave of depolarization that results in increased ventilation by the lungs (34). The involvement of the human BK channel in the physiological responses to hypoxia and the regulation of these responses by heme and CO have been well documented (14,36-38). Both ferric and ferrous heme inhibit the BK channel, while CO stimulates channel activity (16). In addition, co-immunoprecipitation experiments and immunocytochemical analyses indicate that HO-2 binds directly to the BK channel (15). However, the mechanism(s) by which heme inhibits and CO activates the BK channel in response to hypoxic and normoxic conditions, respectively, remains unclear. Mechanisms by which the functions of HO-2 and the BK-channel could be coupled include the direct activation of the BK-channel by CO, regulation of heme availability by HO-2 and protein-protein associations. Our results indicate that a thiol/disulfide redox switch in the HBD of the BK channel affects binding of both heme and CO as well as HO-2-HBD interactions.

Regarding CO activation, two contrasting mechanisms have been recently proposed. Based on the findings that CO affects the binding of Fe^{2+}-heme, but not Fe^{3+}-heme, to the HBD and that mutation of Cys615 and His616 in the CXXCH motif abolish both heme-dependent inhibition and CO-induced activation of the channel, it was proposed that the effects of CO are mediated by binding to heme (17). On the other hand, because substitutions of residues (two His and an Asp) in the high-affinity RCK1 high-affinity Ca^{2+} sensor domain disrupt CO-dependent activation of the BK channel (using the CO donor $[Ru(CO)_3Cl_2]_2$) without affecting the inhibition by heme, and because substitutions in the CXXCH motif (of His and Cys) disrupt heme binding without abrogating activation by CO, it was suggested that CO directly interacts with the His and Asp residues in the RCK1 domain in a heme-*independent* manner (22).

Our results demonstrate that a thiol/disulfide redox switch in the human BK channel regulates binding of both heme and CO. Previous studies have indicated that Cys residues

can affect the regulation and/or activity of the human BK channel. Substitution of Cys911 with Gly decreased the sensitivity of the channel to a CO donor (the tricarbonyldichlororuthenium (II) dimer) by two-fold; furthermore, cysteine oxidation (39,40) and reaction of some cysteine-specific reagents, e.g., DTNB, MTSEA and PCMB, (41) has been reported to decrease BK channel activity. Here we have shown that residues Cys612 and Cys615 in a CXXCH motif between the two RCK domains interconvert between the thiol and disulfide states according to a midpoint reduction potential of -184 mV, while the His residue (His616) serves as an axial heme ligand. This arrangement allows robust control of heme binding, such that the dithiol(ate) state of either the HBP or the HBD binds Fe^{3+}-heme 90- or 14-fold tighter, respectively, than the oxidized disulfide form. The K_d value for the complex between the reduced (disulfide) state of the HBD and Fe^{3+}-heme is 0.21 μM, which is similar to the K_i value (~ 0.1 μM) for inhibition of the BK channel by Fe(III)-heme (14). Importantly, the K_d value for the oxidized HBP of 14.5 μM (or 2.8 μM for the HBD) is well outside the range of intracellular free heme concentrations of 20-100 nM (42-46) (furthermore, free heme levels above 1 μM are toxic (46)). Because the ambient intracellular redox potential ranges from -170 mV to -325 mV (32,33), the CXXC motif in the HBD should undergo redox interconversion under physiologically relevant conditions, e.g., normoxia and hypoxia. Therefore, when the HBD converts to the oxidized state, the BK channel would be expected to release its bound heme.

Heme and CO elicit opposite effects on activity of the BK channel. Our results indicate that CO interacts directly with heme in the HBD, forming a high affinity Fe^{2+}-CO complex (K_d = 0.05 μM), which could be considered to favor the former of the two mechanisms of CO activation described above (17). In comparison, the hemes in NPAS2 (K_d = 1 μM) and a bacterial CO sensor (CooA) (K_d = 11 μM) bind CO with significantly lower affinity (47,48). If the HBD is the sole CO binding site within the BK channel, one possible explanation for the importance of the RCK1 domain in the CO response is that allosteric effects may couple binding of Ca^{2+} and CO to separate sites. Because it is highly unlikely that CO can bind directly to the implicated amino acid residues (H365, H394 and D367) in the RCK1 domain in a metal-independent manner, one possibility is that the His and Asp residues in RCK1 ligate a low-valent metal ion, e.g., Fe^{2+} or Cu^{1+},

which forms a CO binding site. There is evidence that Zn^{2+} can activate the BK channel and that H365 and D367 are required for this activation, suggesting that these residues can bind metal ions. A large class of metalloenzymes, i.e., oxygenases, contains a 2-His-1-carboxylate facial triad motif in which a single metal ion (Zn^{2+} or Fe^{2+}) is coordinated by two His residues and one Asp (or Glu) in a motif that often consists of $HXDX_nH$ (X can be any residue and n represents a variable number of residues) (49,50), which matches the sequence in RCK1 ($H_{365}XD_{367}X_{22}H_{394}$). Although we are unaware of CO binding to the metal center of a protein containing the 2-His-1-carboxylate facial motif, the structure of isopenicillin N synthase has been solved with bound NO (51), a CO analog. If this site does indeed bind Zn^{2+}, being a d^{10} metal ion, it would not be able to bind CO; however, there are examples of Zn^{2+} or Fe^{2+} competing for binding to a metal binding site, e.g., carbonic anhydrase (52). Thus, further studies are required to clarify the relationship between CO and the potential metal binding sites in the RCK1 domain.

As was observed for heme binding, affinity of the HBD-Fe^{2+}-heme for CO appears to be regulated by the CXXC motif. Surprisingly, the affinity of Fe^{2+}-heme in the C612S/C615S variant, which was expected to mimic the reduced protein, is 50-fold weaker than that of the native protein (K_d = 2.68 μM). How Cys612 and Cys615 affect CO binding is unclear. Perhaps one of the Cys residues undergoes ionization, which would alter the micro-environment of the heme in a way that Ser could not. Besides the Cys residues in CXXCH motif, Cys628 and Cys630 form the other intramolecular disulfide bond in HBD. We have been unable to address the properties of these residues because the single and double (C628S/C630S) variants were unable to be purified, suggesting that these residues may play a structural role.

The results of our intrinsic fluorescence quenching experiments indicate that the HBD interacts directly with HO-2. These results support earlier coimmunoprecipitation and immunocytochemical analyses indicating that HO-2 binds directly to the BK channel (15). This interaction could allow HO-2 to locally influence both the heme and CO concentrations to which the BK channel is exposed. The influence of the CXXC motif on heme and CO binding suggests that this motif functions as a thiol/disulfide redox switch. Interestingly, a similar redox regulatory mechanism has been recently identified in human HO-2; however, with an opposite redox regulatory modality (24,25). HO-2 has low

affinity for heme when the Cys residues in a heme response motif (HRM) are in the reduced (free thiol) state; however, when they switch to the oxidized (disulfide) state, the affinity for heme markedly increases (24,25). Thus, it is most significant that redox switches in both HO-2 and the BK channel respond in a seemingly coordinated way to redox changes, with HO-2 releasing heme under redox conditions that optimize heme binding to HBD and HBD releasing heme under oxidizing conditions that stimulate heme degradation by HO-2.

Figure 5.14 describes a working hypothesis for how HO-2 and the BK channel system may coordinately respond to altering intracellular redox conditions and to the related shifts between hypoxia and normoxia. Under hypoxic conditions, where the redox potential would decrease, the thiol/disulfide switches in HO-2 and the BK channel would convert to the dithiol states, with HO-2 having low affinity and BK channel having high affinity for Fe^{3+}-heme. The combined effects of low heme affinity and limited O_2 concentration would decrease heme degradation activity by HO-2, resulting in a local increase in heme and decrease in CO concentrations. Furthermore, the decrease in intracellular redox potential associated with hypoxia would promote binding of heme and to the BK channel. Thus, these coordinated effects of high heme and low CO would promote closing of the BK channel. Under normoxic conditions, the redox active thiols of HO-2 and the BK channel would exist in oxidized states, with HO-2 having high affinity and BK channel having low affinity for Fe^{3+}-heme. Furthermore, the increased O_2 levels would stimulate degradation of heme to generate CO, which would activate the channel. It is likely that CO binding to the HBD would be one of the most rapid responses to the reestablishment of normoxic conditions, which would be followed by release of heme from the BK channel, due to its low heme affinity when the CXXC motif is in the oxidized state. The redox-based control of the BK channel proposed here would of course be interfaced with the many other inputs into regulation of ion channel function, including the major roles of Ca^{2+} and membrane potential and other modulatory properties of the RCK domains.

In conclusion, our research provides strong evidence for a thiol/disulfide switch in the BK channel that involves Cys residues in the CXXCH motif of a HBD. This switch regulates affinity of the HBD for heme and CO and for HO-2. We speculate that this

redox-linked alteration in properties of the HBD has important physiological roles, including the ability to regulate the activity of the human BK channel in response to intracellular hypoxic/normoxic conditions.

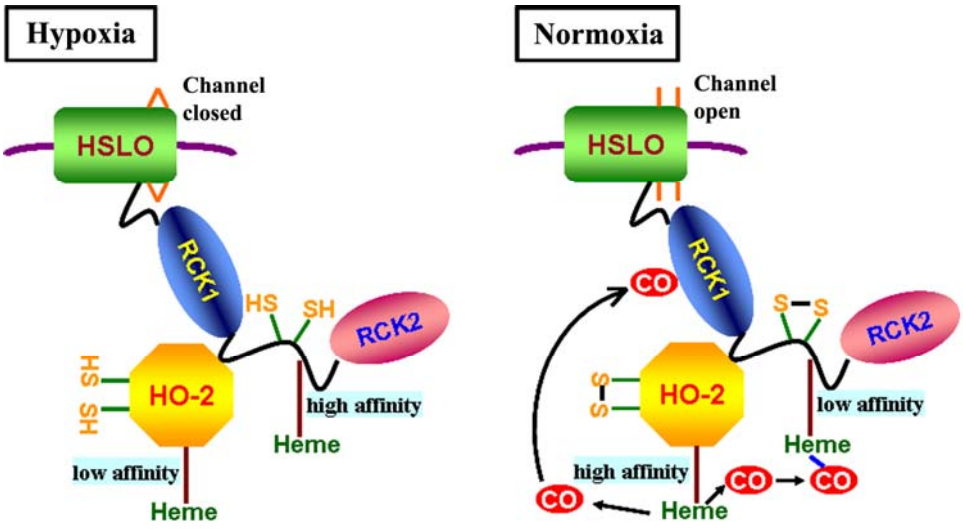

FIGURE 5.14 **Proposed redox regulatory mechanism of human BK channel and HO-2 under hypoxic/normoxic condition.** This figure describes a working hypothesis for how HO-2 and the BK channel system may coordinately respond to intracellular redox changes, e.g. hypoxia and normoxia. Under hypoxic or more reducing conditions, the thiol/disulfide redox switches in HO-2 and the BK channel would be in the dithiol states, with HO-2 having low affinity and BK channel having high affinity for Fe^{3+}-heme. The combined effects of low heme affinity and low O_2 concentration would decrease HO-2 activity, resulting in an increase in heme and a decrease in CO concentrations. Increase in heme affinity of the BK channel, combined with high heme and low CO levels would promote closing of the channel, and depolarization of the cell membrane. Under more oxidizing and/or normoxic conditions, the redox active thiols of HO-2 and the BK channel would exist in oxidized states, with HO-2 having high affinity and the BK channel having low affinity for Fe^{3+}-heme. Furthermore, the increased O_2 levels would stimulate HO-2 activity to generate CO, which would activate the channel, leading to hyperpolarization of the cell membrane.

5.6 Conclusion

In our work described here, a soluble 134-residue linker region, which we refer to as the heme-binding domain (HBD), between RCK1 and RCK2 was cloned, expressed and purified to address the heme binding properties of the human BK channel. We characterized the HBD using EPR and UV-visible spectroscopy. Our results demonstrate that His616 in the $C_{612}XXC_{615}H$ motif serves as the axial heme ligand. The Cys residues were shown to form a thiol/disulfide redox switch that regulates the affinities of the channel for heme and CO. Reduction of the disulfide bond in the CXXCH motif enhances the affinity of HBD for heme by ~14-fold. In addition, replacement of the Cys residues by Ser decreases the CO affinity by over 50-fold. We propose that thiol/disulfide redox modulation of the affinity for heme and CO is one way that the BK channel can rapidly respond to the switch between hypoxic and normoxic conditions.

5.7 References

1. Salkoff, L., Butler, A., Ferreira, G., Santi, C., and Wei, A. (2006) *Nat Rev Neurosci* **7**, 921-931
2. Hou, S., Heinemann, S. H., and Hoshi, T. (2009) *Physiology (Bethesda)* **24**, 26-35
3. Liu, H., Moczydlowski, E., and Haddad, G. G. (1999) *J Clin Invest* **104**, 577-588
4. Lewis, A., Peers, C., Ashford, M. L., and Kemp, P. J. (2002) *J Physiol* **540**, 771-780
5. Cui, J., Yang, H., and Lee, U. S. (2009) *Cell Mol Life Sci* **66**, 852-875
6. Lu, R., Alioua, A., Kumar, Y., Eghbali, M., Stefani, E., and Toro, L. (2006) *J Physiol* **570**, 65-72
7. Adelman, J. P., Shen, K. Z., Kavanaugh, M. P., Warren, R. A., Wu, Y. N., Lagrutta, A., Bond, C. T., and North, R. A. (1992) *Neuron* **9**, 209-216
8. Xia, X. M., Zeng, X., and Lingle, C. J. (2002) *Nature* **418**, 880-884
9. Yusifov, T., Savalli, N., Gandhi, C. S., Ottolia, M., and Olcese, R. (2008) *Proc Natl Acad Sci U S A* **105**, 376-381
10. Hou, S., Xu, R., Heinemann, S. H., and Hoshi, T. (2008) *Nat Struct Mol Biol* **15**, 403-410
11. Dong, J., Shi, N., Berke, I., Chen, L., and Jiang, Y. (2005) *J Biol Chem* **280**, 41716-41724
12. Nakamura, T., Yuda, R., Unemoto, T., and Bakker, E. P. (1998) *J Bacteriol* **180**, 3491-3494
13. Jiang, Y., Pico, A., Cadene, M., Chait, B. T., and MacKinnon, R. (2001) *Neuron* **29**, 593-601
14. Tang, X. D., Xu, R., Reynolds, M. F., Garcia, M. L., Heinemann, S. H., and Hoshi, T. (2003) *Nature* **425**, 531-535
15. Williams, S. E. W., P. Mason, H. S. Bould, J. Iles, D. E. Riccardi, D. Peers, C. and Kemp, P. J. (2004) *Science* **306**, 2093-2097
16. Horrigan, F. T., Heinemann, S. H., and Hoshi, T. (2005) *J Gen Physiol* **126**, 7-21
17. Jaggar, J. H., Li, A., Parfenova, H., Liu, J., Umstot, E. S., Dopico, A. M., and Leffler, C. W. (2005) *Circ Res* **97**, 805-812
18. Kim, H. P., Ryter, S. W., and Choi, A. M. (2006) *Annu Rev Pharmacol Toxicol* **46**, 411-449
19. Baranano, D. E., and Snyder, S. H. (2001) *Proc Natl Acad Sci U S A* **98**, 10996-11002
20. Maines, M. D. (2005) *Antioxidants & redox signaling* **7**, 1761-1766
21. Boehning, D., and Snyder, S. H. (2002) *Science* **298**, 2339-2340

22. Hou, S., Xu, R., Heinemann, S. H., and Hoshi, T. (2008) *Proc Natl Acad Sci U S A* **105**, 4039-4043
23. Venter, J. C., *et al*., (2001) *Science* **291**, 1304-1351
24. Yi, L., and Ragsdale, S. W. (2007) *J Biol Chem* **282**, 21056-21067
25. Yi, L., Jenkins, P. M., Leichert, L. I., Jakob, U., Martens, J. R., and Ragsdale, S. W. (2009) *J Biol Chem* **284**, 20556-20561
26. Berry, E. A., and Trumpower, B. L. (1987) *Anal Biochem* **161**, 1-15
27. Ellman, G. L. (1958) *Arch Biochem Biophys* **74**, 443-450
28. Qiu, Y., Sutton, L., and Riggs, A. F. (1998) *J Biol Chem* **273**, 23426-23432
29. Kubista, M., Sjoback, R., Eriksson, S., and Albinsson, B. (1994) *Analyst* **119**, 417-419
30. Ikeda-Saito, M., Hori, H., Andersson, L. A., Prince, R. C., Pickering, I. J., George, G. N., Sanders, C. R., 2nd, Lutz, R. S., McKelvey, E. J., and Mattera, R. (1992) *J Biol Chem* **267**, 22843-22852
31. Benda, R., Schunemann, V., Trautwein, A. X., Cai, S., Reddy Polam, J., Watson, C. T., Shokhireva, T., and Walker, F. A. (2003) *J. Biol. Inorg. Chem.* **8**, 787-801
32. Dooley, C. T., Dore, T. M., Hanson, G. T., Jackson, W. C., Remington, S. J., and Tsien, R. Y. (2004) *J Biol Chem* **279**, 22284-22293
33. Jones, D. P. (2002) *Methods Enzymol* **348**, 93-112
34. Lopez-Barneo, J., Pardal, R., and Ortega-Saenz, P. (2001) *Annu Rev Physiol* **63**, 259-287
35. Lopez-Barneo, J., Lopez-Lopez, J. R., Urena, J., and Gonzalez, C. (1988) *Science* **241**, 580-582
36. Kumar, P. (2007) *Essays Biochem* **43**, 43-60
37. Dong, D. L., Zhang, Y., Lin, D. H., Chen, J., Patschan, S., Goligorsky, M. S., Nasjletti, A., Yang, B. F., and Wang, W. H. (2007) *Hypertension* **50**, 643-651
38. Franco-Obregon, A., Montoro, R., Urena, J., and Lopez-Barneo, J. (1996) *Adv Exp Med Biol* **410**, 97-103
39. Brazier, S. P., Telezhkin, V., Mears, R., Muller, C. T., Riccardi, D., and Kemp, P. J. (2009) *Adv Exp Med Biol* **648**, 49-56
40. Zhang, G., Xu, R., Heinemann, S. H., and Hoshi, T. (2006) *Biochem Biophys Res Commun* **342**, 1389-1395
41. Tang, X. D., Daggett, H., Hanner, M., Garcia, M. L., McManus, O. B., Brot, N., Weissbach, H., Heinemann, S. H., and Hoshi, T. (2001) *J Gen Physiol* **117**, 253-274
42. Sassa, S. (2004) *Antioxidants & redox signaling* **6**, 819-824
43. Liu, S. C., Zhai, S., and Palek, J. (1988) *Blood* **71**, 1755-1758

44. Garrick, M. D., Scott, D., Kulju, D., Romano, M. A., Dolan, K. G., and Garrick, L. M. (1999) *Biochimica et biophysica acta* **1449**, 125-136
45. Ogawa, K., Sun, J., Taketani, S., Nakajima, O., Nishitani, C., Sassa, S., Hayashi, N., Yamamoto, M., Shibahara, S., Fujita, H., and Igarashi, K. (2001) *Embo J* **20**, 2835-2843
46. Sassa, S. (2006) *J. Clin. Biochem. Nutr.* **38**, 138-155
47. Dioum, E. M., Rutter, J., Tuckerman, J. R., Gonzalez, G., Gilles-Gonzalez, M. A., and McKnight, S. L. (2002) *Science* **298**, 2385-2387
48. Yamashita, T., Hoashi, Y., Watanabe, K., Tomisugi, Y., Ishikawa, Y., and Uno, T. (2004) *J Biol Chem* **279**, 21394-21400
49. Hausinger, R. P. (2004) *Crit Rev Biochem Mol Biol* **39**, 21-68
50. Koehntop, K. D., Emerson, J. P., and Que, L., Jr. (2005) *J Biol Inorg Chem* **10**, 87-93
51. Roach, P. L., Clifton, I. J., Hensgens, C. M., Shibata, N., Schofield, C. J., Hajdu, J., and Baldwin, J. E. (1997) *Nature* **387**, 827-830
52. Macauley, S. R., Zimmerman, S. A., Apolinario, E. E., Evilia, C., Hou, Y. M., Ferry, J. G., and Sowers, K. R. (2009) *Biochemistry* **48**, 817-819

Chapter 6

Ongoing Work and Future Directions

6.1 Evaluate the effect of redox states of HRMs on the enzymatic activity of HO-2 under *in vitro* condition

It was demonstrated in work leading to my MS degree that two Cys residues in the C-terminal region of HO-2 that are within HRM motifs can constitute a thiol/disulfide redox switch, regulating the affinity of human HO-2 for heme, with the oxidized protein (K_d = 33 nM) able to bind heme 10-fold more tightly than the reduced form ($K_{d\text{-reduced}}$ = 350 nM) of HO-2 (1). Since the physiological concentration of heme is approximately 0.02-0.1 μM, the reduced state of HO-2 is expected to be depleted in heme within the cell. Furthermore, the sequences of HO-1 and HO-2 are most divergent in the C-terminus near the HRMs (**Figure 1.4**), while the crystal structure of the human HO-2 core domain is nearly identical to that of HO-1 (2) (**Chapter 3**). These properties indicate that the HRMs may be responsible for the unique properties of HO-2, including its distinct regulatory mechanism in cells. By using the oxICAT technique, the thiol-disulfide switch in HO-2 was found to respond to cellular oxidative stress and reductive conditions, with its midpoint reduction potential at -200 mV (3) (**Chapter 2**). Cys residues in the thiol-disulfide switch are 60-70% reduced under normal growth conditions. Under oxidative stress conditions, these Cys residues in the thiol-disulfide switch exist predominantly (86-89%) in the disulfide state, while treatment with reductants converts these Cys resides largely (81-87%) to the reduced dithiol state. These results indicate that, at physiological heme concentrations, HO-2 with the oxidized form of the thiol-disulfide switch will exhibit higher HO-2 activity than the reduced protein, representing a paradigm for how HRMs can integrate heme homeostasis to confer cytoprotective effects in cells. It is important to test this hypothesis because often the K_d value is quite different from the K_m,

which is the important kinetic parameter that will govern the response of HO-2 to varying heme concentrations in the cell.

In order to investigate whether the different heme affinities between oxidized and reduced HO-2 lead to different heme degradation rates, a new heme degradation activity assay was established. Our standard assay for determining HO-2 activity, which measures bilirubin synthesis (at 468 nm) at saturating heme concentrations (1,4), is unable to distinguish between the heme degradation rates of oxidized and reduced HO-2 at physiological heme concentrations because, although bilirubin has a relatively high extinction coefficient ($\varepsilon_{bilirubin}$ = 43.5 $mM^{-1}\cdot cm^{-1}$ at 468 nm), total conversion of 20 nM heme (close to the K_d value) to bilirubin would give rise to an absorption change of only 0.00086. Increasing the heme concentrations to levels that will allow reproducible activity measurements (e.g., changes in absorbance of 0.05) requires 1 μM heme, which would be saturating for both the oxidized and reduced protein (at 100 nM range). Furthermore, studies at physiological concentrations of heme are not amenable to steady-state kinetic measurements ([substrate] >> [enzyme]). The extinction coefficient for HO-2-Fe^{3+}-heme complex at its soret peak (ε_{HO-2} = 171.4 $mM^{-1}\cdot cm^{-1}$) (1) is 3.9-fold higher than that of bilirubin, which indicates that the absorbance change for HO-2-Fe^{3+}-heme complex caused by the heme degradation would be easier to measure than that of bilirubin.

In order to measure the activities of the oxidized and reduced states of HO-2, we used single turnover conditions with 2 μM heme and 2 μM HO-2, and directly measured the decrease in absorbance of the heme as it underwent conversion to biliverdin (**Figure 6.1A**). Biliverdin reductase is unnecessary in this assay and was omitted to simplify the assay conditions. Because NADPH and cytochrome P450 reductase (CPR) are required for reduction of the heme, it is important to ensure that this single-turnover assay is not rate-limited by CPR. As shown in **Figure 6.2**, the rate of heme degradation is independent of the concentration of CPR, with similar k_{obs} values for heme degradation (0.0072 s^{-1} - 0.0076 s^{-1}) as the concentration of CPR is increased from 12 μM to 20 μM. The physiological reductant of the disulfide bond in the HRMs of HO-2 is unknown and we considered that CPR might serve this function. If so, CPR and NADPH would convert the disulfide of HO-2 to the dithiol form and the measured activities would be

indistinguishable. However, incubating HO-2 with NADPH and cytochrome P450 reductase does not alter the redox status of the Cys residues in HO-2, as measured by titration with 5,5′-Dithiobis(2-nitrobenzoic acid) (DTNB) (**Table 6.1**). Only 0.27 μM thiol groups were detected in 50 μM NADPH solution, indicating that the NADPH does not react with DTNB. 12.8 μM thiol groups were detected for the solution containing 100 μM NADPH and 3 μM CPR, and this number increased to 23.8 μM when 10 μM oxidized HO-2 was present in the mixture. The increase of 11 μM thiol groups after adding HO-2 is mainly from the free thiol in HO-2 (**Table 6.1**) that was identified as Cys127 in my previous research (1). Thus, the combined DTNB results demonstrate that CPR (and NADPH) do not catalyze reduction of the disulfide bonds in the HRMs of HO-2 and that CPR only appears to only reduce the heme. Furthermore, the physiological reductant of the HRMs in HO-2 remains unknown, the results shown in **Figure 6.2** and **Table 6.1** demonstrate that catalytic activity of HO-2 will be rate limiting and that the oxidized or reduced forms of HO-2 will remain in their as-prepared state during the single-turnover measurement.

When a 50 mM phosphate buffer solution containing 2 μM oxidized or reduced HO-2, 0.1 mg/ml BSA, 80 μM NADPH and 15 μM cytochrome P450 reductase was mixed with 2 μM Fe^{3+}-heme, the heme absorbance spectrum was replaced with that of HO-2-Fe^{3+}-heme complex, which has a soret peak at 412 nm. By following the absorbance decrease in the HO-2-Fe^{3+}-heme complex at 412 nm, the enzymatic activity was calculated to be 0.079 ± 0.004 nmol/min/nmol. This indicates that oxidized HO-2 is 1.9- to 2.8-fold more active than the reduced protein, which has an enzymatic activity of 0.035 ± 0.005 nmol/min/nmol. The first-order rate constant for oxidized HO-2 (k_{obs}), obtained from a single exponential fit to the data, is 0.0071 ± 0.0003 s^{-1}, which is 1.25-fold faster than that of reduced HO-2 (0.0057 ± 0.0001 s^{-1}) (**Figure 6.1C**). The lower initial absorbance for the reduced HO-2 is a reflection of lowered heme affinity of the reduced protein, as described in earlier studies (1). Compared to oxidized and reduced HO-2, the H45A variant does not present any measurable heme degradation activity, which is due to the lack of the heme ligand (**Figure 6.1B and 6.1C**).

To evaluate the experimental results from our heme degradation assay, the actual data were compared to the theoretically calculated values. The K_d values of oxidized and

reduced HO-2 for heme were determined as 33 nM and 348 nM, respectively, in my previous research (1). Based on these K_d values, the concentration of HO-2-bound heme in oxidized HO-2 was calculated as 1.77 μM when the assay system contains 2 μM HO-2 and 2 μM heme. This number decreased to 1.36 μM for reduced protein in the same conditions. Based on the different concentrations of HO-2-Fe^{3+}-heme complexes with oxidized and reduced HO-2 in the assays, the ratio of the initial absorbance of oxidized/reduced HO-2- Fe^{3+}-heme complexes should be close to 1.30. In addition, after fitting the K_d values, heme and HO-2 concentrations into the Michaelis–Menten equation ($V/V_{max} = s/(K_m+s)$), the ratio of $V_{oxidized}/V_{reduced}$ is calculated as 1.13. Our experimental values are comparable to these theoretically calculated numbers. The initial absorbances at 412 nm for oxidized and reduced HO-2-Fe^{3+}-heme complexes in the assays are 0.224 and 0.185, respectively, so the ratio of the initial absorbance of oxidized/reduced HO-2-Fe^{3+}-heme complexes is 1.21. This number is comparable to 1.30, which indicates that the heme affinities for oxidized and reduced HO-2 that we determined in our previous studies are reliable. In addition, the k_{obs} was calculated to be 1.25-fold greater for oxidized HO-2 (0.0071 s^{-1}) than for reduced HO-2 (0.0057 s^{-1}) in our heme degradation assay, which is very close to what is theoretically calculated by their different heme affinities (1.13). These combined analyses indicate that the heme degradation efficiency is different between oxidized HO-2 and reduced HO-2.

The finding that the redox state of C-terminal HRMs in HO-2 affects enzymatic activity provides supporting evidence for the hypothetical HRM-mediated regulatory mechanism that we proposed in Chapter 2 (**Figure 2.10**). HO-2 can confer cytoprotective effects through a HRM-mediated mechanism in response to the cellular redox environmental changes. Cysteine residues in C-terminal HRMs of HO-2 largely exist in the disulfide state (**Figure 2.8**) under oxidative conditions, which makes HO-2 catalyze the heme degradation efficiently to generate CO, Fe^{2+}, and biliverdin/bilirubin, activating various cytoprotective pathways. Nevertheless, under reducing conditions, cysteine residues in C-terminal HRMs are mainly in the dithiol state, which leads to moderate heme degradation compared to oxidative conditions. Although the redox state variation of C-terminal HRMs leads to different heme degradation efficiencies of HO-2, further

experiments need to be performed under both *in vitro* and *in vivo* conditions to fully understand the physiological roles of HRMs in cells.

TABLE 6.1 **Quantification of free thiols in HO-2 heme degradation system by the DTNB assay.** Assays for all the proteins were performed in aerobically. All measurements were performed in triplicate with different amounts of protein. The average concentration of free thiols are presented.

	Concentration of free thiols (μM)
NADPH (50 μM)	0.27 ± 0.02
CPR (3 μM)	17.45 ± 0.05
CPR (3 μM) + NADPH (100 μM)	12.8 ± 0.1
Oxidized HO-2 (10 μM)	9.5 ± 0.1
Oxidized HO-2 (10 μM) + CPR (3 μM) + NADPH (100 μM)	23.8 ± 0.6

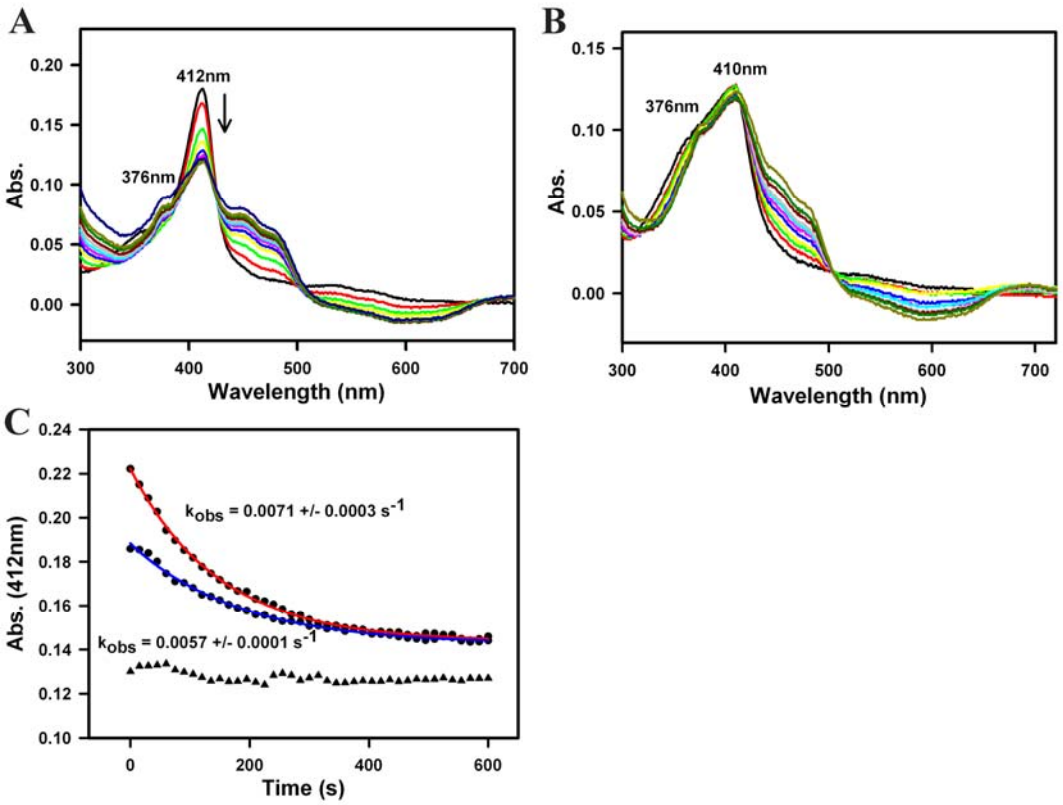

FIGURE 6.1 **Heme degradation activities of oxidized and reduced HO-2.** 2 μM HO-2, 0.1 mg/ml BSA, 80 μM NADPH and 15μM cytochrome P450 reductase were mixed in 50 mM phosphate buffer, pH 7.4. The mixture was incubated under 37 ^{o}C for 5 min before the reaction was initiated by adding 2 μM heme. The absorbance changes at 412 nm and 410 nm, for HO-2 and the H45A variant, respectively, were recorded to calculate the enzymatic activities. The data were fit with a single exponential equation (f=y0+a*exp(-b*x)) to calculate k_{obs}. In the equation, x is time; b is k_{obs}; y0 is the final abs; a is the amplitude. A, representative spectra of oxidized and reduced HO-2. B, representative spectra of the H45A variant. C, fits to data of oxidized and reduced HO-2, and the H45A variant.

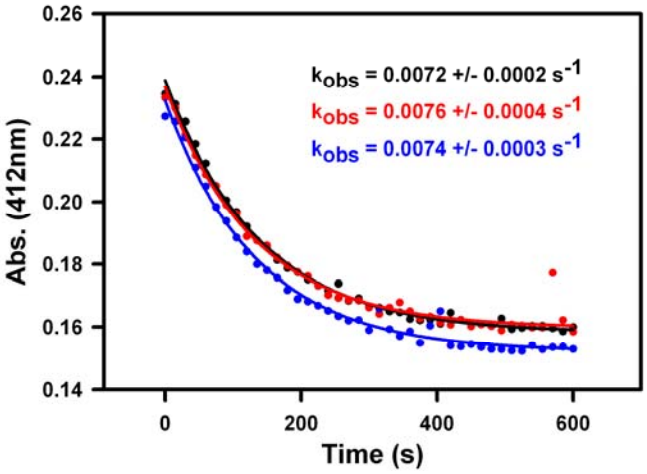

FIGURE 6.2**. The effect of NADPH-cytochrome P450 reductase on heme degradation.** To evaluate if the reaction step in which the NADPH-cytochrome P450 reductase is involved is the limiting step in heme degradation, 2 μM HO-2, 0.1 mg/ml BSA, 80 μM NADPH and various amount of cytochrome P450 reductase (12 μM: black, 15 μM: red, 20 μM: blue) were mixed in 50 mM phosphate buffer, pH 7.4. The mixture was incubated under 37 ^{o}C for 5 min before the reaction was initiated by adding 2 μM heme. The absorbance changes at 412 nm were recorded to calculate the enzymatic activities.

6.2 References

1. Yi, L. (2007) *Master's thesis, University of Nebraska-Lincoln*
2. Bianchetti, C. M., Yi, L., Ragsdale, S. W., and Phillips, G. N., Jr. (2007) *J Biol Chem* 282, 37624-37631
3. Yi, L., Jenkins, P. M., Leichert, L. I., Jakob, U., Martens, J. R., and Ragsdale, S. W. (2009) *J Biol Chem* 284, 20556-20561
4. Ishikawa, K., Matera, K. M., Zhou, H., Fujii, H., Sato, M., Yoshimura, T., Ikeda-Saito, M., and Yoshida, T. (1998) *J Biol Chem* 273, 4317-4322